Origin and development of hematopoietic tumors

in sumoylation mutants of *Drosophila melanogaster*

by

Marta Elzbieta Kalamarz

A dissertation submitted to the Graduate Faculty in Biology

in partial fulfillment of the requirements for the degree of Doctor of Philosophy, The City

University of New York

2010

This manuscript has been read and accepted for the Graduate Faculty in Biology in satisfaction of the dissertation requirement for the degree of Doctor of Philosophy.

Shubha Govind, Ph.D.

Date | Chair of the Examining Committee

Laurel A. Eckhardt, Ph.D.

Date | Executive Officer

Girish Deshpande, Ph.D.

Serafin Piñol-Roma, Ph.D.

Paul Schedl, Ph.D.

Linda Spatz, Ph.D.

Supervisory Committee

THE CITY UNIVERSITY OF NEW YORK

Origin and development of hematopoietic tumors

in sumoylation mutants of *Drosophila melanogaster*

by

Marta Elzbieta Kalamarz

Advisor: Dr. Shubha Govind

ABSTRACT

The larval hematopoietic system of *Drosophila melanogaster* consists of freely circulating cells, the sessile population, and the hematopoietic organ called the lymph gland. Most hemocytes function as macrophages and play a significant role in innate immunity. Hemocytes also remodel tissues, aiding in development of the organism. Constitutive activation of immune signaling pathways, as well as various mutations in genes which are not linked to immune pathways, result in the overabundance of circulating hemocytes and tumor formation. Many aspects of tumor development, such as the identity of the affected hematopoietic population and mechanisms of tumor growth are either not characterized or not well understood. The overall goal of this project was to understand the origin and development of hematopoietic tumor formation in *Ubc9* mutants.

Ubc9 is an E2 enzyme, which conjugates SUMO (small ubiquitin-like modifier) to a range of target proteins. Sumoylation targets vary in function from structural components to enzymes and transcription factors. Thus, sumoylation affects multiple cellular functions via modification of protein localization, stability or activity. Loss-of-

function *Ubc9* mutants of *Drosophila* exhibit severe defects in hematopoietic and immune tissues, including hemocyte overproliferation and tumor formation during larval stages.

In this dissertation, we report that the hemolymph of *Ubc9* mutants contains hematopoietic cells and structures that range from aggregates (composed of only few cells) to small and large tumors. The largest tumors are less than 1 mm^3 in volume. Most cells and aggregates exhibit high ration of mitotic cells, but only a few of the largest tumors in the hemolymph contain actively dividing cells. Based on staining patterns and genetic rescue experiments, we propose that the large tumors are derived specifically from overgrown posterior lobes of the hematopoietic organ. The origin of smaller tumors and aggregates is less clear. Our data suggest that these structures likely derive from circulating hemocytes and fragments of dispersed anterior lobes.

Microtumors in *Ubc9* mutants arise from the highly-mitotic mutant stem/progenitor cells of the lymph gland. Loss of sumoylation cascade enzymes E1 (Aos1/Uba2), E2 (Ubc9), or E3 (PIAS) leads to loss of proliferative quiescence in hematopoietic precursors localized within the lymph gland. Proliferative quiescence of these precursors is at least in part mediated by the activity of the cyclin-dependent kinase inhibitor Dacapo/p21. Expression of Dacapo homolog, human p21, in the *Ubc9* progenitor cells relieves tumor formation. These studies suggest that sumoylation provides a cell-intrinsic mechanism to preserve stem/progenitor cell states for stress response, immunity and development of the fly.

ACKNOWLEDGEMENTS

I express my sincere gratitude and thank Dr. Govind for being my mentor, for never ending and highly contagious enthusiasm, for incredible patience and for continuous support she provided in many dimensions of scientific and ordinary life.

I thank my committee members - Drs. Serafin Piñol-Roma, Linda Spatz, Girish Deshpande and Paul Schedl, for their help, support and constructive criticism.

I offer my deepest gratitude to my family, especially my parents; my mom, Barbara Kałamarz who taught me how to use a microscope, for sparking my interest in science and for her continuous incredible dedication to working for the good of her patients and helping people in every possible way. I thank my dad, Czesław Kałamarz, for sharing his extraordinary love of nature, for his hard work and dedication to family. I thank Izabela Piegdon, the incredible woman who at over 90 years of age has better memory than I will ever have, who supported me throughout years and functioned as my "third grandmother". I thank Daniel Fimiarz, for being my best friend and husband, for sharing experiences and dreams, for love and help in good and bad days. I thank my aunt Marta Deryło for care and invaluable lessons on life. I also thank Ania Deryło and Michał Deryło and their families. I thank Jerry and Sharon Proskurnicki, for offering a life-changing experience, for showing me that life is full of surprises and achieving dreams is indeed possible; for passion for life and incredible joy and sharing of what is best in you. Your presence in my life ultimately made this entire journey possible. I thank my entire family – there are simply too many names to list all of you.

Deepest thanks to all my friends, who, despite sometimes an overwhelming distance, are continuously close and ready to help or poke, depending on the situation, especially Asia Horodecka-Jach, Hülya Kartal and Basia Czerny. This work would not have been accomplished without your love, care and support. You have contributed to my life in many incredible ways. Thank you for that!

I am grateful to Christina Nadar for help with characterization of the hematopoietic tumors. Christina Nadar also helped with p21 rescue experiments with Serpent-Hemo, Hemese, Hemolectin and Collagen drivers. I thank Indira Paddibhatla, with whom I shared the responsibility of performing the 76B-Gal4>p21 rescue experiments. Data in Part II, Fig. 3 panel K, and zoom in panel L were contributed by Indira Paddibhatla. I thank all the members of Dr. Govind's lab for lively discussions and feedback. I thank Jeffrey Uribe and Mena Jorree for their help and great work on several experiments which are not included in this publication. I thank Zoe Papadopol for technical support and friendship. I also especially thank Indira Paddibhatla, our "Ms. Aspirin" and her family, Tamara Goncharuk, Chiyedza "Margarita" Small and Mark "Marky" Lee, Maria "Le Cookie" Otazo and Christina Nadar - for your friendship and support. I am grateful to Jorge Morales for giving away the "tricks of the trade" when I begun working with *Drosophila*. I thank Roma Rajwani, Felix Castellanos-Suarez, Roberto Ferrarese and Gwenaelle "Ms. Chocolat" for help and advice of all sorts.

I thank Daniel Fimiarz for providing valuable help with confocal imaging, data retrieval and advice on image processing. I also thank Drs. Sally Hoskins, Mark Pezzano, Betty Fong and Ralph Zuzolo for teaching and help with carrying out experiments or for critical feedback on writing.

I am grateful to members of the scientific community for sharing stocks and reagents (listed in Material and Methods section).

My sincere gratitude to all who contributed to this work in countless ways.

To my Family and Friends

TABLE OF CONTENTS

LIST OF FIGURES

Part I

Characterization of hematopoietic aggregates and microtumors of sumoylation-deficient *Ubc9* mutants

ABSTRACT

Ubc9 encodes the SUMO-conjugating E2 class enzyme. The *Drosophila* protein is more than 80 % identical to its mammalian counterpart. Loss-of-function mutations in *Drosophila Ubc9* gene cause strong mitotic defects in larval hematopoietic tissues including an increase in the number of hematopoietic precursors in the lymph gland and of mature hemocytes in circulation. In addition, *Ubc9* mutants show signs of genomic instability, as evidenced by the occurrence of polyploid and multinucleate blood cells. In addition, these mutants show high numbers of lamellocytes within lymph glands and hemolymph. Lamellocytes are an activated hemocyte type, which are not found in wild type animals, but differentiate in response to immune stimuli such as wasp parasitization of Drosophila larvae. Some of these lamellocytes present in *Ubc9* mutants take part in forming tumorous masses around self tissues.

The goal of this study was to characterize all the hematopoietic structures found in the mutant hemolymph. From a study of over 932 structures from 58 animals, we found that there are many more aggregates (structures less than ~ 0.5×10^{-3} mm^3) in the larval hemolymph than there are microtumors (0.5×10^{-3} mm^3 -1 mm^3). The abundance of microtumors correlates inversely with their size. Some microtumors are melanized; the

maximum size of the melanized microtumors is somewhat smaller than that of their unmelanized counterparts. Mutant cells of the hematopoietic compartment show higher rates of mitosis and apoptosis in mutants relative to the wild type cells. Antibody staining experiments reveal that some hemocytes are defective in centrosome amplification. Furthermore, microtumors are composed of different cell types; they are morphologically complex with distinct areas of differential gene expression patterns. Our results suggest that most *Ubc9* microtumors are actively-growing structures. Because microtumors do not exceed 1 mm^3 in size and *Drosophila* lacks angiogenesis, the detailed analysis of these microtumors presents a valuable opportunity to understand the earliest steps in tumor formation.

INTRODUCTION

During normal development, pluripotent stem cells give rise to differentiated, post mitotic cell types. In the simplest scenario, a stem cell undergoes asymmetric division leading to the formation of another self-renewing cell and a differentiated sister cell. In many tissues, however, the stem cell first produces a number of progenitors by symmetric division. These transit amplifying cells or progenitors then undergo symmetric division to form fully-differentiated cell types. Mutations in the transit amplifying cell population increase with each generation, and some of them lead to loss of cell cycle controls and tumor growth (Molofsky et al., 2004; Weinberg, 2007).

Despite significant progress in the understanding of the origin of cancers including the discovery of cancer stem cells (Visvader and Lindeman, 2008; Wang, 2010), our understanding of the earliest stages of cancer development remains limited. This is largely because clinical detection of cancer requires presentation of a tumor mass whose structure and biology are different from the initial pre-malignant cell mass. While all tumors arise as microscopic structures, not all grow to become life-threatening. Autopsies and imaging techniques reveal that most do not present symptoms, remain non-invasive, and for the most part remain undetected. Some of these microscopic tumors remain dormant; never growing beyond 1-2 mm in diameter (reviewed in (Almog, 2010)).

The mechanisms behind tumor dormancy remain largely obscure, although the role of angiogenesis in the growth of solid tumors is well-established (Folkman et al., 1971; Carmeliet, 2005; Ribatti, 2005). Molecular characterization of dormant versus fast-growing tumors reveals that angiogenesis genes are among the most significantly affected in the switch (Almog et al., 2009; Almog, 2010). Tumor growth sustained by stem-like cancer cells has been shown to sustain brain tumors in the absence of angiogenesis (Sakariassen et al., 2006).

Drosophila larvae have a simple, unbranched dorsal vessel. Gaseous exchange occurs through the tracheal system and the hemolymph, which circulates in the "open" system; thus, there is no angiogenesis. Hematopoietic microtumors develop in many mutants in the absence of angiogenesis. An interesting class of hematopoietic mutants includes animals in which either the Toll/NF-κB (*cact*$^{-}$, *Ubc9*$^{-}$ *Toll*^{gof}, over-expression of Dorsal or Dif) or JAK-STAT (*hop*$^{Tum\text{-}l}$) signaling is activated (Evans et al., 2003; Meister and Govind, 2003; Minakhina and Steward, 2006). In all cases of this class of mutants, circulating hemocytes (few undifferentiated prohemocytes, plasmatocytes, lamellocytes and crystal cells; (Lanot et al., 2001)) and cells of the lymph gland (Jung et al., 2005) are variously affected ((Qiu et al., 1998; Chiu et al., 2005); see below). These tissues exhibit overproliferation and misdifferentiation and these aberrations are associated with the presence of small aggregates and larger tumorous masses. Aggregates and tumors are easily observed through the larval cuticle due to their melanization. The larger tumor masses often also contain cells of non-hematopoietic tissues (Qiu et al., 1998; Chiu et al., 2005; Minakhina and Steward, 2006).

Hematopoeitic tumors present in *Ubc9* mutants are the most interesting, as they attain relatively large dimensions due to significant developmental delay in these animals. An array of hematopoietic aggregates and microtumors appear within a five-day period in the hemolymph (Chiu et al., 2005).

The goal of this study was to describe all structures of *Ubc9* mutants and to distinguish aggregates from tumors by size and gene expression patterns. Mutant cells are present singly, in clusters or aggregates, as well as in tumors. Aggregates and microtumors are more abundant than larger microtumors and hemocytes in circulation and in aggregates are highly mitotic. The overall rate of turnover is also high, as many more cells in *Ubc9* mutants undergo apoptosis, relative to cells in control animals. Genomic instability observed in mutant hemocytes is partly due to defects in centrosome amplification. Cells which compose aggregates and tumors express high levels of septin protein Peanut and cytoskeletal protein β-tubulin. Hemocytes present in these structures also express integrins α PS1 and β PS in a cell-specific manner. Mutant lamellocytes in circulation and in tumors express high levels of integrin β PS. Mutant plasmatocytes and cells with intermediate morphologies express integrin α PS1. These proteins are highly conserved and their functions are associated with mammalian tumorogenesis. This initial characterization of mutant cells in circulation and in tumors sets the stage for further in-depth analysis of the origin and growth of microtumors.

MATERIAL AND METHODS

Fly lines

y w; Ubc9$^{4\text{-}3}$FRT40A/CyO y^{+}, y w; Ubc9^{5} FRT40A/CyO y^{+}, are described in (Chiu et al., 2005). *Ubc9$^{4\text{-}3}$* was recombined with the *Bc* mutation to generate a *Bc Ubc9$^{4\text{-}3}$ / CyO y^{+}* stock (Chiu et al., 2005). This line was crossed to *y w; Ubc9^{5} FRT40A/CyO y^{+}* to generate *Bc Ubc9$^{4\text{-}3}$/+ Ubc9^{5}* animals. The *msnf>GFP* lines are described in (Tokusumi et al., 2009).

Analysis of tumor size

Developmentally synchronized larvae were collected at day 6 of development and washed with alcohol, water and phosphate-buffered saline (PBS) of pH 7.4. Animals were bled and tumors were dissected onto glass slides and air-dried. Specimens were fixed with freshly prepared 4 % paraformaldehyde in PBS and mounted. Blood smears with tumors and aggregates were imaged, scored and their projections were measured in AxioVision LE Rel. 4.5 software. Data was collected and analyzed in MS Excel.

Apoptosis assays

A fresh solution of 0.5 µg/ml acridine orange (Sigma) and 5 µg/ml Hoechst 33258 (Molecular Probes) was prepared in PBS. On a microscope slide, each larva was bled into a separate 13 µl drop of acridine orange and Hoechst solution covered with a 22 mm x 22 mm cover slip and scored after minimum of two to five minutes of incubation, for up to twenty minutes of incubation. Apoptotic cells were observed in DAPI and FITC channels at 40 x objective and counted. Apoptotic nuclei are light blue-green-yellow in color, while non-apoptotic ones are blue (usually very faint blue of variable intensity). Acridine orange-labeled early apoptotic cells are visible in blue (DAPI) and green (FITC) channel (most intense fluorescence) and late apoptotic cells are also fluorescent in red (TRITC) channel. This protocol was prepared based on Loweth and Morgan (Loweth and Morgan, 1998), Mpoke and Wolfe (Mpoke and Wolfe, 1997) and Lu and Wolfe (Lu and Wolfe, 2001).

Immunostaining of cells and tumors

Hemocyte and tumor samples were dissected, air-dried and fixed with 4 % paraformaldehyde (PFA) in PBS. Tissue samples were permeablized with 0.1 % Triton-X solution in PBS and blocked in 3 % bovine serum albumin with 0.1 % Triton-X in PBS. Primary antibody was applied in blocking solution and incubated overnight at 4 ˚C. Incubation with secondary antibody was performed at room temperature. Tissue samples stained with the secondary antibody only served as negative control. The following primary antibodies were used: mouse monoclonal antibodies against integrin β PS (1:20; (Brower et al., 1984)), integrin α PS1 (1:10; (Brower et al., 1984)), β-tubulin (1:10; (Chu and Klymkowsky, 1989)) and Peanut (1:10; (Neufeld and Rubin, 1994)) obtained from Developmental Studies Hybridoma Bank, University of Iowa; rabbit anti-Phospho Histone H3 (1:200, Molecular Probes), rabbit anti-Cleaved Pro-Caspase 3 (Asp175; 1:200, Cell Signaling Technology), centrosomin (1:500; (Heuer et al., 1995)). Anti-Nimrod C antibody was obtained from Dr. I. Ando (Vilmos et al., 2004; Kurucz et al., 2007). Fluorescent-labeled secondary antibodies were obtained from Jackson

Immunological and Molecular Probes. Tissues were counterstained with fluorescently labeled Phalloidin (Invitrogen) and nuclear dye Hoechst 33258 (Molecular Probes). Images were acquired in a Zeiss Laser Scanning Confocal Microscope and Zeiss Fluorecent Microscope, and formatted in Zeiss LSM5 and AxioVision LE 4.5 software, respectively.

RESULTS

Expressivity of *Ubc9* aggregates and microtumors

To understand the process of their formation, we analyzed 932 structures from blood smears of 58 *Ubc9* mutant larvae. These preparations contained an array of structures from single cells and aggregates (Fig. 1 B) to tumors (Fig. 1 C-E), while controls contained only singly circulating hemocytes (Fig. 1 A). Structures of less than 50 cells (less than 10,000 μm^2 in projection area) were counted as aggregates and they were not measured. The projection area of larger structures (microtumors) was measured and the degree of their melanization was recorded.

By day 6 after egg lay, *Ubc9* mutants contain an average of 8.84 aggregates and 7.22 microtumors per larva. Distribution of the number of structures in 10,000 μm^2 size increment reveals that the most numerous structures are less than 10,000 μm^2 (n = 516) accounting for 55 % of the entire observed population. These structures contain 15-50 cells and are referred to as aggregates (Fig. 1 F). Significantly, the number of all observed structures reduces exponentially as their size increases (Fig. 1 F). This observation suggests that aggregates are not dormant but actively-growing and many of them must contain mitotic cells.

The sizes of the tumors range widely. Structures measuring 10,001 – 110,000 μm^2 (n = 336) and 110,001 – 290,000 μm^2 (n = 66) account for 36 % and 7 % of the tumor population, respectively (Fig. 1 F). The least abundant class of the largest tumors ranges from 290,001 – 940,000 μm^2 and accounts for 1.5 % (n = 14) of all structures. The largest tumors measure up to 931,770.38 μm^2 in projection area and are composed of hundreds of cells.

For a spherical microtumor, the smallest microtumor (surface area approximately 10,000 m^2), translates to roughly 0.5 x 10^{-3} $mm^{3.}$ An average sized microtumor (75527.61 μm^2) is equivalent of 1.5 x 10^{-3} mm^3 and the largest microtumor (surface area 932,000 μm^2) translates to roughly 0.677 mm^3. Structures in this size class are smaller than 1 mm^3 and are called microtumors.

Melanization

The function of melanization in wild type animals is to form an impermeable barrier which aids in wound healing or parasite encapsulation by sealing off the affected region or invader (Lemaitre and Hoffmann, 2007). This reaction is carried out by crystal cells and lamellocytes (Rizki et al., 1980; Irving et al., 2005; Nam et al., 2008). To determine if melanization affects tumor size, we analyzed the melanization patterns of *Ubc9* tumors in relation to their size. We found that small structures (size of these reaching up to 273463.18 μm^2) that include aggregates (n = 516) and small tumors (n = 265) are not melanized (n = 781 out of 932 structures). The larger structures are partially (n = 55 out of 932) or completely melanized (n = 96 out of 932). In general, the size of the microtumor correlates directly with the degree of melanization (also see Fig. 5 D).

Apoptosis in *Ubc9*$^{4\text{-}3/5}$ and *Bc Ubc9*$^{4\text{-}3}$/+ *Ubc9*^{5}animals

To examine if increase in apoptosis and mitosis (see below) will affect the distribution of aggregates and mictrotumors, we examined all hematopoietic structures from *Ubc9* mutants and *Ubc9* mutants carrying one copy of the *Bc* mutation. This dominant mutation causes crystal cells to melanize prematurely, affects their viability, and limits the potential of the hemolymph to melanize (Rizki et al., 1980).

We first examined apoptotic indices of *Ubc9* and control animals in two ways. An overlap of staining signal of acridine orange combined with nuclear dye in living unpermeabilized cells is a convenient assay for apoptosis (Mpoke and Wolfe, 1997; Loweth and Morgan, 1998; Lu and Wolfe, 2001). Using this method we examined circulating hemocytes retrieved from control and mutant animals (Fig. 2 A, B, E). While less than 1 % of hemocytes exhibit signs of apoptosis in control samples, this index increased to 3 % in *Ubc9* mutants (Fig. 2 E). Apoptotic cells were observed more frequently in the aggregates and smaller tumors than in the large tumorous masses (Fig. 2 C, D).

We also stained fixed $Ubc9^{4\text{-}3/5}$ and $Ubc9^{-/+}$ hemocytes with an antibody developed against cleaved pro-Caspase 3 (Fig. 2 F). The index of hemocytes positive for this marker increased from 1.5 % in control animals to 4 % in *Ubc9* mutants, thus corroborating the validity of acridine orange assay and confirming that the cells recognized as apoptotic undergo Caspase 3 cleavage. Similar increase in apoptosis due to loss of function mutations in *Ubc9* has been obtained by Huang (Huang, 2006).

To analyze the effects of cell death in circulation of the modified genetic background, we examined the hemolymph of *Bc*-carrying *Ubc9* mutant animals for apoptosis (Fig. 2 E). No significant change was observed between the $Ubc9^{4\text{-}3/5}$ mutant and $Bc\ Ubc9^{4\text{-}3}/+\ Ubc9^{5}$ mutant hemocytes. However, the control $Bc\ Ubc9^{4\text{-}3}/CyO\ y^{+}$ animals exhibit elevated levels of apoptosis (2 %) compared to $Ubc9^{-}/CyO\ y^{+}$ heterozygotes (less than 1 %).

Mitosis in *Ubc9*$^{4\text{-}3/5}$ and *Bc Ubc9*$^{4\text{-}3}$/+ *Ubc9*^{5}animals

To document changes in mitosis, we stained hemocytes from *Ubc9* animals for phospho-histone H3 and scored the percent of dividing cells. Mitotic index is increased in *Ubc9* mutant individual circulating hemocytes (similar result has been obtained by (Huang, 2006)) as well as in those that are found in small clusters (Fig. 3 A-C). Percentage of circulating hemocytes in division increased from 2 % in heterozygotes (n = 4 larvae; a total of minimum 800 cells was counted) to 11 % in *Ubc9* mutants (n = 4; Fig. 3 G). This difference is statistically significant ($p < 0.05$). As expected, dividing cells appear to be plasmatocytes; mitotic figures were never observed in lamellocytes. Interestingly, while majority of aggregates contain dividing cells, only a few tumors display a low proportion of mitotic cells (Fig. 3 C-F). Thus, mitosis appears to be more frequent in small than large *Ubc9* structures, providing a possible explanation for the high number of the aggregates.

Introducing the *Bc* mutation into the *Ubc9* heterozygous and mutant backgrounds increased mitosis among circulating hemocytes. While heterozygous *Bc Ubc9*$^{4\text{-}3}$/*CyO y*$^{+}$ animals roughly doubled their mitotic index (5 %) compared to the *Ubc9*$^{-}$/*CyO y*$^{+}$ animals, *Ubc9* mutants carrying one copy of the *Bc* mutation exhibit mitotic ratio of 15 % (compared to approximately 11 % in *Ubc9* single mutants; Fig. 3 G). It is likely that the increase in the number of microtumors present in the *Bc Ubc9*$^{4\text{-}3}$/+ *Ubc9*^{5} relative to the *Ubc9*$^{4\text{-}3/5}$ background is related to this increased occurrence of mitosis.

To examine if previously-observed multinucleate cells (Chiu et al., 2005) may arise from abnormality in centrosome amplification, we used stained hemocytes from circulation of control and *Ubc9* mutant animals for centrosomin (CNN; (Heuer et al., 1995)), a component protein of centrosomes (Fig. 4). Overall, the number of centrosomes in mutant larvae is greater than in heterozygotes. Since CNN staining appeared as single, double, and multiple spots in various cells, this distinction was applied to the scoring of cells. The overall trend of larger number of CNN-positive structures in mutant hemocytes than in heterozygotes was true for all categories. Supernumerary centrosomes (more than two per hemocyte) were seen in the *Ubc9* mutant hemocytes, but not in the control hemocytes (Fig. 4).

Microtumors in *Bc Ubc9*$^{4\text{-}3}$/+ *Ubc9*^{5} animals

The overall trend of the frequency distribution among the unmelanized, partially and completely melanized groups of the *Bc Ubc9*$^{4\text{-}3}$/+ *Ubc9*^{5} is similar to the frequency distribution in *Ubc9*$^{4\text{-}3/5}$ mutants (i.e., the aggregates and some of the small tumors are unmelanized, while the large tumors are partially melanized; Fig. 5 A-C). This observation suggests that tumor development due to the *Ubc9* mutation follows a specific course and this process is not significantly perturbed by changes in apoptosis and mitosis. It is important to note that *Bc Ubc9*$^{4\text{-}3}$/+ *Ubc9*^{5} genotype still contains one wild type allele of *Bc* and there is a significant reduction in the number of crystal cells in *Ubc9* animals. Thus, it is not surprising that the overall effect of *Bc* is weak.

Second, in the *Bc Ubc9*$^{4\text{-}3}$/+ *Ubc9*^{5} background, while the proportion of completely-melanized structures is not significantly affected, the proportion of partially-melanized structures increases at the expense of the unmelanized aggregates (Fig. 5 D). Thus, the overall melanization level, presumably lower in the double mutants, and the presence of dead crystal cells is sufficient to alter aggregation and distribution of cells into small versus larger structures. This interpretation suggests that the formation of these two classes of structures is somehow linked and may share cells from a common source.

We analyzed microtumors from *Bc* $Ubc9^{4\text{-}3}/+$ $Ubc9^{5}$ background and found that, while the ratio of completely melanized structures is not affected, significantly the ratio of partially melanized structures increased greatly at the cost of the unmelanized aggregates. These data suggest that either aggregates contribute directly to the partially melanized tumor formation, or the two classes have common origin. Considering the fact that the increase in number of the partially melanized structures (Fig. 5 D; up by 21.56 %, from 5.9 % in $Ubc9^{-/-}$ to 27.46 % in *Bc* $Ubc9^{4\text{-}3}/+$ $Ubc9^{5}$) corresponds closely in number to the decrease in aggregates number (down by 25.39 %, from 55.36 % in $Ubc9^{-/-}$ to 29.98 % in *Bc* $Ubc9^{4\text{-}3}/+$ $Ubc9^{5}$), we speculate that the high incidence of lamellocyte differentiation might account for increase in size of a large number of aggregates whose differentiative potential is skewed towards lamellocyte fate. An average plasmatocyte is about 10 μm (78.5 μm^2) in diameter, while a lamellocyte may reach a size of about 50 μm in diameter (7850 μm^2). It is therefore possible that an aggregate of 50 cells of 3925 μm^2 could expand up to 392500 μm^2, assuming that all cells form a flat single layer sheet.

Microtumors are morphologically complex structures

Microscopic observation of microtumors reveals that they are composed of various mutant cell types that are not found among circulating hemocytes of control animals: spherical cells morphologically corresponding to plasmatocytes but of a smaller size, large and flat lamellocytes, and cell types that are intermediate in size (Fig. 6 and

Fig. 8). Some of these mutant cells are also present singly in circulation, whereas others group in small or large aggregates. Occasionally, fragments of fat body tissue are found associated with microtumors (Fig. 6 A). Fat body cells have been found both, adhering to the microtumor and within the tumorous mass.

The microtumors themselves contain discrete morphological substructures and different cell types. We found regions of microtumors containing tightly packed small and round cells with smaller than usual nuclei (Fig. 6 B). The unusual morphological structure and compactness of these regions suggest that they may be rich in proliferative cells. Indeed, the anti-phospho-histone H3 staining of microtumors allowed for visualization of center of proliferation localized to such region (Fig. 3 E-F). Furthermore, such centers of small cells are occasionally found associated with melanized regions of tumors (Fig. 6 B) and thus, may play a role in initiation of microtumor melanization.

Expression of highly conserved proteins in aggregates and tumors

The molecular structures which allow larval hemocytes to form tumorous masses in *Drosophila Ubc9* mutants are not known. To explore tumor cellular composition and identify antigens which would help in distinguishing early tumors from random hemocyte aggregates, we tested a variety of antibodies including those against β-tubulin and Peanut (Fig. 7) and integrins α PS1 and β PS (Fig. 8).

Both, β-tubulin and Peanut (septin) proteins are needed for proper cell division. Surprisingly, we found that both of these proteins are highly expressed in the microtumor structures (Fig. 7 C, F), but not in free hemocytes in control (not shown) or mutant animals (Fig. 7 A, B, D, E). The staining pattern of β-tubulin and Peanut indicates their possible involvement in cytoskeleton assembly which is specific to the microtumors but not freely circulating hemocytes.

In addition to β-tubulin and Peanut, two proteins that are expressed both in control (not shown) and mutant hemocytes (Fig. 8 C, D, G) are integrins β PS and α PS1. Both of them are expressed within the microtumors and circulating hemocytes of *Ubc9* animals (Fig. 8 A-I). Interestingly, integrin β PS was found to be highly expressed in lamellocyte type cells and as such, present at high levels in tumors. We performed a co-labeling of *Ubc9* mutant hemocytes with integrin β PS and MSNF 9 #83 strain (Tokusumi et al., 2009) and found that these markers overlap largely among circulating hemocytes and those composing tumors (Fig. 8 D-F, F').

Integrin α PS1 appears to be expressed at comparable levels in mutant and heterozygote plasmatocytes (based on cellular morphology) and cells of intermediate morphology (larger and often elongated cells; Fig. 8 G-I). Its expression is lower in lamellocytes (Fig. 8 I). In addition, large oval cells which are possibly precursors of lamellocytes or misdifferentiated cells stained more intensely than all other cells (not shown).

Together, these observations suggest that the cytoskeleton of cells composing tumors may play an essential role in tumor formation and integrity. Furthermore, hemocyte interactions with extracellular matrix and basement membrane proteins are cell-type specific and critical for the formation of microtumors.

DISCUSSION

It is widely accepted that mammalian tumors arise as vascular aggregates of malignant cells and pre-existing vessels are recruited only later to induce microtumor growth (Weinberg, 2007). The critical size at which tumors become angiogenic is 1-3 mm^3. Indeed there is evidence that multicellular glioma cell suspensions or aggregates of less than 1 mm^3 can initiate vascular growth by regulating the expression of angiogenic factors (Vajkoczy et al., 2002). The microtumors in *Ubc9* mutants are significantly smaller than 1mm^3. *Drosophila* do not have blood vessels and tiny tumors that are formed in mutant larvae develop in the absence of factors and processes involved in angiogenesis. Because of the presence of all of the intermediate stages of tumorogenesis in the same animal at any given time, our system represents a powerful model for studying the earliest steps of proliferation, differentiation, micrometastasis, adhesion and microtumor growth, and their relationships *in vivo*.

A comprehensive analysis of all mutant hematopoietic structures from $Ubc9^{4\text{-}3/5}$ and *Bc* $Ubc9^{4\text{-}3}$/+ $Ubc9^{5}$ backgrounds clearly suggest that aggregates and microtumors are not dormant; instead, they are actively-growing. In both genotypes, the frequency of aggregates correlates inversely with increase in the size of the aggregate. Cells in circulation and aggregates are frequently mitotic whereas the largest structures appear to have low number of mitotic cells. A significant level of cellular turnover is also associated with these cell populations.

Not only is the cell turnover highly dynamic in the aggregates and microtumors; they also express proteins that are known to be important in mammalian tumor biology. These include septins, β-tubulin and the members of integrin family receptors. Peanut is a septin and has been shown to function in cytokinesis and can form cytoskeletal filaments (Neufeld and Rubin, 1994; Cooper and Kiehart, 1996). β-tubulin is needed for mitotic spindle formation and this function is conserved across species (Kanbe et al., 1990; Wright and Hunter, 2003). However, studies also link expression of septins and β-tubulin to tumors (Kinoshita et al., 1997; Katsetos et al., 2003; Kim et al., 2004; Jouhilahti et al., 2008; Cerveira et al., 2009). Both, β-tubulin and Peanut are strongly and selectively expressed in larval microtumors present in *Ubc9* mutants.

Integrins are a large family of transmembrane calcium-dependent glycoproteins involved in cell-cell and cell-extracellular matrix interactions during cell adhesion and migration. They act as receptors for intracellular signaling (Mizejewski, 1999; Devenport and Brown, 2004; Wiesner et al., 2005). Furthermore, integrins are important for tumor formation and metastasis (Mizejewski, 1999; Weaver et al., 2002). They are ultimately involved in various processes which require cytoskeleton rearrangements, including cell migration and anchoring to other cells, basement membrane and ECM interactions. Integrins form heterodimers consisting of alpha and beta subunits, of which five types of integrin alpha are known in *Drosophila* (at least thirteen types in mammals) and one type of integrin beta (at least six in mammals) (Mizejewski, 1999; Brower, 2003). *Drosophila* integrin β PS is structurally similar to mammalian integrin β1, of which increased levels have been observed in transformed mouse keratinocytes (Gomez and Cano, 1995). In addition, leukocyte integrin αMβ2 (Mac-1), which takes part in regulation of phagocytosis and cell adhesion, has been implicated to activate NF-κB (Mizejewski, 1999; Shi et al., 2001).

In the next chapter we have addressed the question of the origin of these tumors directly. Once the origin of these tumors is clearly defined and the structures are characterized morphologically, it will be possible to further dissect the genetic mechanisms behind individual steps in greater detail. A detailed understanding of this system will yield insights that will be pertinent to the question of how these earliest stages in microtumor formation influence their environment to recruit factors that confer the unique morphological properties to the microtumor.

Drosophila has a short life cycle and it is easy to obtain large numbers of animals in a relatively short time. A variety of genetic and genomic tools are available for *Drosophila* research, which requires low costs of maintenance making it a valuable model system. Genetic approaches in model organisms such as *Drosophila* are rapidly increasing our understanding of stem cell biology and its relation to tumor formation (Morrison and Spradling, 2008). The fly hematopoietic system is much simpler than its mammalian counterpart and the molecular and genetic mechanisms that control blood cell development and functions are highly conserved (Evans et al., 2003; Meister and Govind, 2003). This molecular conservation and availability of genetic strains provides a unique opportunity to gain insights into how undifferentiated and misdifferentiated progenitor cells contribute to the development of hematopoietic microtumors *in vivo*.

Fig. 1. *Ubc9* hemocyte aggregates and tumors vary in size and the degree of melanization.

(A) Control *Ubc9*$^{-/+}$ hemolymph contains single cells. *Ubc9*$^{-/-}$ animals form aggregates (B), and tumors of various sizes and melanization pattern – unmelanized small tumors (C), partially melanized (D) or fully melanized (E) larger tumors.

(F) Histogram of *Ubc9*$^{-/-}$ tumor size distribution in 10,000 μm^2 increments. Tumor sizes were measured and structures below 10,000 μm^2 in projection size were counted.

Scale bars: 10 μm (A-C) and 100 μm (D, E). Images were acquired in Zeiss confocal (A, B) and fluorescent microscopes (C-E).

Figure 1

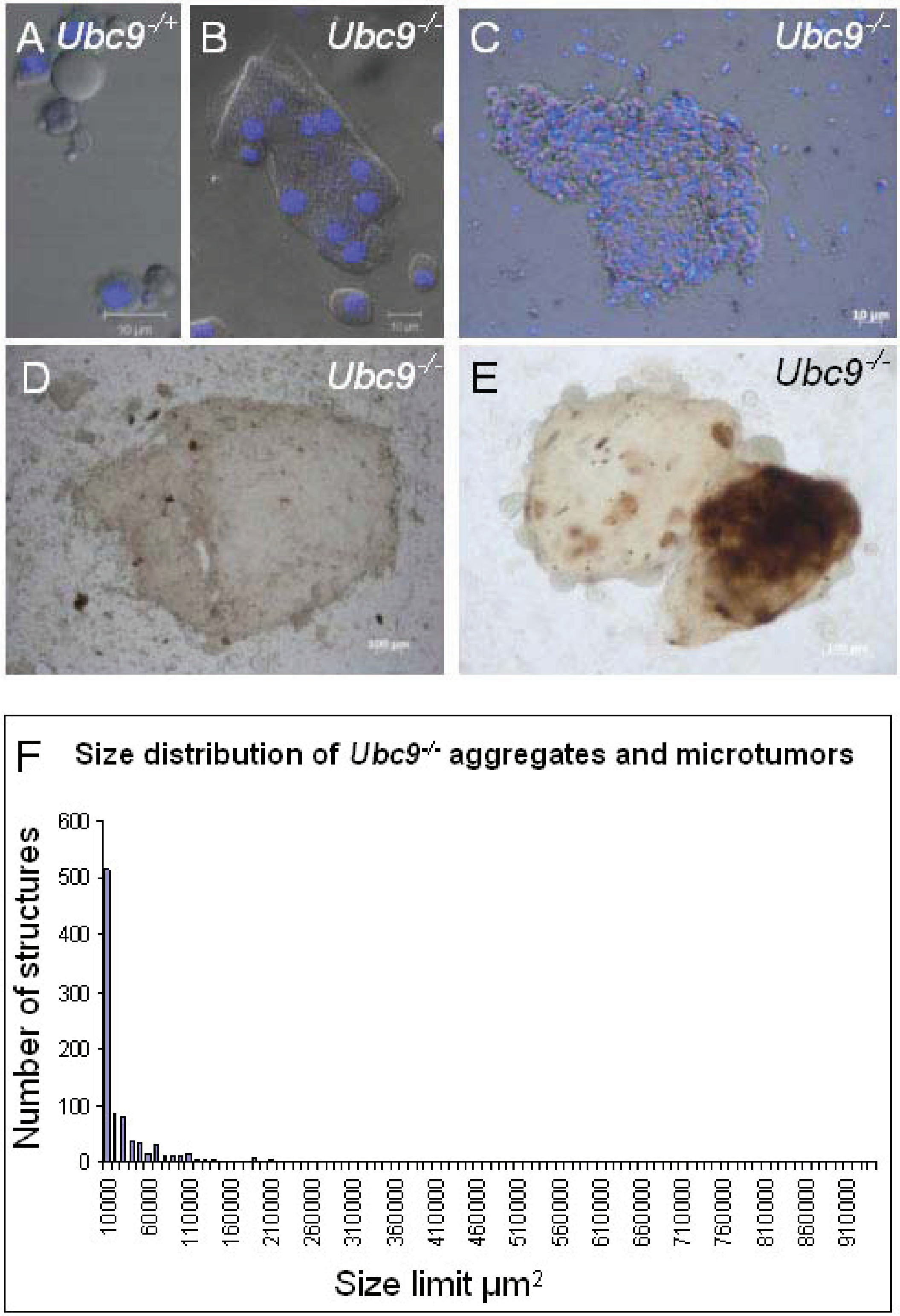
A Ubc9-/+
B Ubc9-/-
C Ubc9-/-
D Ubc9-/-
E Ubc9-/-
F Size distribution of Ubc9-/- aggregates and microtumors
Number of structures
600
500
400
300
200
100
0
10000
60000
110000
160000
210000
260000
310000
360000
410000
460000
510000
560000
610000
660000
710000
760000
810000
860000
910000
Size limit µm2

Fig. 2. Apoptosis is elevated in circulating hemocytes and aggregates of *Ubc9$^{-/-}$* and *Bc Ubc9$^{4-3}$*/+ *Ubc9^{5}* animals.

Larval hemocytes stained with acridine orange (green to red spectrum imaged) and nuclear dye (Hoechst, blue) to visualize dying cells, here visible as bright green-blue round structures. Apoptosis is rarely seen in (A) control *Ubc9$^{-/+}$* hemocytes. Frequency of apoptotic cells is increased in *Ubc9$^{-/-}$* circulating hemocytes (B) and aggregates (C), but it is rare in *Ubc9$^{-/-}$* tumors (D).

(E) The percent of apoptotic hemocytes, which were labeled by acridine orange and nuclear dye Hoechst, was scored in *Ubc9$^{-/-}$* and *Bc Ubc9$^{4-3}$*/+ *Ubc9^{5}* mutants (red squared bars) and their respective heterozygous siblings (blue bars). Data in the graph are represented as average ± SE. (F) The percent of apoptotic hemocytes positive for cleaved pro-caspase 3 was scored in heterozygous control (blue bar) and mutant *Ubc9$^{-/-}$* (red squared bar) animals.

Scale bars: 10 μm (A) and 50 μm (B-D). Images were acquired in Zeiss confocal microscope (A-D).

Figure 2

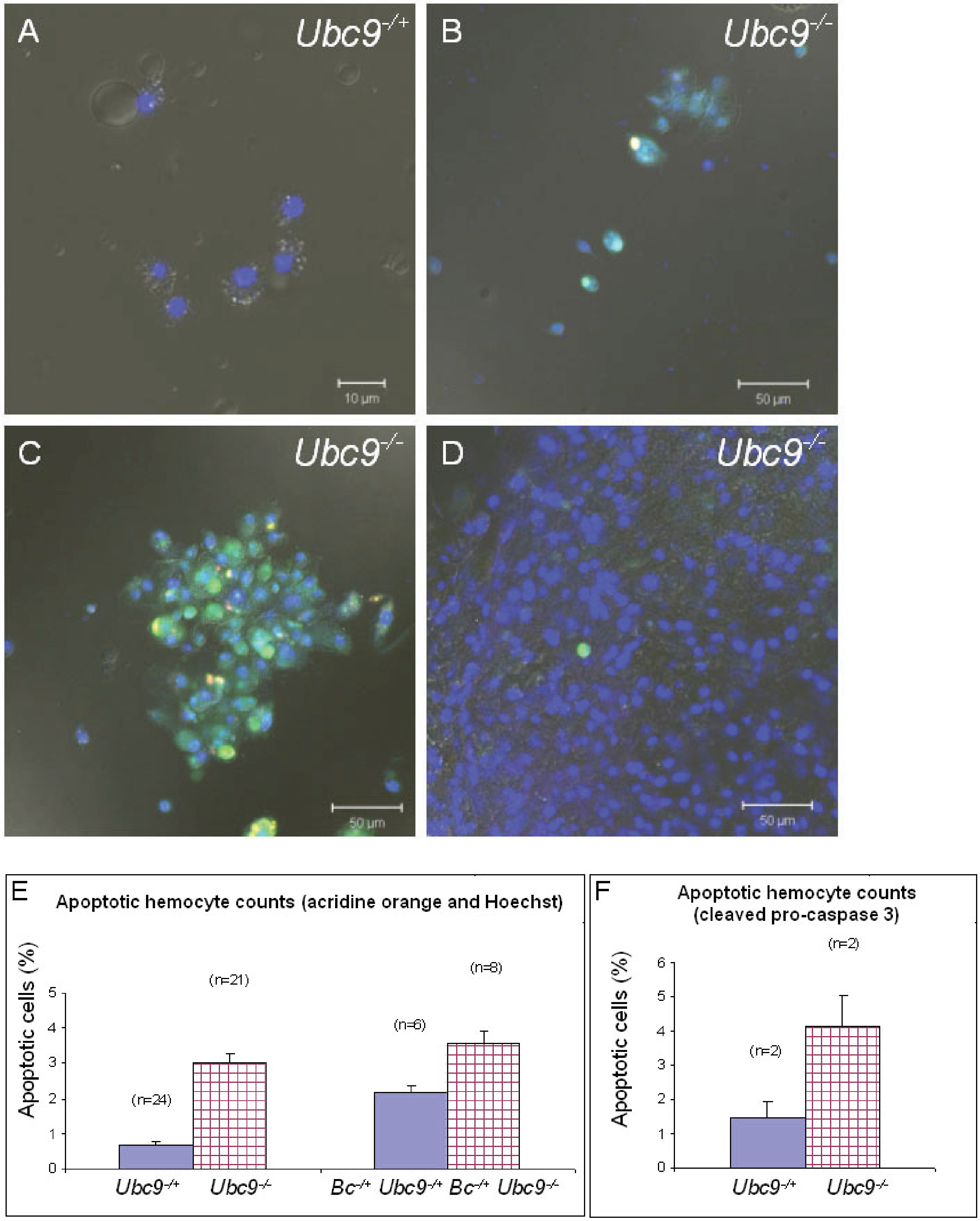
A
Ubc9-/+
10 µm
B
Ubc9-/-
50 µm
C
Ubc9-/-
50 µm
D
Ubc9-/-
50 µm
E
Apoptotic hemocyte counts (acridine orange and Hoechst)
Apoptotic cells (%)
(n=24)
(n=21)
(n=6)
(n=8)
Ubc9-/+
Ubc9-/-
Bc-/+ Ubc9-/+
Bc-/+ Ubc9-/-
F
Apoptotic hemocyte counts (cleaved pro-caspase 3)
Apoptotic cells (%)
(n=2)
(n=2)
Ubc9-/+
Ubc9-/-

Fig. 3. Mitosis is increased in *Ubc9*$^{-/-}$ background and is frequent in aggregates but rarely visible in microtumors.

Circulating hemocytes in aggregates and in tumors from *Ubc9*$^{-/-}$ larvae were stained with anti-phospho histone H3 antibody. (A-C) Cells in circulation are found singly in control (A) and *Ubc9*$^{-/-}$ mutant (B) hemolymph, or are present in *Ubc9*$^{-/-}$ clusters (C). In both cases mitotic cells are evident.

(D) A fragment of an unmelanized microtumor shows high number of actively dividing cells. This is an exceptional piece of tissue; in most instances, the number of positive cells is lower, but clearly significant. (E, F) Small regions of tightly-packed cells are found in hematopoietic microtumors of *Ubc9* mutants; here such center exhibits high index of proliferating cells. Panel F shows a higher magnification of region indicated by the white square in E.

(G) Percent of mitotic cells was scored in *Ubc9*$^{-/-}$ and *Bc Ubc9*$^{4-3}$/+ *Ubc9*^{5} mutants (red squared bars) and their heterozygous siblings (blue bars). Data in the graph are represented as average ± SE.

Scale bars: 20 µm (A, B) and 50 µm (C-F). Images were acquired in Zeiss confocal microscope (A-F).

Figure 3

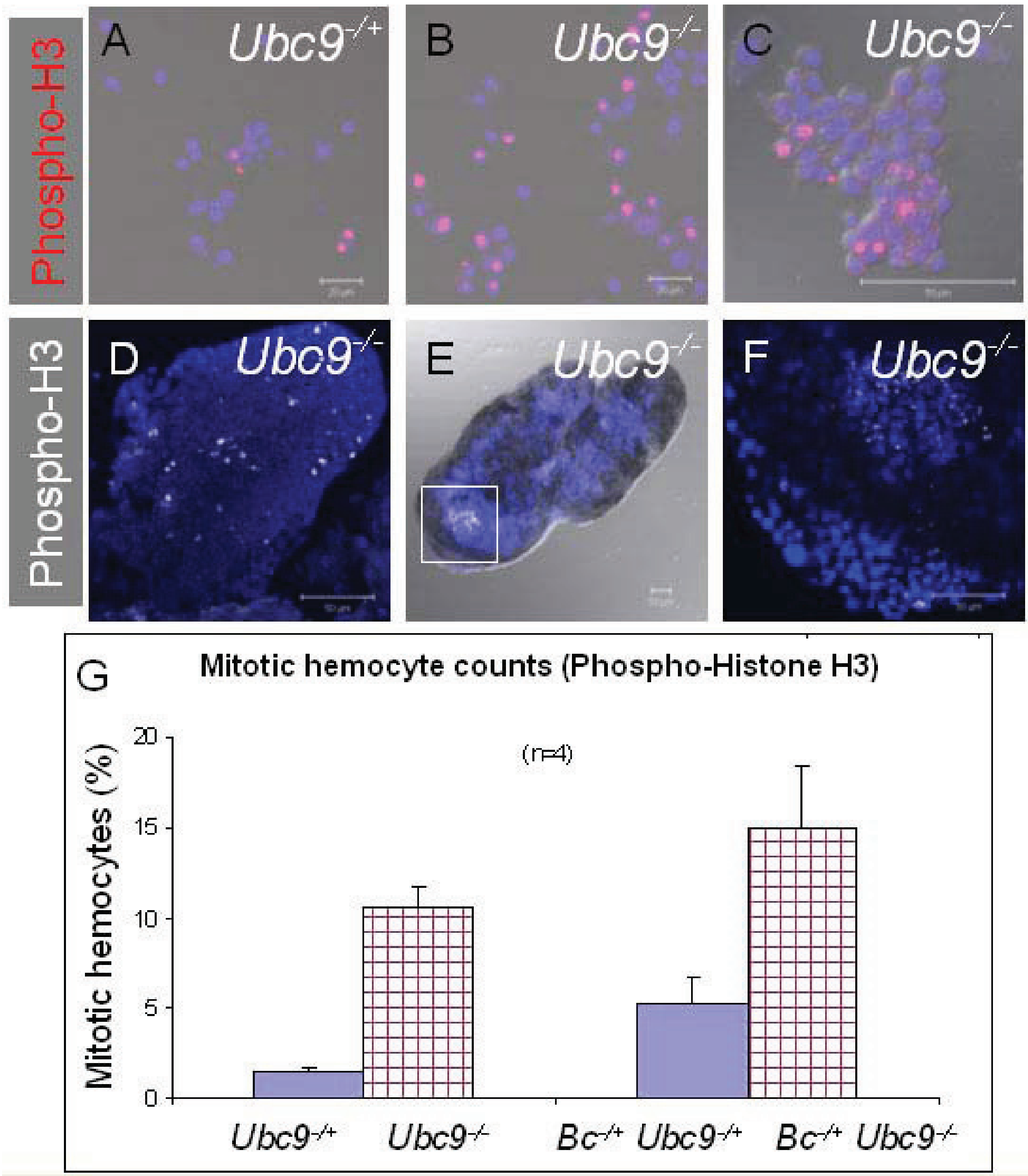
Phospho-H3
A
$Ubc9^{-/+}$
B
$Ubc9^{-/-}$
C
$Ubc9^{-/-}$
Phospho-H3
D
$Ubc9^{-/-}$
E
$Ubc9^{-/-}$
F
$Ubc9^{-/-}$
G
Mitotic hemocyte counts (Phospho-Histone H3)
Mitotic hemocytes (%)
(n=4)
20
15
10
5
0
$Ubc9^{-/+}$
$Ubc9^{-/-}$
$Bc^{-/+}$ $Ubc9^{-/+}$
$Bc^{-/+}$ $Ubc9^{-/-}$

Fig. 4. Loss of *Ubc9* affects centrosome number and morphology.

Circulating hemocytes from control and mutant larvae were stained with antibody against centrosomin (CNN), a component of centrosomes. Control hemocytes show presence of one (A, B) or two centrosomes per cell. *Ubc9* mutant hemocytes contain one, two (C, D), or three and more (E-H) centrosomes. Some of the single centrosomes in *Ubc9* mutant hemocytes appear abnormally large (I, J).

(K) Percentage of hemocytes containing all (first set of bars) and single (supranumerary), double (wt) and multiple (supernumerary) centrosomes in heterozygous *Ubc9*$^{-/+}$ (black bars) and mutant *Ubc9*$^{-/-}$ hemolymph (orange bars). Data represented as average ± SE. The differences were statistically significant (stars).

Panels A, C, E, G, I show centrosomin (red) and Hoechst (blue, nuclear) staining, while corresponding panels B, D, F, H, J show only the centrosomin staining for clarity. Images were acquired in Zeiss fluorescent microscope at 40 x (A-D) and 100 x magnification (E-J).

Figure 4

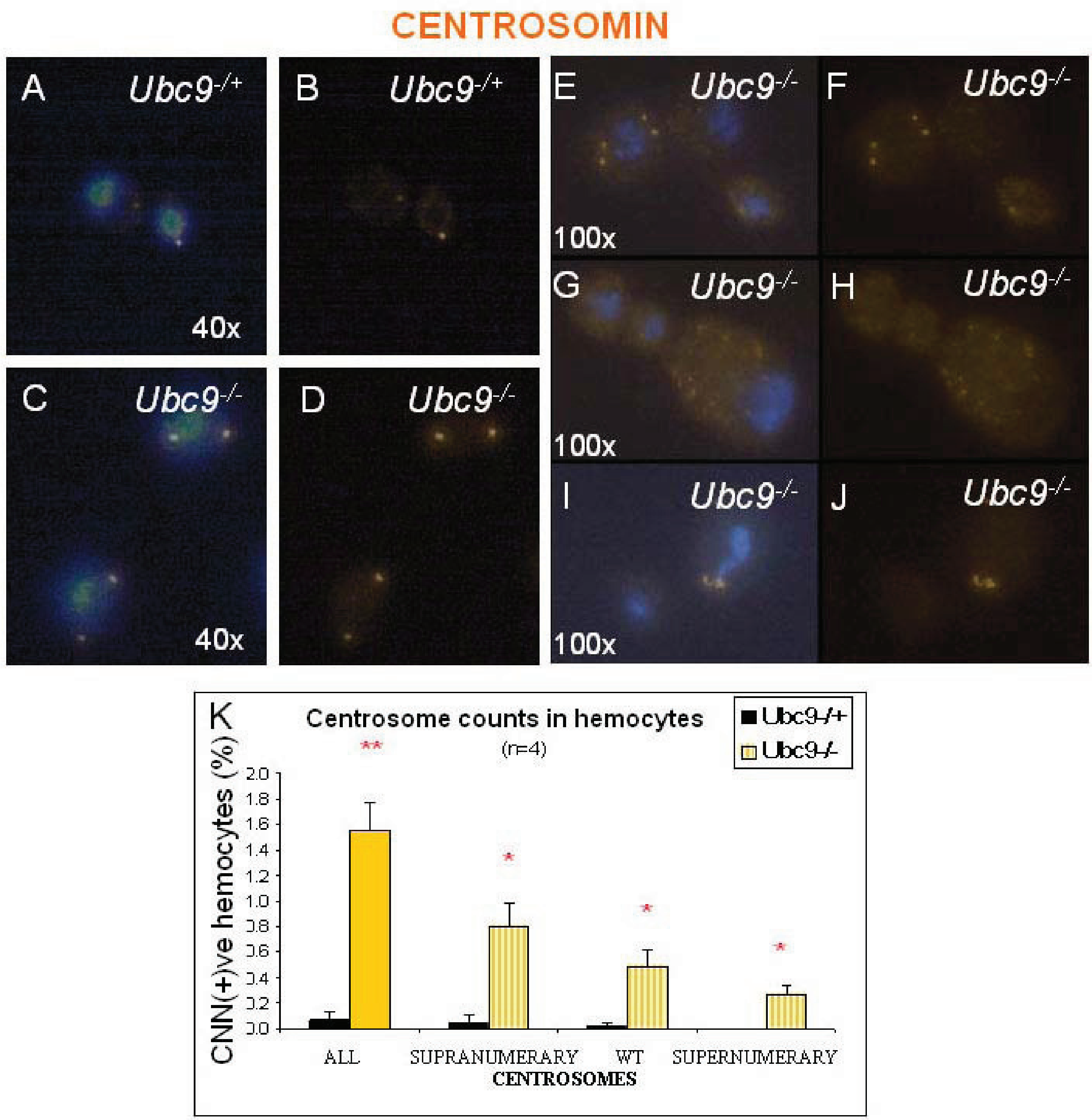
CENTROSOMIN
A Ubc9-/+
40x
B Ubc9-/+
C Ubc9-/-
40x
D Ubc9-/-
E Ubc9-/-
100x
F Ubc9-/-
G Ubc9-/-
100x
H Ubc9-/-
I Ubc9-/-
100x
J Ubc9-/-
K
Centrosome counts in hemocytes
(n=4)
Ubc9-/+
Ubc9-/-
CNN(+)ve hemocytes (%)
2.0
1.8
1.6
1.4
1.2
1.0
0.8
0.6
0.4
0.2
0.0
**
*
*
*
ALL
SUPRANUMERARY
WT
SUPERNUMERARY
CENTROSOMES

Fig. 5. *Bc* mutation affects the frequency of tumor classes in *Ubc9*$^{-/-}$ background.

(A-C) A comparison of size distribution of aggregates and microtumors dissected from *Ubc9*$^{-/-}$ (red data points) and *Bc Ubc9*$^{4\text{-}3}$/+ *Ubc9*^{5} (black data points) animals; unmelanized structures (A), partially melanized structures (B) and largely melanized structures (C).

(D) The overall ratio of the unmelanized aggregates (light blue areas) and partially melanized structures (red stripe areas) of *Ubc9*$^{-/-}$ animals are modified in *Bc Ubc9*$^{4\text{-}3}$/+ *Ubc9*^{5} mutants. The ratio of unmelanized and fully melanized microtumors (dark blue and black areas, respectively) is not affected.

Figure 5

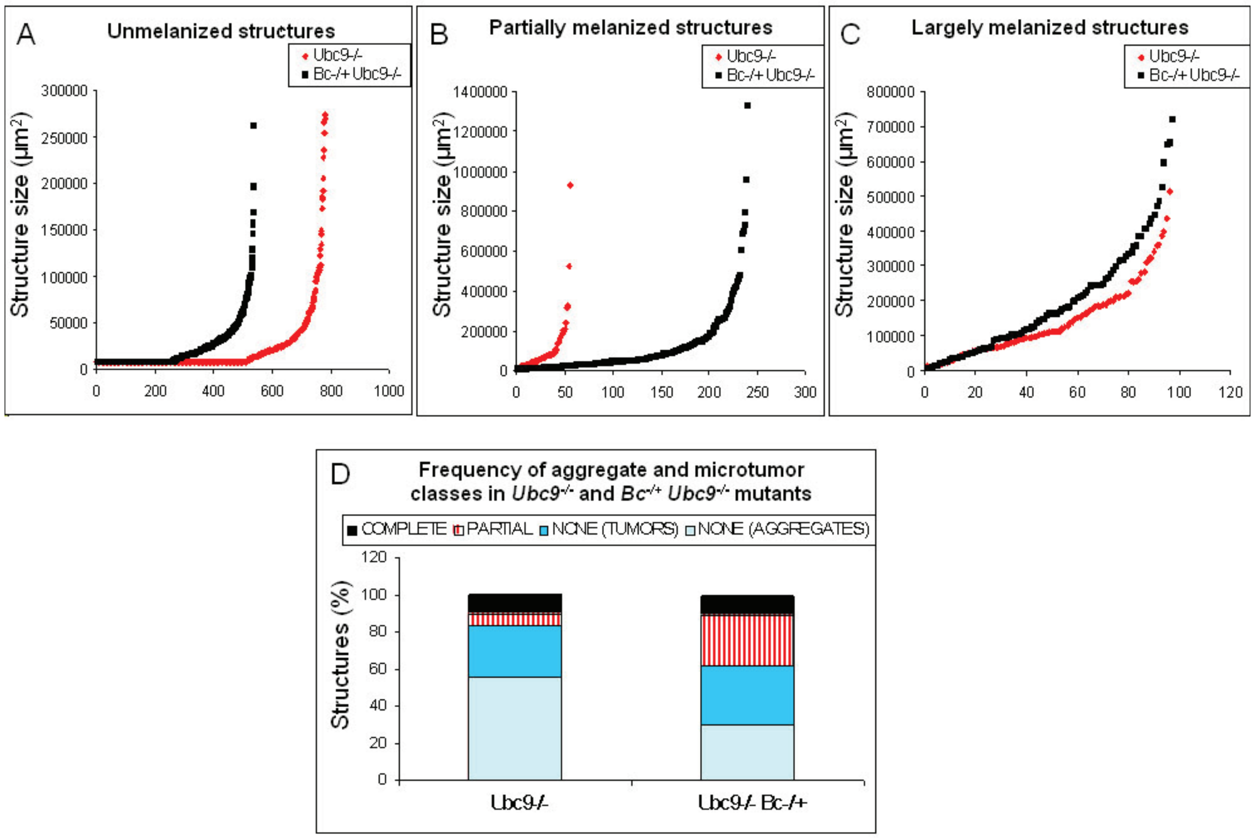
A
Unmelanized structures
Ubc9-/-
Bc-/+ Ubc9-/-
Structure size (µm2)
300000
250000
200000
150000
100000
50000
0
0
200
400
600
800
1000
B
Partially melanized structures
Ubc9-/-
Bc-/+ Ubc9-/-
Structure size (µm2)
1400000
1200000
1000000
800000
600000
400000
200000
0
0
50
100
150
200
250
300
C
Largely melanized structures
Ubc9-/-
Bc-/+ Ubc9-/-
Structure size (µm2)
800000
700000
600000
500000
400000
300000
200000
100000
0
0
20
40
60
80
100
120
D
Frequency of aggregate and microtumor classes in Ubc9-/- and Bc-/+ Ubc9-/- mutants
COMPLETE
PARTIAL
NONE (TUMORS)
NONE (AGGREGATES)
Structures (%)
120
100
80
60
40
20
0
Ubc9-/-
Ubc9-/- Bc-/+

Fig. 6. Cellular composition of *Ubc9$^{-/-}$* microtumors.

Hemocytes make up large proportion of *Ubc9$^{-/-}$* microtumors. (A) On occasion, the fat body (FB) tissue was found attached to or incorporated within the microtumor body. Notice larger nuclei of fat body cells relative to hemocyte nuclei. (B) Some of *Ubc9$^{-/-}$* microtumors contain morphologically distinct areas (arrows) where numerous small cells are tightly packed in a restricted area, which is occasionally associated with local melanization.

Tissue samples were stained with Hoechst to visualize nuclei (blue). Images were acquired in Zeiss confocal (A) and fluorescent (B) microscopes. Scale bars: 100 µm (A) and 50 µm (B).

Figure 6

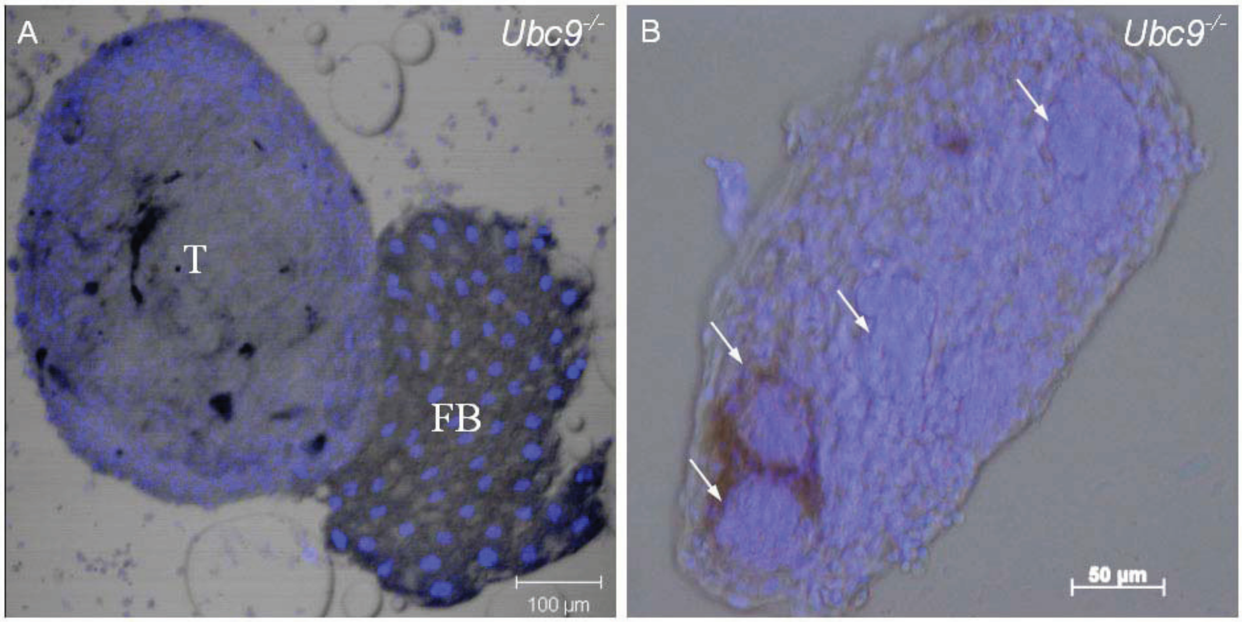

Fig. 7. High level of β-tubulin and Peanut expression differentiates microtumors from circulating hemocytes.

(A-C) Peanut (green) expression is enriched in *Ubc9*$^{-/-}$ circulating hemocytes only in cells which appear to be phagocytosed (A) or form clusters (B), and it is present at a high level in tumor cells. Specimens were counterstained with Phalloidin to visualize F-actin (red) and Hoechst for nuclei (blue).

(D-F) High β-tubulin (red) expression is characteristic of *Ubc9*$^{-/-}$ cells in circulation which closely interact with each other (D, E) and cells of the microtumor body (F). Specimens were counterstained with Phalloidin to visualize F-actin (green) and Hoechst for nuclei (blue).

Enriched expression of β-tubulin and Peanut is infrequent in controls (not shown).

Images were acquired in Zeiss confocal microscope. Scale bars: 10 μm (A-F).

Figure 7

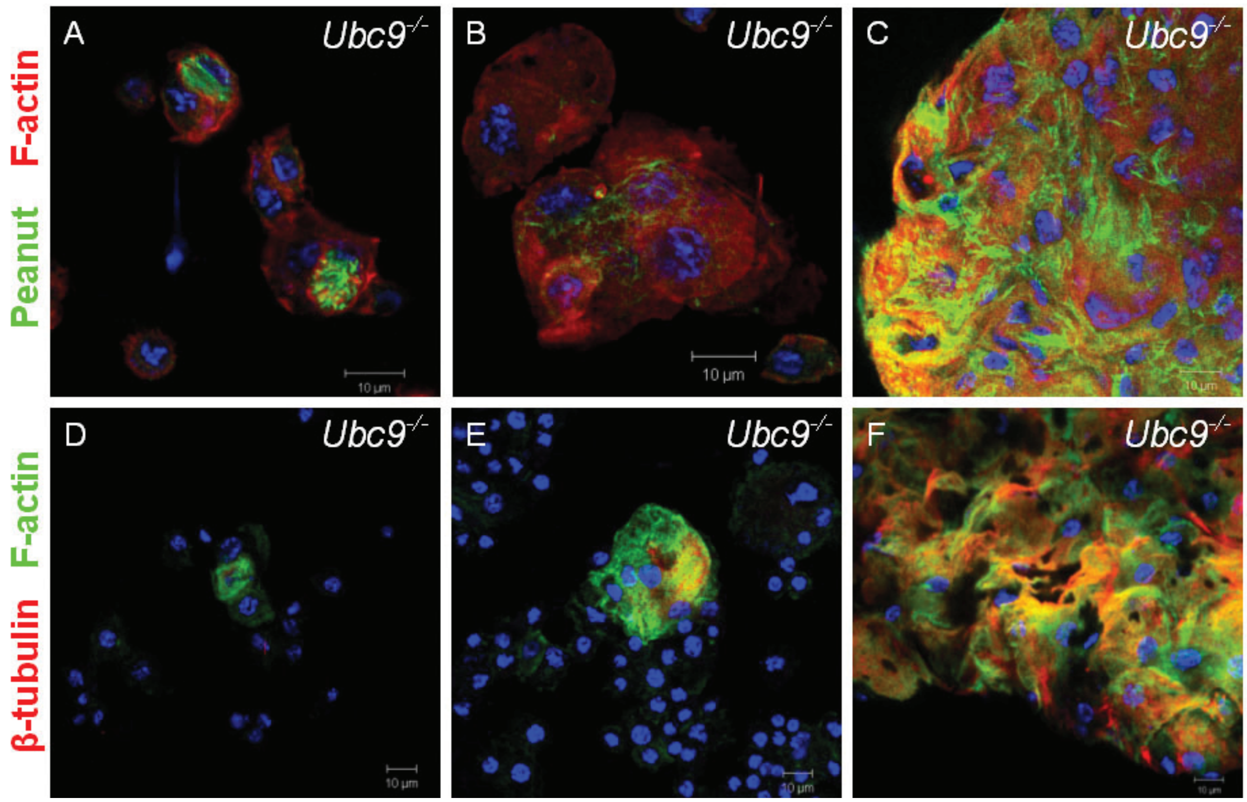

Fig. 8. Integrin expression in various hemocyte classes.

(A-F) Integrin β PS marks lamellocytes present among circulating hemocytes and microtumor cells of *Ubc9*$^{-/-}$ mutants.

(A) The lamellocyte marker MSNF 9 #83 expression (GFP, green) is abundant in the large *Ubc9*$^{-/-}$ microtumors (A) and smaller aggregates (B) and does not overlap with Nimrod C staining (red in B).

Circulating *Ubc9*$^{-/-}$ hemocytes which are positive for MSNF 9 #83 (green), often have active cytoskeleton as indicated by rich F-actin staining (red, panel C).

(D-F) *Ubc9*$^{-/-}$ lamellocytes present in circulation which are positive for MSNF 9 #83 (green) also express high levels of integrin β PS (red), when present in both, circulation (D) and microtumors (E, F). Panels F and F' show magnified region indicated by white rectangle in panel E. In panel F, the green channel (MSNF 9 #83 expression) was omitted for clarity of integrin β PS staining (red).

(G-I) Integrin α PS1 (green) marks cells of plasmatocyte and intermediate morphology, but not lamellocytes. *Ubc9*$^{-/-}$ mutant hemocytes of plasmatocyte morphology show high expression of integrin α PS1 in circulation (G) and in tumors (H, I). Panel I shows magnified region labeled with white frame in panel H. Cells of lamellocyte morphology (labeled with "L" in panel I) which show active cytoskeleton (F-actin, red) do not express integrin α PS1 (green), as opposed to elongated (arrow) or ruffled (arrowhead) cells of unknown identity.

All tissue samples were counterstained with Hoechst to visualize nuclei (blue).

Images were acquired in Zeiss confocal microscope. Scale bars: 50 μm (A, C, E, F, F', H, I), 20 μm (B) and 10 μm (D, G).

Figure 8

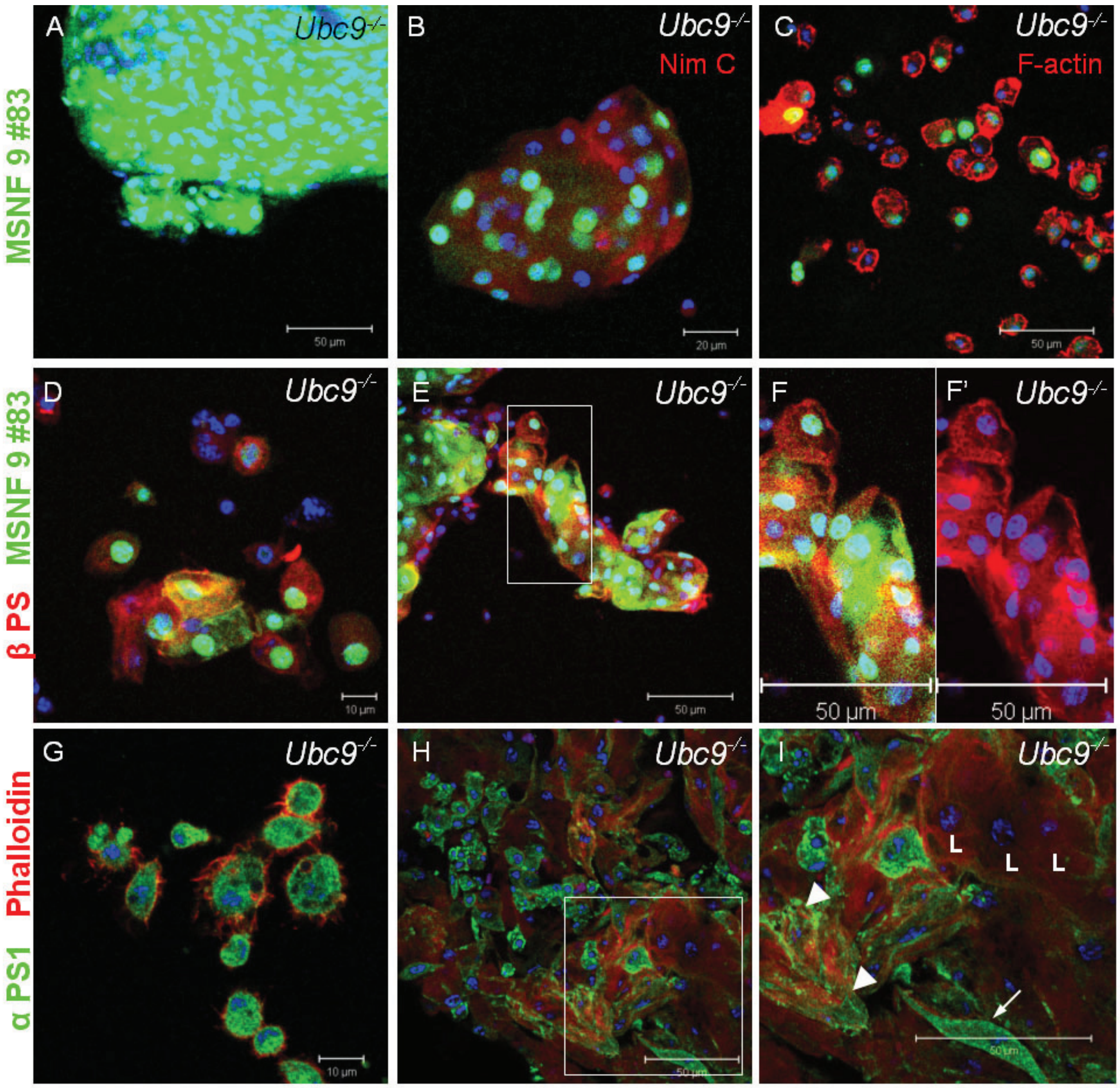
A
Ubc9-/-
B
Ubc9-/-
Nim C
C
Ubc9-/-
F-actin
MSNF 9 #83
50 µm
20 µm
50 µm
D
Ubc9-/-
E
Ubc9-/-
F
F'
Ubc9-/-
β PS MSNF 9 #83
10 µm
50 µm
50 µm
50 µm
G
Ubc9-/-
H
Ubc9-/-
I
Ubc9-/-
L
L
L
α PS1 Phalloidin
10 µm
50 µm
50 µm

REFERENCES

Almog, N. (2010). Molecular mechanisms underlying tumor dormancy. *Cancer Lett* 294, 139-146.

Almog, N., Ma, L., Raychowdhury, R., Schwager, C., Erber, R., Short, S., Hlatky, L., Vajkoczy, P., Huber, P. E., Folkman, J. et al. (2009). Transcriptional switch of dormant tumors to fast-growing angiogenic phenotype. *Cancer Res* 69, 836-844.

Brower, D. L. (2003). Platelets with wings: the maturation of Drosophila integrin biology. *Curr Opin Cell Biol* 15, 607-613.

Brower, D. L., Wilcox, M., Piovant, M., Smith, R. J. and Reger, L. A. (1984). Related cell-surface antigens expressed with positional specificity in Drosophila imaginal discs. *Proc Natl Acad Sci U S A* 81, 7485-7489.

Carmeliet, P. (2005). VEGF as a key mediator of angiogenesis in cancer. *Oncology* 69 Suppl 3, 4-10.

Cerveira, N., Santos, J. and Teixeira, M. R. (2009). Structural and expression changes of septins in myeloid neoplasia. *Crit Rev Oncog* 15, 91-115.

Chiu, H., Ring, B. C., Sorrentino, R. P., Kalamarz, M., Garza, D. and Govind, S. (2005). dUbc9 negatively regulates the Toll-NF-kappa B pathways in larval hematopoiesis and drosomycin activation in Drosophila. *Dev Biol* 288, 60-72.

Chu, D. T. and Klymkowsky, M. W. (1989). The appearance of acetylated alpha-tubulin during early development and cellular differentiation in Xenopus. *Dev Biol* 136, 104-117.

Cooper, J. A. and Kiehart, D. P. (1996). Septins may form a ubiquitous family of cytoskeletal filaments. *J Cell Biol* 134, 1345-1348.

Devenport, D. and Brown, N. H. (2004). Morphogenesis in the absence of integrins: mutation of both Drosophila beta subunits prevents midgut migration. *Development* 131, 5405-5415.

Evans, C. J., Hartenstein, V. and Banerjee, U. (2003). Thicker than blood: conserved mechanisms in Drosophila and vertebrate hematopoiesis. *Dev Cell* 5, 673-690.

Folkman, J., Merler, E., Abernathy, C. and Williams, G. (1971). Isolation of a tumor factor responsible for angiogenesis. *J Exp Med* 133, 275-288.

Gomez, M. and Cano, A. (1995). Expression of beta 1 integrin receptors in transformed mouse epidermal keratinocytes: upregulation of alpha 5 beta 1 in spindle carcinoma cells. *Mol Carcinog* 12, 153-165.

Heuer, J. G., Li, K. and Kaufman, T. C. (1995). The Drosophila homeotic target gene centrosomin (cnn) encodes a novel centrosomal protein with leucine zippers and maps to a genomic region required for midgut morphogenesis. *Development* 121, 3861-3876.

Huang, L. (2006). Functions and regulatory mechanisms of the Rel family transcription factors, Dorsal and Dif, and the Ubc9 family SUMO conjugase, lesswright, in Drosophila hematopoiesis. Ph. D. Dissertation College of Arts and Sciences of Ohio University.

Irving, P., Ubeda, J. M., Doucet, D., Troxler, L., Lagueux, M., Zachary, D., Hoffmann, J. A., Hetru, C. and Meister, M. (2005). New insights into Drosophila larval haemocyte functions through genome-wide analysis. *Cell Microbiol* 7, 335-350.

Jouhilahti, E. M., Peltonen, S. and Peltonen, J. (2008). Class III beta-tubulin is a component of the mitotic spindle in multiple cell types. *J Histochem Cytochem* 56, 1113-1119.

Jung, S. H., Evans, C. J., Uemura, C. and Banerjee, U. (2005). The Drosophila lymph gland as a developmental model of hematopoiesis. *Development* 132, 2521-2533.

Kanbe, T., Hiraoka, Y., Tanaka, K. and Yanagida, M. (1990). The transition of cells of the fission yeast beta-tubulin mutant nda3-311 as seen by freeze-substitution electron microscopy. Requirement of functional tubulin for spindle pole body duplication. *J Cell Sci* 96 (Pt 2), 275-282.

Katsetos, C. D., Legido, A., Perentes, E. and Mork, S. J. (2003). Class III beta-tubulin isotype: a key cytoskeletal protein at the crossroads of developmental neurobiology and tumor neuropathology. *J Child Neurol* 18, 851-866; discussion 867.

Kim, D. S., Hubbard, S. L., Peraud, A., Salhia, B., Sakai, K. and Rutka, J. T. (2004). Analysis of mammalian septin expression in human malignant brain tumors. *Neoplasia* 6, 168-178.

Kinoshita, M., Kumar, S., Mizoguchi, A., Ide, C., Kinoshita, A., Haraguchi, T., Hiraoka, Y. and Noda, M. (1997). Nedd5, a mammalian septin, is a novel cytoskeletal component interacting with actin-based structures. *Genes Dev* 11, 1535-1547.

Kurucz, E., Markus, R., Zsamboki, J., Folkl-Medzihradszky, K., Darula, Z., Vilmos, P., Udvardy, A., Krausz, I., Lukacsovich, T., Gateff, E. et al. (2007). Nimrod, a putative phagocytosis receptor with EGF repeats in Drosophila plasmatocytes. *Curr Biol* 17, 649-654.

Lanot, R., Zachary, D., Holder, F. and Meister, M. (2001). Postembryonic hematopoiesis in Drosophila. *Dev Biol* 230, 243-257.

Lemaitre, B. and Hoffmann, J. (2007). The host defense of Drosophila melanogaster. *Annu Rev Immunol* 25, 697-743.

Loweth, A. C. and Morgan, N. G. (1998). Methods for the study of NO-induced apoptosis in cultured cells. *Methods Mol Biol* 100, 311-320.

Lu, E. and Wolfe, J. (2001). Lysosomal enzymes in the macronucleus of Tetrahymena during its apoptosis-like degradation. *Cell Death Differ* 8, 289-297.

Meister, M. and Govind, S. (2003). Hematopoietic development in Drosophila: a parallel with vertebrates. In Hematopoietic Stem Cells (eds I. Godin and A. Cumano): Eurekah.com.

Minakhina, S. and Steward, R. (2006). Melanotic mutants in Drosophila: pathways and phenotypes. *Genetics* 174, 253-263.

Mizejewski, G. J. (1999). Role of integrins in cancer: survey of expression patterns. *Proc Soc Exp Biol Med* 222, 124-138.

Molofsky, A. V., Pardal, R. and Morrison, S. J. (2004). Diverse mechanisms regulate stem cell self-renewal. *Curr Opin Cell Biol* 16, 700-707.

Morrison, S. J. and Spradling, A. C. (2008). Stem cells and niches: mechanisms that promote stem cell maintenance throughout life. *Cell* 132, 598-611.

Mpoke, S. S. and Wolfe, J. (1997). Differential staining of apoptotic nuclei in living cells: application to macronuclear elimination in Tetrahymena. *J Histochem Cytochem* 45, 675-683.

Nam, H. J., Jang, I. H., Asano, T. and Lee, W. J. (2008). Involvement of pro-phenoloxidase 3 in lamellocyte-mediated spontaneous melanization in Drosophila. *Mol Cells* 26, 606-610.

Neufeld, T. P. and Rubin, G. M. (1994). The Drosophila peanut gene is required for cytokinesis and encodes a protein similar to yeast putative bud neck filament proteins. *Cell* 77, 371-379.

Qiu, P., Pan, P. C. and Govind, S. (1998). A role for the Drosophila Toll/Cactus pathway in larval hematopoiesis. *Development* 125, 1909-1920.

Ribatti, D. (2005). The crucial role of vascular permeability factor/vascular endothelial growth factor in angiogenesis: a historical review. *Br J Haematol* 128, 303-309.

Rizki, T. M., Rizki, R. M. and Grell, E. H. (1980). A Mutant Affecting the Crystal Cells in Drosophila melanogaster. *Wilhelm Roux's Archives* 188, 91-99.

Sakariassen, P. O., Prestegarden, L., Wang, J., Skaftnesmo, K. O., Mahesparan, R., Molthoff, C., Sminia, P., Sundlisaeter, E., Misra, A., Tysnes, B. B. et al. (2006). Angiogenesis-independent tumor growth mediated by stem-like cancer cells. *Proc Natl Acad Sci U S A* 103, 16466-16471.

Shi, C., Zhang, X., Chen, Z., Robinson, M. K. and Simon, D. I. (2001). Leukocyte integrin Mac-1 recruits toll/interleukin-1 receptor superfamily signaling intermediates to modulate NF-kappaB activity. *Circ Res* 89, 859-865.

Tokusumi, T., Sorrentino, R. P., Russell, M., Ferrarese, R., Govind, S. and Schulz, R. A. (2009). Characterization of a lamellocyte transcriptional enhancer located within the misshapen gene of Drosophila melanogaster. *PLoS One* 4, e6429.

Vajkoczy, P., Farhadi, M., Gaumann, A., Heidenreich, R., Erber, R., Wunder, A., Tonn, J. C., Menger, M. D. and Breier, G. (2002). Microtumor growth initiates angiogenic sprouting with simultaneous expression of VEGF, VEGF receptor-2, and angiopoietin-2. *J Clin Invest* 109, 777-785.

Vilmos, P., Nagy, I., Kurucz, E., Hultmark, D., Gateff, E. and Ando, I. (2004). A rapid rosetting method for separation of hemocyte sub-populations of Drosophila melanogaster. *Dev Comp Immunol* 28, 555-563.

Visvader, J. E. and Lindeman, G. J. (2008). Cancer stem cells in solid tumours: accumulating evidence and unresolved questions. *Nat Rev Cancer* 8, 755-768.

Wang, J. C. (2010). Good cells gone bad: the cellular origins of cancer. *Trends Mol Med* 16, 145-151.

Weaver, V. M., Lelievre, S., Lakins, J. N., Chrenek, M. A., Jones, J. C., Giancotti, F., Werb, Z. and Bissell, M. J. (2002). beta4 integrin-dependent formation of polarized three-dimensional architecture confers resistance to apoptosis in normal and malignant mammary epithelium. *Cancer Cell* 2, 205-216.

Weinberg, R. A. (2007). The Biology of Cancer. New York: Garland Science, Taylor and Francis Group, LLC.

Wiesner, S., Legate, K. R. and Fassler, R. (2005). Integrin-actin interactions. *Cell Mol Life Sci* 62, 1081-1099.

Wright, A. J. and Hunter, C. P. (2003). Mutations in a beta-tubulin disrupt spindle orientation and microtubule dynamics in the early Caenorhabditis elegans embryo. *Mol Biol Cell* 14, 4512-4525.

PART II

Sumoylation is tumor-suppressive and confers developmental quiescence to hematopoietic progenitors in *Drosophila* larvae

ABSTRACT

Blood cells of the *Drosophila* pupa and adult derive from the larval lymph gland. The gland has three sets of paired lobes. In third instar larvae, a small pool of stem/progenitor cells acquires quiescence. This cell state is in part achieved by a multicellular niche that is in contact with the dorsal vessel. Here we show that this stem/progenitor cell population is heterogeneous; cells express one or both, *Dome>GFP* and *ZCL2897* markers. Zygotic loss of *Ubc9* (the SUMO-conjugating E2 enzyme) leads to lymph gland hyperplasia, development of microtumors, developmental delay and larval death. We show that microtumors arise from the highly-mitotic mutant stem/progenitor cells that are *Dome>GFP*-negative, but *ZCL2897*-positive. Mutant phenotypes are rescued by specific $Ubc9^{wt}$ expression in progenitor cells, but not when $Ubc9^{wt}$ is provided in the niche. Whereas normal stem/progenitor cells express high levels of the *Drosophila* cyclin-dependent kinase inhibitor p21 homolog, Dacapo, the corresponding hyperplastic mutant population exhibits a marked reduction in Dacapo/p21 levels. Expression of human p21 in mutant stem/progenitor cells limits their expansion and rescues tumorogenesis. Akin to *Ubc9* mutants, removal of the SUMO E1 activating-enzyme subunits *Aos1/Uba2,* or the E3 SUMO ligase, *PIAS*, results in loss of stem/progenitor cell quiescence. Surprisingly, onset of cells release from the prepupal/pupal anterior lobes of wild type animals

correlates with decrease of *Dome>GFP* expression, similar to the premature decrease of this marker observed in *Ubc9* mutants. Our data suggest that sumoylation provides a cell-intrinsic mechanism to preserve stem/progenitor cell states for stress response, immunity and development of the fly.

INTRODUCTION

Tissue and organ regeneration in patients following normal loss of tissue integrity due to ageing or after lesions from disease or surgery is a primary challenge in biomedical research. Tissue engineering requires understanding how normal tissues originate, develop, renew themselves, maintain their proliferative quiescence and are kept from overgrowing. One mechanism by which tissues and organs maintain their integrity over time is through the functions of stem cells (Morrison and Spradling, 2008). A characteristic property of stem cells, as compared to their more differentiated progenitors, is that of infrequent division, often referred to as 'proliferative quiescence'. Loss of proliferative quiescence in pre-malignant cells frequently accompanies the development of cancer. Mammalian cancers are composed of heterogeneous cell populations that include few stem (or stem-like) cells with abundant capacity for self-renewal and the many more differentiated cells with limited proliferative potential (Morrison and Spradling, 2008; Wang, 2010). The growth and development of a tumor depends on the complex interplay of both the intrinsic (genetic and epigenetic) cell states as well as on the tumor microenvironment. Many tumors are further characterized by dormancy or metastasis, and the nature of these processes in relation to their origin remains largely unclear (Morrison and Spradling, 2008; Wang, 2010).

In this study, we used the *Drosophila* model to analyze the origin of hematopoietic microtumors in larvae that result from loss of *Ubc9* function. Along with the SUMO activating E1 enzymes, Aos1 and Uba2, and the SUMO E3 ligase, PIAS, the SUMO-conjugating enzyme, Ubc9 participates in a protein modification system that is conserved from yeast to humans (Talamillo et al., 2008). Relative to wild type, *Ubc*9 mutant third instar larvae exhibit anomalous heterochrony (here referring to differential timing in development of lymph gland lobes); they are developmentally delayed, and most die without entering pupal stage. Mutants develop an array of hematopoietic formations which can be classified as microtumors, as the largest of these reach sizes below 1 mm^3 in volume. Most of these structures float freely in the hemolymph (Chiu et al., 2005; Huang et al., 2005). The precise origin of these microtumors is not known.

Blood cells or hemocytes in normal *Drosophila* larvae can be found in three compartments: hemocytes circulate in hemolymph, or remain localized under the cuticle as sessile cells, or within the hematopoietic organ called lymph gland. The predominant (>95%) cell type of the larval hemolymph is the plasmatocyte. These cells express Nimrod C (Vilmos et al., 2004; Kurucz et al., 2007a) and phagocytose microbes and dead cells. The remaining lineages are crystal cells and lamellocytes, both of which express pro-phenol oxidase and facilitate melanization reactions (Kurucz et al., 2007a; Nam et al., 2008). A very small fraction of undifferentiated cells is also present in the hemolymph (Holz et al., 2003).

Hemocytes in all three compartments are summoned when the fly larva is infected by parasitic wasps. Parasitization induces differentiation of numerous flat adhesive lamellocytes, which, along with plasmatocytes and crystal cells, encapsulate the wasp egg. Parasitization also induces lamellocyte differentiation within the lymph gland lobes. The basement membrane of the anterior lobes is disrupted and the peripheral cells of the lobes disperse (Sorrentino et al., 2002; Krzemien et al., 2007). Not surprisingly, mutations in immune pathways affect hemocyte number and differentiation (Rizki and Rizki, 1980; Rizki and Rizki, 1992; Qiu et al., 1998; Chiu et al., 2001; Sorrentino et al., 2002; Crozatier et al., 2004). Lamellocytes express high levels of Atilla (Vilmos et al., 2004; Kurucz et al., 2007a) and may account for up to 15 % of all circulating hemocytes in parasitized animals (Rizki and Rizki, 1992).

Lymph gland is the hematopoietic organ of *Drosophila* larva. The primordium for lymph gland is established during embryogenesis (Mandal et al., 2004). The lymph gland continues to develop through the early larval instars and undergoes significant changes upon metamorphosis (Lanot et al., 2001; Holz et al., 2003). The lobes of the larval lymph gland are arranged bilaterally and flank the dorsal vessel in the anterior body segments. The dorsal vessel is a simple aorta or heart tube, which runs along the dorsal midline and constitutes the open circulatory system of the animal (Shrestha and Gateff, 1982; Lanot et al., 2001; Jung et al., 2005); (Fig. 1 A, B, D).

Post-embryonic lymph gland development is heterochronic and lobe development is synchronous with the larval molts. The second instar larval lymph gland has two pairs of small posterior lobes, and a pair of larger anterior lobes. By the late third instar, the lymph gland grows significantly in size, although, the arrangement of the lobes and pericardial cells remains unchanged (Shrestha and Gateff, 1982; Lanot et al., 2001; Sorrentino et al., 2002; Jung et al., 2005). Cells of the anterior pair of lobes continue to divide frequently until the third instar stage, while all posterior lobes remain relatively small.

Lymph gland lobes harbor hematopoietic precursors. The division and differentiation of some of these is prompted by parasitic wasp infection (Shrestha and Gateff, 1982; Lanot et al., 2001; Jung et al., 2005). Precursors from the lobes also differentiate and are released into the hemolymph upon metamorphosis. Thus, the larval structure is also the source of hemocytes of the adult fly (Lanot et al., 2001; Holz et al., 2003).

Cellular morphologies and differentiation markers reveal the existence of three zones within anterior lobes. The cortical zone contains mature hemocytes while the progenitors or stem cells occupy the medullary zone. Cells of the cortical zone show expression of several genes, among others, *Hemolectin* (*Hml*) or *Collagen* (*Cg*), Nimrod C or Pro-phenol oxidase (Jung et al., 2005; Kurucz et al., 2007b). Medullary zone cells express such markers as Dome-Gal4, an indicator of promoter activity for *Domeless* gene, the receptor of JAK/STAT pathway, or ZCL2897 (P element, GFP trap in an uncharacterized gene) (Morin et al., 2001; Jung et al., 2005; Krzemien et al., 2007). Both cell populations divide actively until the third instar, when cells of the medullary zone become proliferatively quiescent (Jung et al., 2005; Mandal et al., 2007; Talamillo et al., 2008). The cell states in both medullary and cortical zones are controlled by cells of the niche (Crozatier et al., 2004; Jung et al., 2005; Krzemien et al., 2007; Mandal et al., 2007).

The exact nature of the cells in the medullary zone is not entirely clear. The earliest studies refer to the least differentiated precursors as prohemocytes, or progenitors of hemocytes (Shrestha and Gateff, 1982; Lanot et al., 2001; Jung et al., 2005), while more recent studies label cells in the medullary zone as stem-like hematopoietic precursors (Sinenko et al., 2009), or indicate the presence of stem cells (Minakhina and Steward, 2010). We refer to this population as hematopoietic progenitors.

We show that the posterior lymph gland lobes of *Ubc9* mutants are hyperplastic. The mutant hemolymph has an overabundance of normal and aberrant hemocytes, and some of these occur in groups, referred here as aggregates. The hematopoietic defects are strongly suppressed in the absence of the Rel/NF-kappaB-family transcription factors Dorsal and Dif, or in the presence of a non-signaling allele of Cactus, the I-kappaB protein in *Drosophila* (Chiu et al., 2005; Huang et al., 2005)

Ubc9 also regulates the arm of innate immunity mediated by anti-microbial peptides in the larval fat body, where it serves to keep Toll-dependent immune response in check. Whereas in wild type larvae wasp infection activates the Toll pathway and *drosomycin* (*drs*) expression, *drs* is constitutively expressed in *Ubc9* mutants in the absence of wasp infection (Chiu et al., 2005). Ubc9 is essential for the stability of Cactus protein and together these proteins confer immune homeostasis that is essential for resolution of the encapsulation response of the wasp egg ((Paddibhatla et al., 2010), in revision). While expression of wild type Ubc9 in the fat body and plasmatocytes restores the regulation of *drs* expression in the mutant fat body, hematopoietic defects and tumorogenesis persist (Chiu et al., 2005), suggesting that microtumors do not arise from freely-circulating plasmatocytes.

Tumors in *Drosophila* may affect various tissues (Minakhina and Steward, 2006). The goal of this study was to define the precise origin of *Ubc9* microtumors. We report that *Ubc9* microtumors are derived specifically from a heterogeneous lymph gland progenitor population in the medullary zone, that otherwise becomes quiescent in third instar larvae. This overgrowth of immature cells in all lymph gland lobes is independent of the niche. In genetic experiments, we functionally link all sumoylation cascade components to cells of this progenitor population. Our data suggest that proliferative quiescence is instilled by the *Drosophila* cyclin-dependent kinase inhibitor Dacapo, a functional homolog of mammalian p21. Based on our analysis of the organ in pre-pupal and pupal stages, we propose that proliferative quiescence in hematopoietic progenitors is developmentally regulated and sumoylation is a key player in maintaining this cell state. Loss of cell cycle control and heterochrony yields solid microtumors.

Drosophila has served as an excellent model system for cancer research (Watson et al., 1994; Vidal and Cagan, 2006). Because of its simple organization and genetic accessibility, the fruit fly continues to facilitate discoveries pertinent to cancer biology. Our studies broaden the understanding of the links between normal cell cycle control mechanisms in tissue maintenance and disease development *in vivo*. The system offers opportunities to dissect the contributions of epigenetic and biochemical mechanisms to the growth and development of microtumors.

MATERIAL AND METHODS

Fly strains and culture

Strains: *y w; Ubc9$^{4\text{-}3}$ FRT40A/ CyO y^{+}* and *y w; Ubc9^{5} FRT40A/ CyO y^{+}* (obtained from Dr. S. Tanda, described in (Chiu et al., 2005)). *Ubc9* is maternally expressed (Ohsako and Takamatsu, 1999). However, larval functions rely on zygotic transcription and hematopoietic larval defects arise due to lowered *Ubc9* function. *w^{1118}; PBac[w^{+mC}=PB]Aos1^{c06048}/TM6B, Tb^{1}* (line 17744) and *y w; Smt3^{K06307}/CyO GFP* (line 10419) stocks were obtained from *Drosophila* Bloomington Stock Center. *PIAS* alleles *Su(var)2-10^{1}/CyO GFP* and *Su(var)2-10^{2}/CyO GFP* were obtained from Dr. G. Karpen (Hari et al., 2001).

The following UAS lines were used: RNAi lines for *Su(var)2-10* and *Aos1* (Vienna Stock Center), RNAi for *Uba2* (TRiP, Harvard Medical School); *UAS-lwr^{wt}* (obtained from Dr. S. Tanda, (Apionishev et al., 2001)), *UAS-p21* (de Nooij and Hariharan, 1995), *UAS-mCD8-GFP* (Bloomington, line 5137), *UAS-DsRed* (Bloomington, line 6280). *ZCL2897* was obtained from Yale GFP Protein Trap Collection (Morin et al., 2001); expression in hematopoietic tissue described in (Jung et al., 2005).

The following Gal4 lines were used: *Domeless-Gal4* obtained from Dr. M. Crozatier (Bourbon et al., 2002); described in (Ghiglione et al., 2002). In addition to cells of the medullary zone, *Dome>GFP* is highly expressed in the prothoracic cells of the ring gland (our unpublished observations). *Antennapedia-Gal4* received through Dr. S. Minakhina (from Dr. Cohen, S.M.; (Emerald and Cohen, 2004)), *HemolectinΔ-Gal4* (Sinenko and Mathey-Prevot, 2004), *Collagen-Gal4* (Bloomington Stock Center, line 7011; (Asha et al., 2003), *Hemese-Gal4* (obtained from Dr. I. Ando; (Zettervall et al., 2004), *Serpent-*

Gal4 (Bruckner et al., 2004) and *76B-Gal4* (Harrison et al., 1995). The *ZCL2897* and *Gal4* transgenes (*Dome*, *Antp*, *Hml*, *Cg*, *Hemese*, *Srp*, *76B*) were integrated into specific mutant backgrounds by standard genetic crosses. *ZCL2897* and *Dome>myr-mRFP* combination was lethal in the *Ubc9* background. The *Gal4* expression, or *Gal4*-driven fluorescent protein expression (e.g. *Dome*>GFP) in cells and tissues reflects transcriptional activity of the promoter (or its fragment) of a given gene, while *ZCL2897* is a protein trap line, where GFP is expressed as part of the protein encoded by this gene. All *Drosophila* cultures and crosses were maintained at standard culture conditions. Six to twelve hour egglays were cultured at 23.5 °C, until animals developed to specific larval stage. To minimize effects of unrelated mutations, heteroallelic combinations of $Ubc9^{4\text{-}3}/Ubc9^{5}$ and $Su(var)2\text{-}10^{1}/Su(var)2\text{-}10^{2}$ were studied. Heterozygotes served as controls. Comparison of mutant and heterozygote was done on the same day, where available. At day 8 some of the *Ubc9* mutants remain in their larval L3, while heterozygous animals pupate at day 6.

Rescue experiments

The rescue experiments were performed using the Gal4/UAS system (Brand and Perrimon, 1993). To obtain the class of animals with the rescuing transgene, males *y w UAS-*$Ubc9^{wt}$*/Y;* $Ubc9^{5}$*, UAS-mCD8-GFP/CyO* y^{+} and females *y w Dome-Gal4/FM7c;* $Ubc9^{4\text{-}3}$*/CyO* y^{+} were crossed. To obtain animals of mutant and heterozygous genotype, the following parents were crossed: males *y w/Y;* $Ubc9^{5}$*, UAS-mCD8-GFP/CyO* y^{+} and females *y w Dome-Gal4/FM7c;* $Ubc9^{4\text{-}3}$*/CyO* y^{+}. The F1 classes (heterozygote *Dome-Gal4/y w;* $Ubc9^{5}$*, UAS-mCD8-GFP/CyO* y^{+}, mutant *Dome-Gal4/y w;* $Ubc9^{5}$*, UAS-*

mCD8-GFP/Ubc9$^{4-3}$, rescue *Dome-Gal4/y w UAS-Ubc9^{wt}; Ubc9^{5}, UAS-mCD8-GFP/Ubc9$^{4-3}$*) were simultaneously scored for the expression of the *Dome* promoter, differentiation of the anterior lobes (Atilla/L1 or PPO2/Pro-phenol oxidase 2 staining), microtumor penetrance (6 and 7-day old larvae), time of pupariation, and adult viability. Tumor penetrance in larvae was scored after dissection (at a magnification of 200 x), and in adults, it was scored through the cuticle in a dissecting microscope.

For rescue with the *Antp-Gal4*, F1 progeny of the following two crosses were observed: (1) females *y w UAS-Ubc9^{wt}; Ubc9^{5}, UAS-mCD8-GFP/CyO y^{+}* and males *y w/Y; Ubc9$^{4-3}$/CyO y^{+}; Antp-Gal4/TM6B* and (2) females *y w; Ubc9^{5}, UAS-mCD8-GFP/CyO y^{+}* and males *y w/Y; Ubc9$^{4-3}$/CyO y^{+}; Antp-Gal4/TM6B*. The number of niche cells (GFP), presence of membranous projections, tumor penetrance, differentiation of anterior lobes (Phalloidin staining) and posterior lobe overgrowth, pupariation and adult eclosure were scored.

For rescue with the *Collier driver (Col-Gal4)*, the F1 progeny of the following crosses were observed: (1) males *y w UAS-Ubc9^{wt}/Y; Ubc9^{5}/CyO y^{+}* and females *y w/y w; Ubc9$^{4-3}$, Col-Gal4/CyO y^{+}* and (2) females *y w UAS-Ubc9^{wt}/y w UAS-Ubc9^{wt}; Ubc9^{5}/CyO y^{+}* and males *y w/Y; Ubc9$^{4-3}$, Col-Gal4/CyO y^{+}* and (3) females *y w/y w; Ubc9^{5}/CyO y^{+}* and males *y w/Y; Ubc9$^{4-3}$, Col-Gal4/CyO y^{+}*. Tumor penetrance and adult eclosure were scored.

The rescue experiments involving p21 were designed in a similar way as above; flies carrying *UAS-p21* in the *Ubc9* mutant background (*y w, UAS-p21; Ubc9^{5}, UAS-mCD8-GFP/CyO y^{+}*) were crossed to those carrying respective *Gal4* (*Dome*, *76B*, *Hemolectin*, *Collagen*, *Hemese* and *Serpent*) in the background of *y w; Ubc9*$^{4\text{-}3}$*/CyO y*$^{+}$ and F1 larvae were utilized.

Experiments were performed in duplicate or triplicate. Data analysis and graphic representation were prepared in MS Excel 2002.

Immunohistochemistry

Tissue preparation: Developmentally-synchronized larvae from six- or twenty-four hour egglays were collected at indicated day of development (four to seven days), washed with PBS, distilled water and alcohol and bled on glass slides. Lymph glands were dissected in PBS. Air-dried specimens were fixed with freshly prepared solution of 4 % paraformaldehyde in PBS.

Immunolabeling: Standard antibody staining protocol was used for all antigens. Tissue samples were permeabilized with 0.5 % Triton-X solution prepared in PBS, and blocked in 3 % bovine serum albumine in PBS with Triton-X. Incubations with primary and secondary antibodies were performed overnight at 4 ˚C, or for two to five hours at room temperature, depending on antigen. Blood smears and lymph glands stained with only the secondary antibody served as negative controls.

Antibodies against following antigens were used: rabbit anti-phospho-histone H3 (1:200, Molecular Probes), mouse anti-P1/Nimrod C1 and mouse anti-L1/Atilla (1:10, (Vilmos et al., 2004; Kurucz et al., 2007a)), rabbit anti-PPO2/Pro-phenoloxidase 2 (1:2000, George Christophides) rabbit anti-SUMO (1:1000, received from Dr. A. Courey (Smith et al., 2004)). Fluorescently-labeled secondary antibodies were obtained from Molecular Probes and Jackson Immunological and used according to manufacturer specifications.

Counterstaining was performed with fluorescently labeled phalloidin (Invitrogen) and nuclear dye Hoechst 33258 (Molecular Probes).

Image acquisition: Images were acquired in a Zeiss Laser Scanning Confocal Microscope and Zeiss Fluorescent Microscope, and formatted in Zeiss LSM5 and AxioVision LE 4.5 software, respectively. Figures were assembled in Adobe Photoshop CS5.

RESULTS

Loss of Ubc9 affects lobes size and Dome>GFP expression in third instar lymph gland

Post-embryonic lymph gland development is heterochronic. By the first instar, anterior lobes form compact structures and acquire zonation (Jung et al., 2005). From the onset of the third instar, the posterior lobes of wild type lymph glands expand and coalesce with one another so that the initially distinct multiple strips form only two pairs of posterior lobes. The growth of these posterior groups of lobes is synchronized developmentally in that the first set develops and expands earlier than the second set (Fig. 1 B and D, Fig. 2 A and C). We call them posterior lobes, set 1 (PL1), and posterior lobes, set 2 (PL2) (Fig. 1A). The *Dome-Gal4* is expressed in the medullary zone cells (Jung et al., 2005; Krzemien et al., 2007). Like in the medullary zone of the anterior lobes, majority of cells in the posterior lobes do not express mature hemocyte markers, but some cells express *Dome>GFP* (Fig. 1B, D). *Domeless* encodes the receptor for JAK-STAT signaling (Brown et al., 2001); here, it is used as a marker and a driver for the expression of proteins in the medullary zone (see rescue experiments).

A comparison of the expression patterns and relative sizes of lobes from heterozygous and *Ubc9* lymph glands revealed no significant difference in late second or even early third instar (day four after egg lay) animals. All glands of both genotypes are *Dome>GFP*-positive in medullary zone of anterior lobes and very few cells of first posterior lobes (Fig. 1 B, C and data not shown). Only half (n = 5 out of 10) of the glands of either genotype express *Hml>GFP* in anterior lobes (Fig. 2 A, B). Few cells in the posterior lobes of some (roughly one-fifth, n = 2 out of 10) mutant but not heterozygous animals express *Hml>GFP* (Fig. 2 B). We did not observe a clear difference between lobe sizes until day 5 suggesting that *Ubc9* zygotic functions in hematopoiesis are essential during and past the mid third instar stage.

At mid- to late third instar (day five to six), all heterozygous anterior lobes remain relatively small and structurally intact, while anterior lobes of the mutant glands are either larger than control, or they disperse. Posterior lobes of mutants expand dramatically, but remain largely intact (Fig. 1 D, E, Fig. 2 C, D, Fig. 4 A-D). The expression of *Dome>GFP* in heterozygous lymph glands remains high, while it is virtually absent in mutant glands (Fig. 1 D, E). *Dome>GFP* expression is undetectable in circulating hemocytes of both controls and mutants. Single *Dome>GFP* cells are extremely rare in circulation or within microtumors (Fig. 3 A-D). Surprisingly, while *Dome>GFP* is expressed at a low level in the dorsal vessel of control animals, it is upregulated after anterior lobe dispersal in the mutant background (marked with a star in Fig. 1 D, E, and Fig. 5 B, C). These results suggest that a primary hematopoietic effect of *Ubc9* loss is on the cells of the medullary zone, but Ubc9 also appears to regulate gene expression in the dorsal vessel.

The expression of *Hml>GFP* is limited largely to the periphery in all control anterior lobes and in approximately 10 % (n = 1 out of 8) of the first set of posterior lobes (Fig. 2 C). In all mutant anterior lobes and some (nearly 40 %, n = 3 out of 8) of first posterior lobes, *Hml>GFP* cells are scattered throughout the body of the lobe (Fig. 2 D). The expanded posterior lobes of mutant glands contain more *Hml>GFP*-expressing cells than the control posterior lobes (Fig. 2 C). The fact that *Dome>GFP* and *Hml>GFP* transgenes are expressed in the first posterior lobes of control glands supports the notion that these lobes also acquire zonation, although this capacity is attained progressively in development only after the anterior lobes have matured. Second, specific changes in gene expression patterns of third instar glands correlate with overgrowth of mutant lobes.

The medullary zone exhibits heterogeneity

To understand the effects of the *Ubc9* mutation on cells of the medullary zone, we examined simultaneous expression of *Dome>DsRed* with *ZCL2897* (GFP) in wild type glands. *ZCL2897* is expressed in the subset of cells of the medullary zone (Fig. 1 J). Despite substantial overlap of the two markers, *Dome>DsRed* and *ZCL2897*, there is surprisingly significant heterogeneity in gene expression (Fig. 1 F-I). At least four cell types are observed: those that express both markers (*Dome*^{hi} *ZCL2897*^{hi}, Fig. 1 F, G - cells with yellow hue), those that are positive for just one marker (*Dome*^{hi} *ZCL2897*^{lo}, red cells, or *Dome*^{lo} *ZCL2897*^{hi} green cells, Fig. 1 F, G), or those that express neither. Among the doubly-positive cells, there is no apparent correlation in signal intensity of the two markers, suggesting that the medullary zone population consists of distinct cell types.

We next monitored *ZCL2897* expression in heterozygous and *Ubc9* mutant third instar animals and found that, in contrast to *Dome>GFP*, loss of *Ubc9* strongly enhances *ZCL2897* expression in anterior and posterior lymph gland lobes (Fig. 1 J-M). Unlike *Dome>GFP*, very high expression of *ZCL2897* is also found in mutant circulating hemocytes and microtumors (Fig. 3 E-H). Together, our data suggest that *Ubc9* has a differential effect on gene expression in the heterogeneous progenitor population. Furthermore, increase in the number of cells expressing *ZCL2897* suggests that *Ubc9* restrains division and differentiation of hematopoietic progenitors.

Ubc9⁻ microtumors arise from progenitor hyperplasia of anterior and posterior lobes

To directly confirm that *Ubc9* primary effect is through the regulation of cell proliferation, we stained lymph glands for phospho-histone H3 (Fig. 4 A-H). By late third instar stage (day 6.5-7), mutant lymph glands have numerous mitotically active cells. The first and second posterior lobes are consistently more severely affected (Fig. 4 A-D); cells of second posterior lobes become progressively more mitotic in days seven and eight.

To define the location of the dividing cells and to clarify their identity, we stained *Dome>GFP* lymph glands and visualized differentiated plasmatocytes (anti-Nim C antibody) or lamellocytes (anti-Atilla antibody) along with phospho-histone H3. *Ubc9* lymph glands have very few crystal cells (Chiu et al., 2005) and therefore were not examined. First, most of the *Dome>GFP* cells in control glands are phospho-histone H3-negative, confirming proliferative quiescence of this cell population. The phospho-histone H3-positive cells are mostly observed outside the medullary zone (Fig. 4 E, G, arrowheads). Second, the mitosis and Nim C markers rarely colocalized in cells of either genotype (Fig. 4 E, F, arrow). None of the lamellocytes were in division (Fig. 4 G, H).

In six days old (late L3) wild type glands, posterior lobes remain relatively small (Fig. 1 D, K, Fig. 4 B, schematic in Fig. 5A) and disperse only after the onset of pupariation (day six to seven; see also Fig. 16. A-P), while in six to seven days old mutant lymph glands, posterior lobes grow significantly (Fig. 1 E, M and Fig. 2 D). Mutant cells at the periphery of the entire anterior and part of first posterior lobes often disperse, whereas the remaining posterior lobes grow but remain intact (Fig. 1 E and Fig. 2 D) and become strongly *ZCL2897*-positive (Fig. 1 M). Taken together, these results suggest that the largest solid *Ubc9* microtumors are directly derived from the overgrown posterior lobes.

Ubc9 function is essential in hematopoietic progenitors

Our previous results indicate that microtumors could not be rescued with *Collagen>Ubc9*^{wt} (Chiu et al., 2005). *Cg-Gal4* driver is expressed in cortical zone and circulating hemocytes (Asha et al., 2003). This observation is consistent with the interpretation that *Ubc9* primary effect is on progenitors localized within the medullary zone and posterior lobes. To test this idea, we provided wild type *Ubc9* to the affected mutant populations (*Dome>Ubc9*^{wt}; see Methods). *Dome>Ubc9*^{wt} animals of the experimental rescue class exhibit remarkable amelioration from the effects of the mutation. The normal temporal and spatial regulation of the *Dome* promoter is restored almost fully within the anterior and posterior lobes and dorsal vessel cells (Fig. 5 B-D). The size of the rescued posterior lobes is comparable to control posterior lobes. Even though the cortical zone of the rescue class glands shows differentiating lamellocytes (stained for Atilla antigen, data not shown), the overall proportions of the medullary and cortical zones return to normal.

Furthermore, the decrease in crystal cell number, visualized with antibody against Pro-phenol oxidase 2, apparent in 80 % of *Ubc9* mutant animals examined (n = 5 larvae) is rescued by the *Dome>Ubc9*^{wt} expression (Fig. 6 A-D). Similarly, the trend of mild increase of mitotic cell number in the anterior lobes of the *Ubc9* mutant animals is suppressed by the *Dome>Ubc9*^{wt} transgene expression (Fig. 6 E), although the differences between all of the data points are not statistically significant.

Significantly, microtumor penetrance and expressivity are strongly suppressed in the rescued animals (Fig. 7 A-E). Whereas approximately 75 % of mutants at late third instar exhibit microtumors, only about 11 % of rescued animals contain any microtumors and the tumors are smaller (Fig. 7 A-D). Similar pattern of rescue was observed for hemocyte aggregates (Fig. 7 E). Taken together, these data implicate that Ubc9 not only prevents excessive mitosis in hematopoietic progenitors, but also serves as a tumor-suppressor.

Dome>Ubc9^{wt} restored normal larval/pupal development (onset of pupariation, Fig. 8 A) and adult viability (Fig. 8 B). The rescued adults carry no visible microtumors (Fig. 8 C). These effects are likely to be linked to *Dome* expression in the larval ring gland (our unpublished results).

Ubc9 hyperplasia is niche-independent

To examine if Ubc9 inhibitory function is required in the niche, we compared the niche morphology and size, and the membranous projections emanating from the niche into the medullary zone (Krzemien et al., 2007; Mandal et al., 2007) in heterozygous and mutant glands. We found no significant difference in the niche size, measured either as the number of cells expressing Antennapedia protein (Fig. 9 A-C), or *Antp>GFP* (Fig. 9 D-F). There was no difference in the presence of niche projections (Fig. 9 D, E). In addition, we observed that the cells of the dorsal vessel immediately adjacent to the niche express *Antp* (by both criteria), although there is no apparent difference in its expression between heterozygous and mutant glands (Fig. 9 A, B, D, E, stars).

To test if Ubc9 function in the niche can be linked to overproliferation, we examined *Ubc9⁻, Antp>Ubc9*^{wt} progeny. Larvae of this “rescue” class did not exhibit any relief from hematopoietic defects, neither in the lymph glands (Fig. 10 A-C), nor in circulation (Fig. 10 D-H) and died during pupal stages, just like their mutant siblings (Fig. 11 A-C). Likewise, adult viability and tumor incidence of the *Ubc9* mutant animals were not rescued when wild type protein was supplied in the niche by *Collier-Gal4* (Fig. 11 D and data not shown) (Crozatier et al., 2004). These observations suggest that progenitor hyperplasia in mutants is niche-independent and that its function is autonomous with respect to the progenitor population.

Loss of Ubc9 is linked to reduction of Dacapo levels

Protein interaction data suggest direct association of Ubc9 with CDK inhibitor Dacapo (Dap) (Stanyon et al., 2004). To test if Dap levels are affected by loss of *Ubc9*, we stained lymph glands with anti-Dap antibody. Dap expression is high in the *Dome>GFP* cells of control glands and cells with weak *Dome>GFP* intensity express low levels of Dacapo (Fig. 12 A, D, areas outlined with white dotted line). In *Ubc9* lymph glands, the overall Dap expression is significantly reduced throughout the gland and this reduction parallels the decrease in the *Dome>GFP* signal (Fig. 12 B, C, E, F, regions of higher intensity in Dacapo staining are outlined with orange dotted line). This close temporal correlation suggests that *Dome>GFP* expression marks progenitor quiescence in third instar lymph glands and one role for sumoylation is to keep cells in a quiescent state by controlling cell cycle exit through Dacapo function.

Expression of human p21 relieves Ubc9 overproliferation

To test the functional significance of reduced Dap in the *Ubc9* medullary zone, we expressed human p21 in the mutant medullary zone (*Dome>p21*). By early day six, when the mutant glands overgrow, *Dome>p21* expression rescues overgrowth. The sizes of the rescued lobes and zone proportions return to normal (Fig. 13 A-C). However, 6.5 days old (and older) animals of rescue group have overgrown posterior lobes, and their anterior lobes disperse (data not shown). All of the 6.5 days and older *Dome>p21* rescue class larvae bear tumors. Thus, although rescue of *Ubc9* lymph glands in early mid-third instars with *Dome>p21* is clear (Fig. 13 A-C), it is transient, most likely because the *Dome-Gal4* itself is downregulated in the mutants and does not depend on Dacapo/p21 expression.

We pursued this issue with a second Gal4 driver, *76B-Gal4*, which is expressed continuously high in developing mutant lymph glands. Expression of *76B-Gal4* (Harrison et al., 1995) in the control lymph gland is largely limited to cells of the medullary zone of anterior lobes and some cells of the posterior lobes (Fig. 12 G, and data not shown). Significantly, regulation of *76B* expression in *Ubc9* mutants is reminiscent of *ZCL2897* in the lymph glands (Fig. 12 G, H, compare to *ZCL2897* in Fig. 1 L, M), circulating hemocytes and tumors (Fig. 3 I-L compare to *ZCL2897* in Fig. 3 E-H). *76B>p21* expression partially restores *Ubc9* overgrowth clearly visualized by the reduction of GFP-positive cells (in these animals, *76B* simultaneously drives the expression of p21 and GFP). In contrast to the *Dome>p21*, relief of the mutant phenotype continues past day 6, anterior lobes do not disperse, and tumors do not appear in circulation (Fig. 12 I and data not shown). These results support the idea that Dap requirement continues at least until the onset of pupariation.

When p21 was provided in cells of the cortical zone and circulating hemocytes (with *SrpHemo-Gal4*, *Hemese-Gal4*, *Hml-Gal4*, or *Cg-Gal4*, which are specifically expressed in the aforementioned cells), we found no evidence of tumor rescue (data not shown). Thus, Dap expression in lymph gland progenitor cells and p21 rescue results with specific drivers confirm *Ubc9* tumor suppressive function in the hematopoietic progenitors and suggest that sumoylation of Dap is a likely mechanism for cell cycle exit.

SUMO pathway components in hematopoiesis

If Ubc9 function is to modify specific proteins like Dacapo in progenitor populations of the lymph gland, then other enzymes of the sumoylation cascade should be required similarly to Ubc9. *Drosophila* SUMO is closely related to the vertebrate SUMO-3 (Talamillo et al., 2008) and its expression is strongly nuclear in both, heterozygous and mutant lymph glands (Fig. 14 A-L). Although the staining intensity varies somewhat among some nuclei, we found no clear difference in expression levels or patterns among various classes of lymph gland cells.

We next examined larvae carrying loss-of-function mutations in E1 ($Aos1^{c06048}$) and E3/PIAS ($Su(var)2\text{-}10^{1}/Su(var)2\text{-}10^{2}$) genes. E1 is a heterodimer of Aos1 and Uba2 subunits, while PIAS, encoded by *Su(var)2-10* serves as the E3 ligase. Mutant *Aos1* and *PIAS* glands are similar to *Ubc9* mutants, albeit the phenotypes are less severe. Cells of the medullary zone of both mutants exhibit significantly increased *ZCL2897* expression (Fig. 15 A-C compare to Fig. 1 J-M). *ZCL2897* expression is also clearly detected in tumors from each mutant background (Fig. 15 D, E compare to Fig. 3 G, H). Lamellocytes are abundant within dispersing anterior lobes and in circulation (data not shown).

To test if *Dome>GFP* expression is compromised by loss of sumoylation enzymes, we expressed RNAi constructs for each of the two E1 subunits in the medullary zone. Knock-down of either Aos1 or Uba2 led to significant loss of the *Dome>GFP* expression, lamellocyte differentiation, anterior lobe dispersal (Fig. 15 F-H) and tumorogenesis (Fig. 15 I, J). These observations confirm that sumoylation plays essential role in proliferative quiescence of hematopoietic progenitors.

Quiescence is developmentally controlled; Dome>GFP expression is downregulated in prepupal lymph glands

Our results thus far point to the idea that the regulated expression of the *Dome* promoter correlates with "stemness" of cells in this region; i.e., strong *Dome>GFP* expression coincides with quiescence (compact medullary zone population) at third larval instar, whereas weak or no *Dome>GFP* expression correlates with loss of quiescence (loosely packed cells). Because mutant *Ubc9* animals show significant developmental delay, we hypothesized that precocious loss of *Dome>GFP* expression (due to loss of sumoylation) indicates loss of heterochrony in normal organ development in these mutants.

We tested this idea by examining *Dome>GFP* expression during normal metamorphosis, in pre-pupal and pupal glands. We found that the number of *Dome>GFP*-expressing cells peaks during wandering third instars in both anterior and posterior lobes, and upon pupariation, there is a significant reduction in the number of *Dome>GFP*-positive cells as well as in the intensity of GFP signal (Fig. 16 A-D and I-L). In the prepupal stage, these cells are found at or near the periphery of the anterior lobes. The cortical zone (*Dome>GFP*-negative but F-actin-positive cells in Fig. 16) comprises only a narrow rim around the medulla (Fig. 16 C). All GFP-positive cells (regardless of their fluorescence intensity) appear more loosely packed than their third instar predecessors. In contrast, *ZCL2897* expression does not decrease during pupariation (data not shown). Changes seen in Ubc9 mutant third instar glands resemble some of the changes seen in the prepupal and pupal wild type lymph glands. This correlation suggests that quiescence of the medullary zone in the anterior and first posterior lobes is lost upon pupariation (Fig. 17).

DISCUSSION

Excessive mitoses, misdifferentiation of progenitors, and loss of heterochrony contribute to tumor development

The goal of our study was to identify the source of the large solid microtumors of *Ubc9* and understand why its loss leads to severe hematopoietic overgrowth. We discovered that microtumors are essentially hyperplastic, misdifferentiated progenitors of the lymph gland lobes, whose detachment from the dorsal vessel allows them to freely float in the hemolymph. We also found that while sumoylation directly imposes proliferative quiescence on progenitors of all lobes, it also, indirectly, helps maintain the timely maturation and dispersal of the lobes. The latter effects are likely mediated through SUMO functions in the ring gland and metamorphosis (Talamillo et al., 2008). Accordingly, *Dome*> *Ubc9*^{wt} expression in the medullary zone and in prothoracic cells of the ring gland (our unpublished results) is sufficient to free the mutants of the major effects of the mutation (Fig. 5).

An important reason for the significant gain in tumor size is loss of heterochronic development of the mutant animals. Delay or failure of pupariation allows mutants to continue tumor development in the larval body for up to ten days. However, tumor ontogeny during this period follows a course that can be understood in the context of normal lymph gland ontogeny during the pre-pupal and pupal stage (Fig. 17). The anterior lobes of mutants disperse ahead of schedule (at mid-to-late third instar) while both posterior lobes remain mitotic, but largely intact. Due to space constraint, the growing masses frequently overlap, appearing to merge with one another. This comparison of mutant organ development with control organs using expression markers over roughly five days of the animal life (Fig. 17) suggests that all three lymph gland lobe sets are under somewhat different developmental influences and the loss of heterochrony and cell cycle regulation in mutants strongly affects the posterior lobes.

The onset of the effect of the *Ubc9* mutation is at the mid third instar stage which coincides with the period when the progenitor population undergoes proliferative restraint (Jung et al., 2005). We show that at this time in development, this cell population is heterogeneous (*vis-a-vis Dome>GFP* and *ZCL2897* expression), and one of the earliest detectable effects of the mutation on this population is on the expression of both markers. Loss of sumoylation leads to loss of *Dome>GFP* expression in third instar lobes (Fig. 1 and Fig. 5), but *ZCL2897* expression continues and increases in the expanding population in all three sumoylation mutant backgrounds tested (*Ubc9* in Fig. 1, and *Aos1* and *PIAS* in Fig. 15).

It may not be a coincidence that in some wild type cells of early prepupal lobes, *Dome>GFP* expression is reduced or undetectable (Fig. 16), while *ZCL2897* expression remains continuously high (our unpublished results). We interpret this correlation in the context of heterochronic development and propose that the misdifferentiation program of the mutant cells is due to a series of hierarchical loss of cellular controls, of which loss of cell cycle constraint is among the first (Fig. 18).

The heterogeneity of progenitors from which the tumors arise (Fig. 1) argues for the presence of some fate-restricted progenitors, in addition to (or instead of) multipotent stem cells (Krzemien et al., 2010). Extrinsic influence of the niche and autonomous biochemical mechanisms such as sumoylation appear to be essential to help maintain these progenitors in a dormant state through late larval/prepupal stages. In wild type animals, at least some of these progenitors appear to be released from the constraints of quiescence at late larval/prepupal stage as novel cell types; cells identified as secretory and phagocytic cells (Lanot et al., 2001) appear in the dispersing gland. Thus, the progenitors in the anterior lobes may be preserved temporarily so that they do not mature precociously in the larva. Alternatively, some cells of this population may be kept in reserve in the event of an environmental stress or wasp infection (Sorrentino et al., 2002) and may provide the additional cells including lamellocytes for host defense. Regardless of the fate of these progenitors, this strategy to maintain cells in quiescence is also seen in mammals. For example, in mice, hematopoietic stem cells exit proliferation about three weeks after birth, whereas in humans this occurs at about four years of age, when hematopoietic stem cells (HSCs) become adult HSCs. The dormant adult HSCs are activated as the organism recovers from injury (Trumpp et al., 2010).

The tumor-suppressive role of sumoylation is mediated, in part, by Dacapo/p21

Protein modification by sumoylation is a general post-translational regulatory mechanism of eukaryotic cells (Talamillo et al., 2008). We have shown that SUMO protein expression is strong in all lymph gland cells and the functions of all sumoylation cascade components tested control proliferative quiescence in the lymph gland progenitor population. Our results clearly link sumoylation to cell cycle control through Dacapo/p21, which is a cyclin-dependent kinase inhibitor. Dacapo binding to cyclin E/Cdk2 complexes blocks the G1/S transition in cell cycle (Lane et al., 1996). Dacapo/p21 and Ubc9 proteins interact with one another in a yeast two hybrid screen (Stanyon et al., 2004). We found that high levels of Dacapo/p21 coincide with high

Dome>GFP levels in the wild type glands. In the mutant glands, the expression of Dap is lost or reduced shortly after *Dome>GFP* is downregulated. This fact provides an explanation for the transient rescue observed in *Dome>p21*-expressing *Ubc9* mutants, but also suggests that high levels of Dacapo/p21 are continually required to maintain cells in a non-mitotic state. Furthermore, human p21 expression in these cells, but not cells of the cortical zone or circulating hemocytes, blocks overgrowth of *Ubc9* lymph glands (Fig. 12 and Fig. 13). Whereas *Dome>Ubc9*^{wt} expression restores the normal regulation of the Dome promoter (Fig. 5), *Dome>p21* does not have such an effect (Fig. 13). These observations suggest that simply blocking additional mitoses in the mutants is not sufficient to restore *Dome>GFP* regulation. They also support a role for Dap that is downstream of Ubc9. The mechanism by which sumoylation regulates Dap protein levels is not known. The significant but incomplete rescue of Ubc9 overgrowth via *76B>p21* can be attributed to the fact that the targeted population of *76B>GFP* cells does not correspond to the entire progenitor population in either the control or mutant glands, or Ubc9 tumor suppressive effect ensures the timely activation of signaling mechanisms important for proper hematopoietic development.

Other contributors of tumor growth

Even though our studies link the progenitor cell status to the process of sumoylation, they do not rule out its requirement in controlling hematopoietic development of cells that are partially committed and await post-mitotic terminal differentiation. This notion is supported by the fact that, first, p21 rescue by both drivers is partial, and second, knock-down of sumoylation enzymes in cells outside the medullary zone promotes aberrant hematopoieitic division and differentiation (our unpublished observations). In fact, loss of sumoylation in the non-hematopoietic fat body is sufficient to trigger mild differentiation of hemocytes in wild type larvae ((Paddibhatla et al., 2010), in revision). Thus, even though the primary requirement of Ubc9 in hematopoiesis is in the progenitor population, tumorogenesis in *Ubc9* mutants is supported by other intrinsic and extrinsic mechanisms.

The niche is a source of ligands, which influence the microenvironment of a very small number of stem cells remaining in direct contact with it (Trumpp et al., 2010). The lymph gland niche restrains progenitors of the anterior lobes in an undifferentiated state (Crozatier et al., 2004; Krzemien et al., 2007; Mandal et al., 2007; Trumpp et al., 2010). While the requirement for sumoylation does not appear essential to cells in the niche, it is intriguing that one of the niche markers, Antp, is also expressed in the dorsal vessel (Fig. 9). Furthermore, the expression of *Dome>GFP* in the dorsal vessel is under the control of sumoylation; its expression is undetectable in normal cells, but is activated in mutant cells (Fig. 1 and Fig. 5). Thus, it is possible that in addition to the cells in the niche, cues from the cells of the dorsal vessel influence the state of the hematopoietic progenitors, especially those that are immediately adjacent to the dorsal vessel.

Recent proteomic studies have identified Dorsal and Ras as direct targets of sumoylation in the *Drosophila* embryo (Nie et al., 2009). Both these proteins affect hematopoiesis (Asha et al., 2003; Chiu et al., 2005). It is therefore likely that sumoylation provides a multi-step mechanism for coupling cues from the niche, cortical zone and even the dorsal vessel. The uncoupling of these signals and their effects leads to uninhibited proliferation and differentiation, opening a gate for malignancy.

Loss of controlled proliferation underlies the development of human hematopoietic malignancies. In human leukemias, uncontrolled proliferation of progenitors can occur independently of the signals from the niche (Passegue et al., 2003). Understanding how stem–like cells govern tissue integrity is ultimately important for developing novel cancer therapies. The *Drosophila* model offers opportunities for identification and testing of drugs targeting highly-conserved biochemical mechanisms, such as sumoylation, which oversee self renewal pathways in progenitor populations.

Fig. 1. Aberrant gene expression in progenitors of *Ubc9* lymph glands.

(A) Schematics of second and third instar lymph glands. Labeling corresponds to images in all remaining panels. Three groups of lobes are aligned symmetrically along the antero-posterior axis of dorsal vessel (gray, labeled with a star, DV): (I) anterior lobes, (II) first set of posterior lobes consist of 2-3 pairs of smaller lobes at second instar, (III) second set of posterior lobes consist of 2-3 pairs of smaller lobes, clearly distinguishable at second instar and forming a large lobe at third instar. In the anterior lobes, progenitor cells (light green) are in the medullary zone (MZ), mature cells are localized to the outer cortical zone (CZ, dark green); the niche (N, orange) is localized to the posterior part of the anterior lobes and anterior-most part of the first posterior lobe. Cells in navy blue (P) have not been classified. Pericardial cells (PC, light blue) function as nephrocytes and physically separate the lobes.

(B-E) *Dome>GFP* (green) expression is similar in lymph glands of 4 days old L2 larvae – control (B, *Ubc9*$^{-/+}$) and mutant (C, *Ubc9*$^{-/-}$). *Dome>GFP* (green) expression remains strong in 6 days old *Ubc9*$^{-/+}$ glands (D) while it is reduced in the *Ubc9*$^{-/-}$ lymph glands (E).

(F-I) *ZCL2897* (green) and *Dome>DsRed* (red) expression in wild type anterior (F) and posterior (H) lobes of L3 animal; yellow hue is a result of an overlap of green and red. Zoomed fragments contained in white squares (labeled in F and H) are shown in G and I, respectively.

(J-M) *ZCL2897* (green) is expressed at a low level in anterior (J) and posterior (K) lobes of 6 days old third instar *Ubc9*$^{-/+}$ animals. *ZCL2897* expression is increased in 6 days old L3 *Ubc9*$^{-/-}$ mutant anterior (L) and posterior (M) lobes.

All samples were stained with Hoechst to visualize nuclei (blue), omitted for clarity in G and I. AL – anterior lobe(s), PL1 – set of first posterior lobes, PL2 – set of second posterior lobes. Star marks the dorsal vessel. Confocal sections (B-M). Scale bars correspond to 50 µm.

Figure 1.

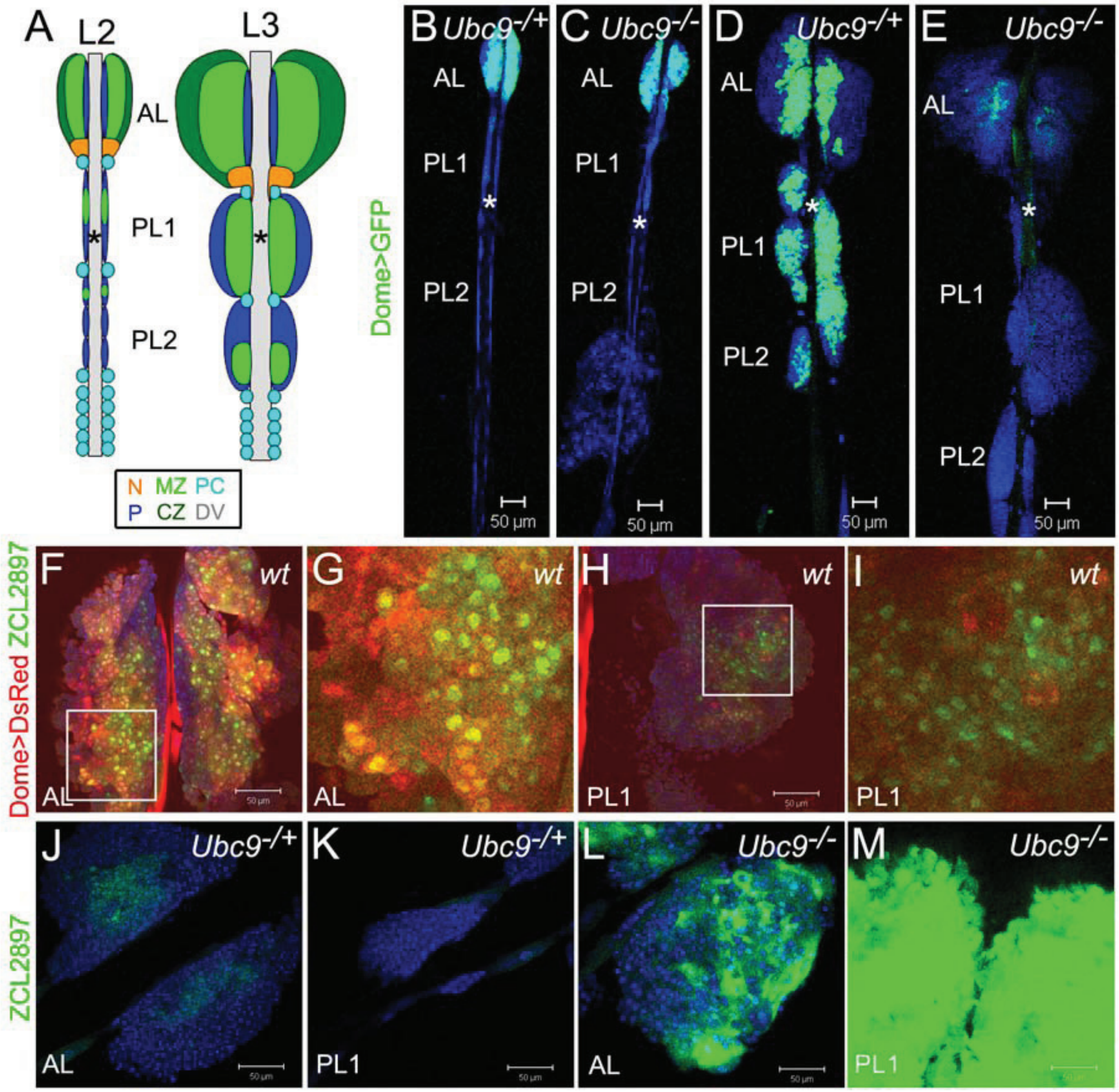
A
L2
L3
AL
PL1
PL2
N MZ PC
P CZ DV
B Ubc9-/+
C Ubc9-/-
D Ubc9-/+
E Ubc9-/-
Dome>GFP
50 µm
F wt
G wt
H wt
I wt
Dome>DsRed ZCL2897
J Ubc9-/+
K Ubc9-/+
L Ubc9-/-
M Ubc9-/-
ZCL2897

Fig. 2. Hemolectin expression pattern is similar in control and *Ubc9*$^{-/-}$ animals.

(A-B) *Hml>GFP* (green) expression in early third instar (4.5 days old) lymph glands of *Ubc9*$^{-/+}$ (A) and *Ubc9*$^{-/-}$ (B) animals.

(C-D) *Hml>GFP* (green) expression pattern in 6.5 days old third instar lymph glands of *Ubc9*$^{-/+}$ (C) and *Ubc9*$^{-/-}$ (D) animals is similar between the two genotypes.

All samples were stained with Hoechst to visualize nuclei (blue). AL – anterior lobe(s), PL1 – set of first posterior lobes, PL2 – set of second posterior lobes. Star marks the dorsal vessel. Confocal sections (A-D). Scale bars correspond to 50 µm.

Figure 2.

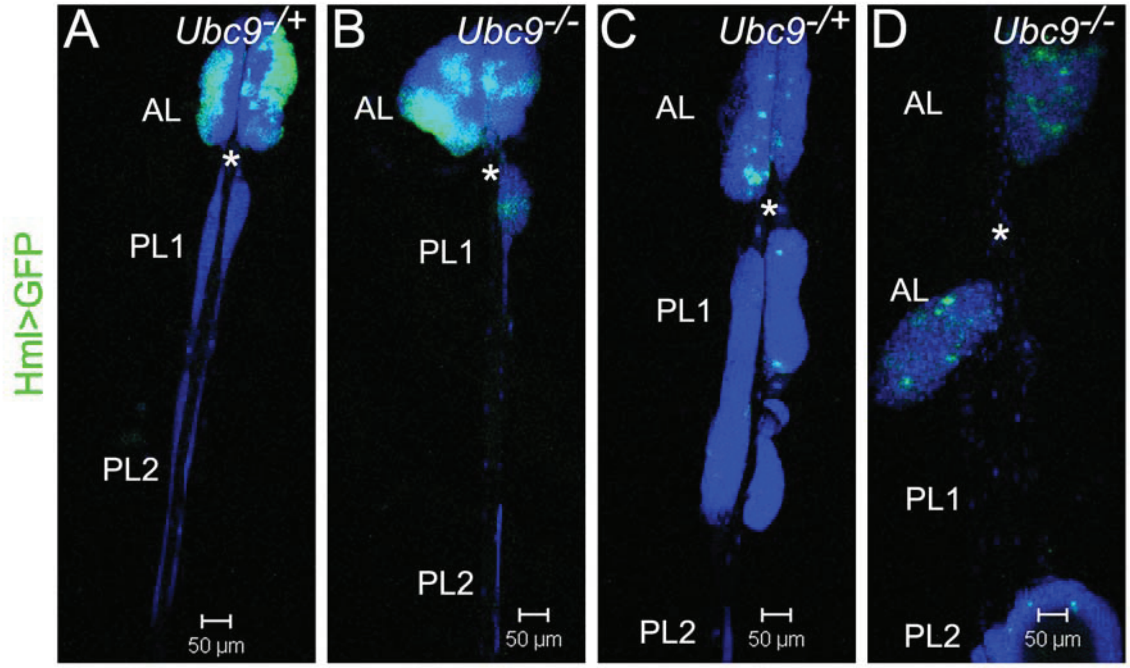
Hml>GFP
A
Ubc9-/+
AL
*
PL1
PL2
50 µm
B
Ubc9-/-
AL
*
PL1
PL2
50 µm
C
Ubc9-/+
AL
*
PL1
PL2
50 µm
D
Ubc9-/-
AL
*
AL
PL1
PL2
50 µm

Fig. 3. Expression of the progenitor markers is present in tumors and resembles patterns seen in the lymph glands.

(A-D) *Dome>GFP* (green) expression is absent from circulating hemocytes in *Ubc9*$^{-/+}$ animals (A), and is rarely observed in the *Ubc9*$^{-/-}$ circulating hemocytes (B) or tumors (C, D).

(E-H) *ZCL2897* (green) expression is not detectable in heterozygous circulating cells (E). *Ubc9*$^{-/-}$ animals show numerous *ZCL2897*-expressing cells in circulation (F) and in tumors (G, H). m refers to melanized region of the microtumor. (H) is a zoomed area of microtumor in panel G.

(I-L) *76B>GFP* (green) expression is absent in heterozygous circulating hemocytes (I), but like *ZCL2897*, it is abundant in circulating *Ubc9*$^{-/-}$ mutant hemocytes (J) and microtumors (K, L).

All samples were stained with Hoechst to visualize nuclei (blue). Confocal sections (A-L). Scale bars correspond to 50 µm.

Figure 3.

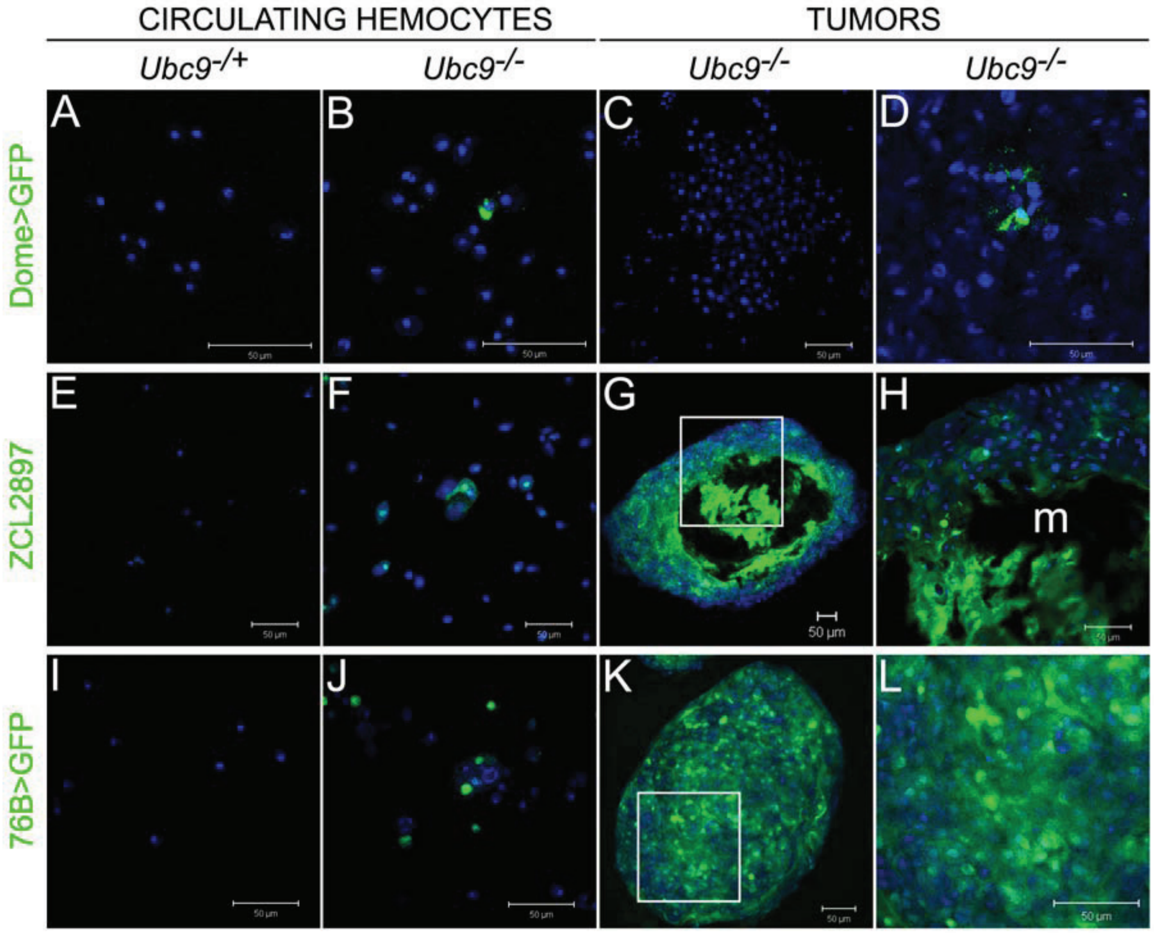
CIRCULATING HEMOCYTES
TUMORS
Ubc9-/+
Ubc9-/-
Ubc9-/-
Ubc9-/-
Dome>GFP
ZCL2897
76B>GFP
A
B
C
D
E
F
G
H
m
I
J
K
L
50 µm

Fig. 4. Overproliferation of immature cells in *Ubc9*$^{-/-}$ lymph gland.

(A-D) Mitosis (anti-phospho-histone H3 antibody, PH3, white) in anterior (A) and posterior (B) lobes of late third instar (6.5 day old) *Ubc9*$^{-/+}$ glands. At this stage *Ubc9*$^{-/-}$ mutants lose their anterior lobes, and posterior lobes (first pair in C, second pair in D) are overgrown and show numerous mitotic cells (white).

(E-H) Anterior lobes of 6 days old animals expressing *Dome>GFP* (green) were stained for mitosis (white) and mature hemocyte markers, anti-Nimrod C (red) antibody for plasmatocytes (E, F), and anti-Atilla antibody (red) for lamellocytes (G, H). Phospho-Histone H3 (PH3, white) and Nim C (red) only rarely localized to the same cells in third instar anterior lobes of *Ubc9*$^{-/+}$ (E, arrow) and *Ubc9*$^{-/-}$ (F) animals. Expression of lamellocyte marker Atilla (red) is absent in control *Ubc9*$^{-/+}$ lobes (G), and cells marked with it in mutant *Ubc9*$^{-/-}$ (H) do not pick up the mitotic marker (white).

Samples were stained with Hoechst to visualize nuclei (blue). Arrowheads point to examples of mitotic cells. Confocal sections (A-H). Scale bars correspond to 50 μm.

Figure 4.

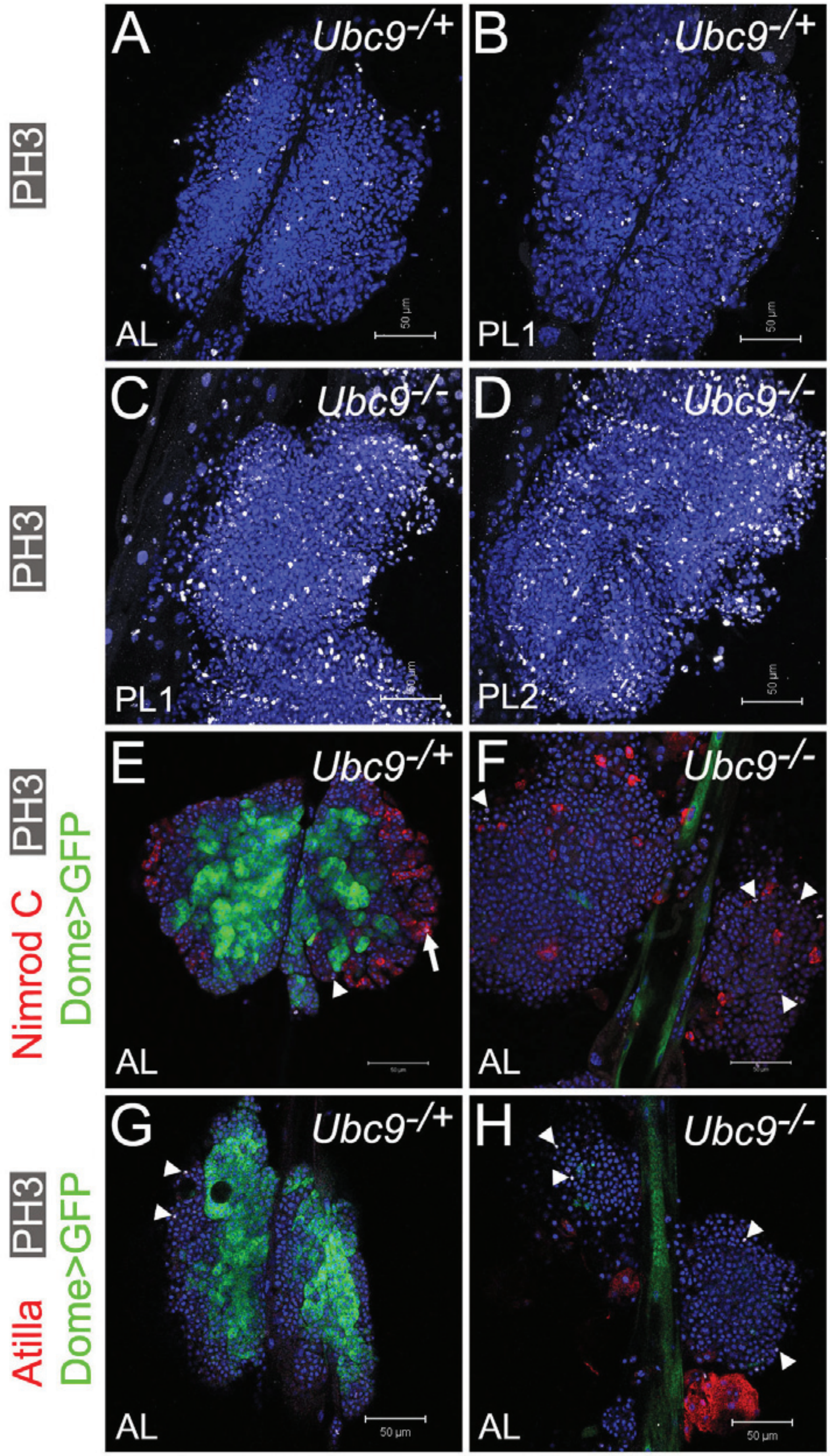

PH3
A
Ubc9-/+
AL
50 µm
B
Ubc9-/+
PL1
50 µm
PH3
C
Ubc9-/-
PL1
D
Ubc9-/-
PL2
50 µm
Nimrod C
PH3
Dome>GFP
E
Ubc9-/+
AL
F
Ubc9-/-
AL
Atilla
PH3
Dome>GFP
G
Ubc9-/+
AL
50 µm
H
Ubc9-/-
AL
50 µm

Fig. 5. *Dome>Ubc9^{wt}* restores *Ubc9$^{-/-}$* lymph gland size and *Dome>GFP* gene expression.

Schematic (A) summarizes the *Ubc9$^{-/-}$* lymph gland phenotype (lobes to the right) in relationship to the control (lobes to the left).

(B-D) *Dome>GFP* expression in control lymph gland (B) is high in anterior and posterior lobes, while it is severely decreased in *Ubc9$^{-/-}$* lobes (C) and increased in the dorsal vessel (star in panel C). *Dome>Ubc9^{wt}* expression restores the *Dome>GFP* level in the lobes and the dorsal vessel, as well as the sizes of all lobes (D).

Samples were stained with Hoechst to visualize nuclei (blue). AL – anterior lobe(s), PL1 – set of first posterior lobes, PL2 – set of second posterior lobes. Star marks the dorsal vessel. Confocal sections (B-D). Scale bars correspond to 50 µm.

Figure 5.

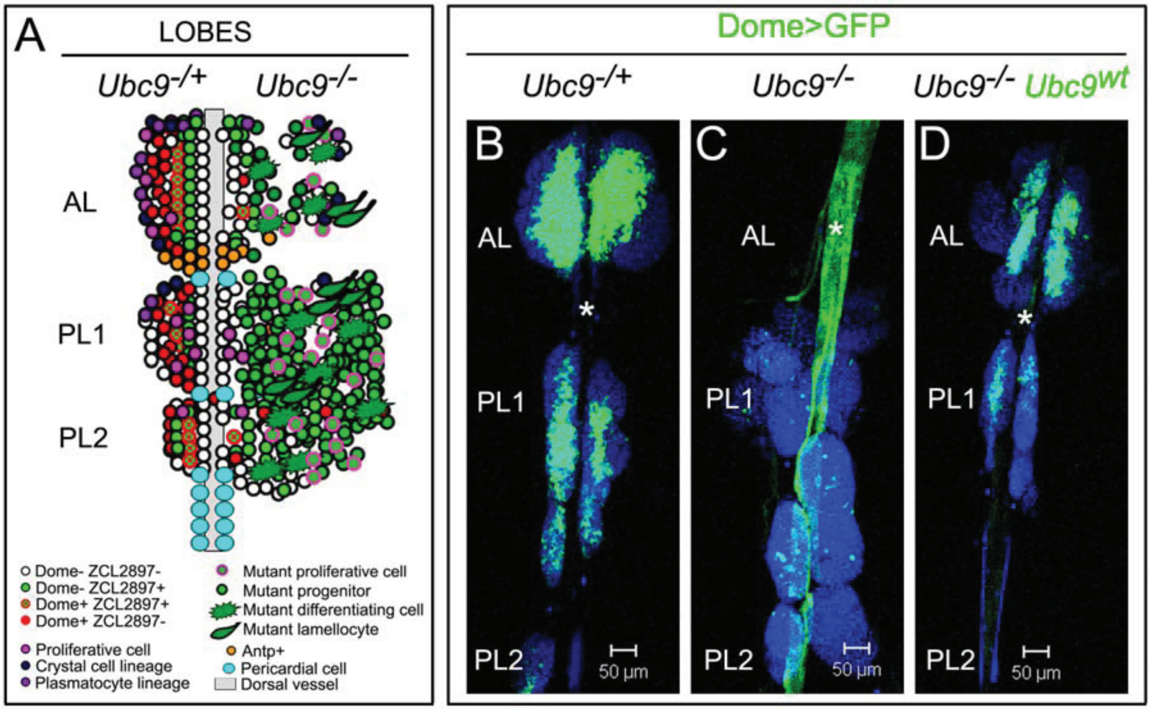
A
LOBES
Ubc9-/+
Ubc9-/-
AL
PL1
PL2
Dome- ZCL2897-
Dome- ZCL2897+
Dome+ ZCL2897+
Dome+ ZCL2897-
Proliferative cell
Crystal cell lineage
Plasmatocyte lineage
Mutant proliferative cell
Mutant progenitor
Mutant differentiating cell
Mutant lamellocyte
Antp+
Pericardial cell
Dorsal vessel
Dome>GFP
Ubc9-/+
Ubc9-/-
Ubc9-/- Ubc9wt
B
C
D
AL
PL1
PL2
50 µm

Fig. 6. *Dome>Ubc9^{wt}* effect on crystal cells and mitosis in anterior lobes of the lymph gland.

(A-C) Pro-phenol oxidase 2 (PPO2, red) expression marks crystal cells and *Dome>GFP* (green) marks the medullary zone. Crystal cells are present in control lymph gland (A), while their number is somewhat decreased in *Ubc9$^{-/-}$* lobes (B). *Dome>Ubc9^{wt}* expression restores the crystal cell number in the anterior lobes (C).

Samples were stained with Hoechst to visualize nuclei (blue). Confocal sections merged in Z plane (A-C) to show all crystal cells present in each set of anterior lobes. Scale bars correspond to 50 μm.

(D) Crystal cells were counted in *Ubc9$^{-/+}$*, *Ubc9$^{-/-}$* and “rescue” *Ubc9$^{-/-}$* with *Dome>Ubc9^{wt}* group (black, red and dashed red bars, respectively). Data were collected from n = 5 larvae and is represented in the graph as an average of total crystal cell number present in both anterior lobes per animal ± SE. The differences between mutant and heterozygous or “rescue” group data points are not statistically significant (t-test; lack of significant difference is symbolized by letter “a”) due to an outstanding value for one of the mutant animals.

(E) Mitotic cell numbers scored in *Ubc9$^{-/+}$*, *Ubc9$^{-/-}$* and “rescue” *Ubc9$^{-/-}$* with *Dome>Ubc9^{wt}* group (black, red and dashed red bars, respectively); n = 4 larvae (8 anterior lobes) per each genotype were scored. Collected data is represented in the graph as an average of mitotic cell number per anterior lobe ± SE. The differences between all data points are not statistically significant (t-test; lack of significant difference symbolized by letter “a”).

Figure 6.

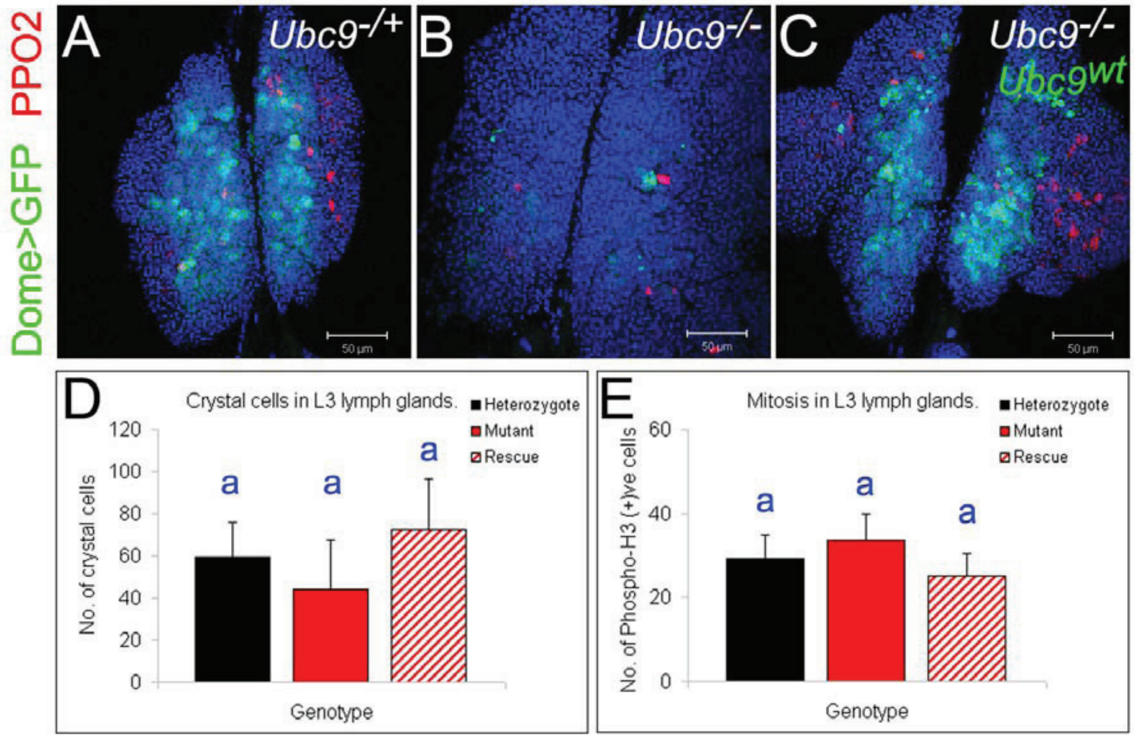
Dome>GFP PPO2
A
$Ubc9^{-/+}$
B
$Ubc9^{-/-}$
C
$Ubc9^{-/-}$
$Ubc9^{wt}$
50 µm
50 µm
50 µm
D
Crystal cells in L3 lymph glands.
Heterozygote
Mutant
Rescue
No. of crystal cells
120
100
80
60
40
20
0
a
a
a
Genotype
E
Mitosis in L3 lymph glands.
Heterozygote
Mutant
Rescue
No. of Phospho-H3 (+)ve cells
60
40
20
0
a
a
a
Genotype

Fig. 7. Dome>Ubc9^{wt} suppresses generation of *Ubc9$^{-/-}$* tumors and aggregates.

(A-C) Hemolymph from heterozygous *Ubc9$^{-/+}$* animals does not contain tumors (A), while *Ubc9$^{-/-}$* animals often exhibit microtumors (B). Tumorogenesis is suppressed in *Ubc9$^{-/-}$* larvae expressing *Dome>Ubc9^{wt}* (C). Tissue samples were stained with Hoechst to visualize nuclei (blue). Images acquired in Zeiss fluorescent microscope (A-C). Scale bars correspond to 100 µm.

(D, E) Penetrance of tumors (D) and aggregates (E), shown as percentage of larvae carrying given structures in *Ubc9$^{-/+}$* (n = 25 larvae), *Ubc9$^{-/-}$* (n = 40 larvae) and “rescue” *Ubc9$^{-/-}$* with *Dome>Ubc9^{wt}* (n = 63 larvae) group (black, red and dashed red bars, respectively in both panels); data represented as average ± SE. The differences between all data points are statistically significant (p value below 0.001). Significance of the difference among genotypes is represented in the graph by varying letters (“a”, “b”, “c”).

Figure 7.

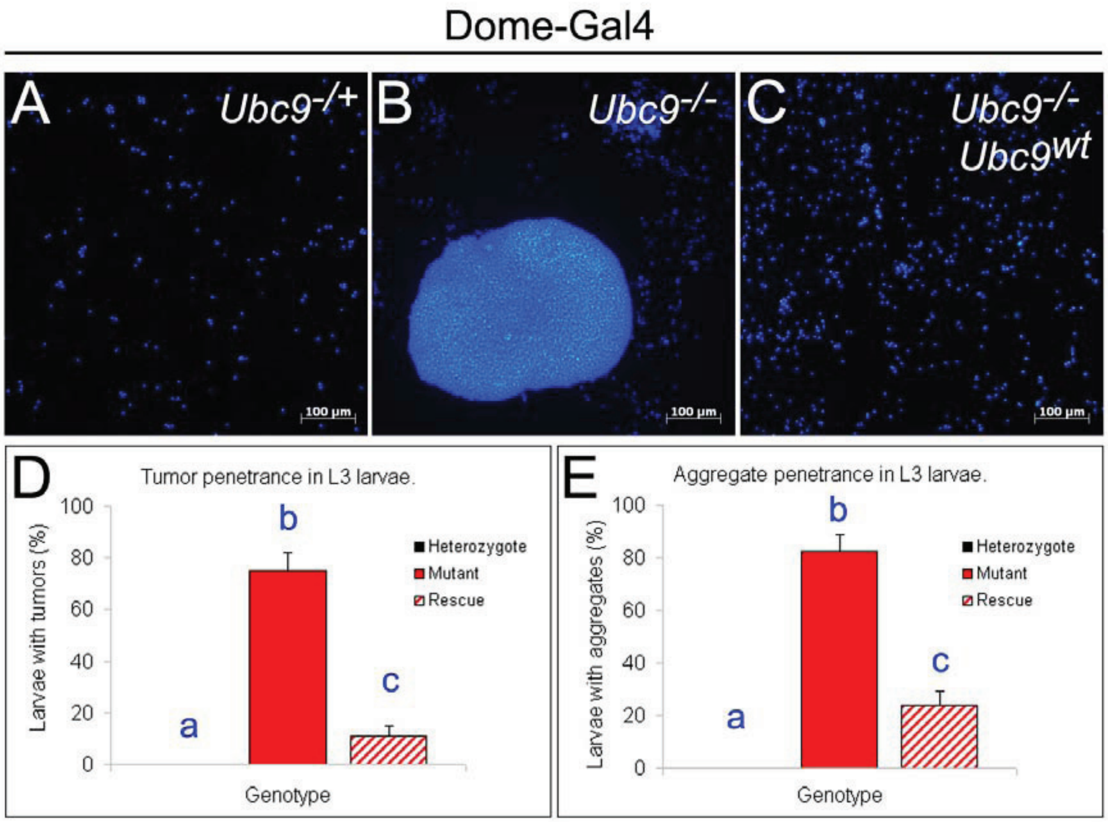

Dome-Gal4
A
$Ubc9^{-/+}$
B
$Ubc9^{-/-}$
C
$Ubc9^{-/-}$
$Ubc9^{wt}$
100 µm
100 µm
100 µm
D
Tumor penetrance in L3 larvae.
Larvae with tumors (%)
100
80
60
40
20
0
a
b
c
Heterozygote
Mutant
Rescue
Genotype
E
Aggregate penetrance in L3 larvae.
Larvae with aggregates (%)
100
80
60
40
20
0
a
b
c
Heterozygote
Mutant
Rescue
Genotype

Fig. 8. *Dome>Ubc9^{wt}* rescues developmental delay and tumor penetrance in adults.

(A-C) Developmental aspect of Ubc9 function was assessed by scoring the number of control *Ubc9$^{-/+}$* (black line and bars), mutant *Ubc9$^{-/-}$* (red bars and lines) and "rescue" *Ubc9$^{-/-}$* with *Dome>Ubc9^{wt}* animals (dashed red bars and lines) undergoing pupariation (A) and eclosing as adult flies (B), in which tumor penetrance was also recorded (C).

(A) Expression of *Dome>Ubc9^{wt}* in *Ubc9$^{-/-}$* animals slightly relieves retardation seen at the onset of pupariation in *Ubc9$^{-/-}$* mutants at day 5 and 6 after egglay. A total of n > 100 animals were scored.

(B) The number of eclosing "rescue" *Ubc9$^{-/-}$* with *Dome>Ubc9^{wt}* flies is higher than that of mutant animals and (C) tumor penetrance (percent of flies with visible tumors) is strongly suppressed in this group compared to mutant class. A total of n > 400 adults were scored.

Figure 8.

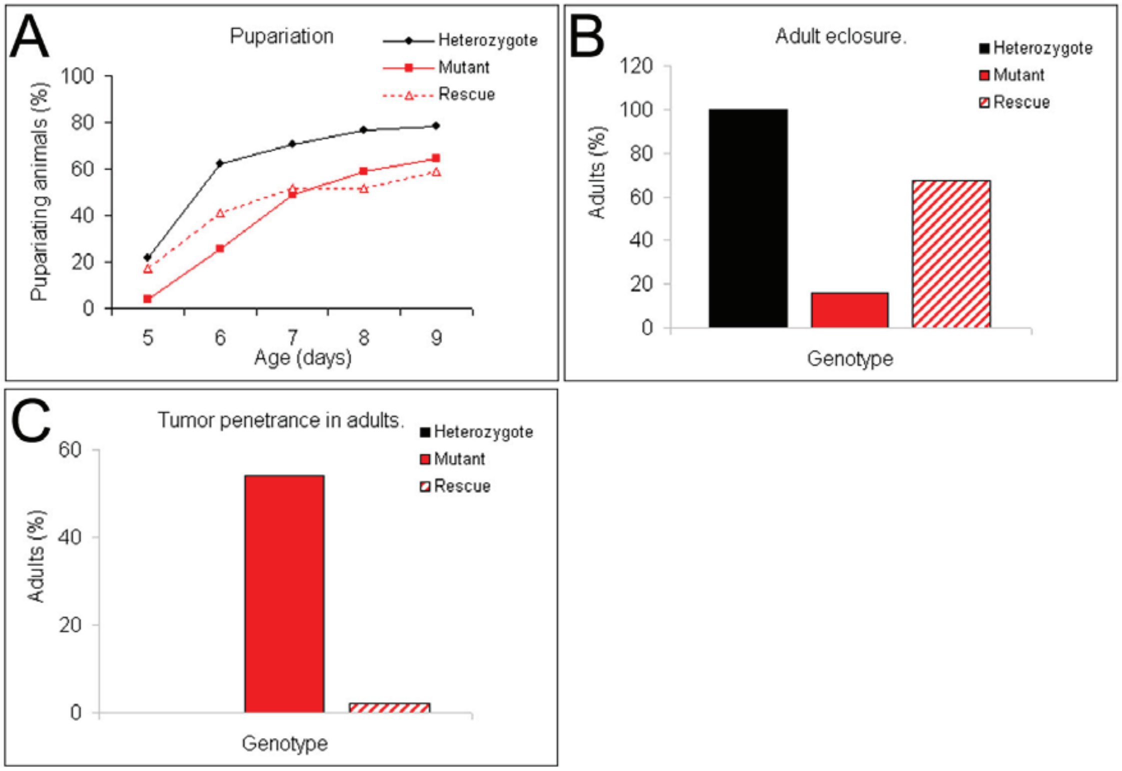
A
Pupariation
Heterozygote
Mutant
Rescue
Pupariating animals (%)
100
80
60
40
20
0
5
6
7
8
9
Age (days)
B
Adult eclosure.
Heterozygote
Mutant
Rescue
Adults (%)
120
100
80
60
40
20
0
Genotype
C
Tumor penetrance in adults.
Heterozygote
Mutant
Rescue
Adults (%)
60
40
20
0
Genotype

Fig. 9. *Ubc9*$^{-/-}$ niche is not significantly affected.

(A-C) Antennapedia protein expression in control *Ubc9*$^{-/+}$ (A) and *Ubc9*$^{-/-}$ (B) anterior lobes was quantified. The average numbers of Antp-expressing cells (± SE) per anterior lobe per genotype are represented in the graph (n = 3 larvae, a total of 6 anterior lobes scored per genotype).

(D-F) *Antp>GFP* expression in anterior lobes of control *Ubc9*$^{-/+}$ (D) and *Ubc9*$^{-/-}$ (E) glands. *Antp>GFP* expressing cells were counted and the averages ± SE are shown in the graph (C) for each genotype (n = 5 larvae, and a total of 10 anterior lobes per genotype were scored).

Differences in number of cells between control and mutant samples by both criteria in (C, at p = 0.267) and (F, at p = 0.632) are not statistically significant (indicated by letter “a”). Tissue samples were stained with Hoechst to visualize nuclei (blue). Confocal sections (A, B, D, E). Scale bars correspond to 50 µm.

Figure 9.

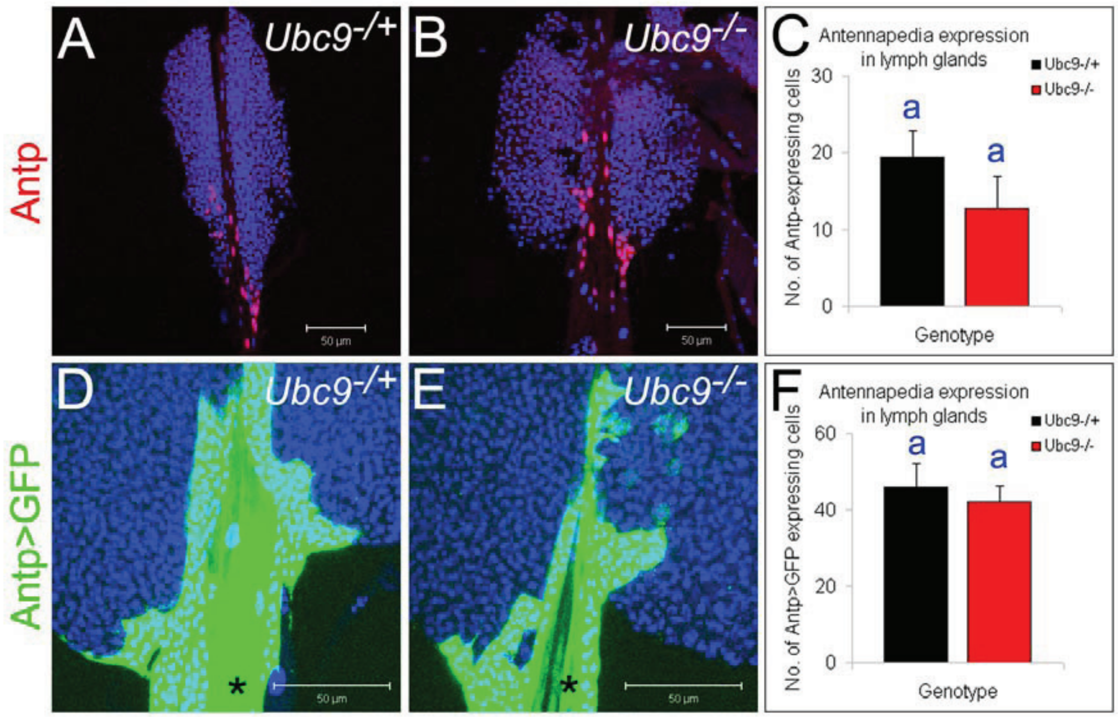
A
Ubc9-/+
B
Ubc9-/-
C
Antennapedia expression
in lymph glands
Ubc9-/+
Ubc9-/-
No. of Antp-expressing cells
30
20
10
0
a
a
Genotype
Antp
50 µm
D
Ubc9-/+
E
Ubc9-/-
F
Antennapedia expression
in lymph glands
Ubc9-/+
Ubc9-/-
No. of Antp>GFP expressing cells
60
40
20
0
a
a
Genotype
Antp>GFP
*
50 µm

Fig. 10. ***Antp>Ubc9^{wt}*** **expression does not rescue the** ***Ubc9$^{-/-}$*** **phenotype.**

(A-C) The anterior lobes of control lymph gland are intact (A) and posterior lobes remain relatively small (PL1, inset in A), while anterior lobes of the *Ubc9$^{-/-}$* animal are dispersed and posterior lobes are severely overgrown (B and inset in B). *Antp>Ubc9^{wt}* expression does not restore the integrity or size of *Ubc9$^{-/-}$* lymph gland lobes (C and inset in C). Lymph glands (A-C) were stained with Phalloidin to visualize F-actin (red) and with Hoechst to visualize nuclei (blue). AL – anterior lobe(s), PL1 – set of first posterior lobes. Confocal sections (A-C). Scale bars correspond to 50 µm.

(D-H) Rescue of *Ubc9* mutants via *Antp>Ubc9^{wt}*. Blood smears stained with Hoechst for nuclei (blue) from *Ubc9$^{-/+}$* (D) reveal circulating hemocytes, while large tumors are present in hemolymph samples collected from *Ubc9$^{-/-}$* (E), or *Antp>Ubc9^{wt}* in *Ubc9$^{-/-}$* background (F) animals. Images acquired in Zeiss fluorescent microscope (D-F). Scale bars correspond to 50 µm.

Penetrance of tumors (G) and aggregates (H) is not significantly different between the *Ubc9$^{-/-}$* mutants (red bars, n = 99 larvae) and *Ubc9$^{-/-}$* with *Antp>Ubc9^{wt}* rescue class (red dashed bar, n = 75 larvae). Heterozygotes do not show any tumors (black bars not visible at 0 % in both, G and H; n = 75 larvae). Data represented as average ± SE. Statistical significance (t-test, $p < 0.05$) of the differences among genotypes is represented in the graph by varying letters ("a", "b").

Figure 10.

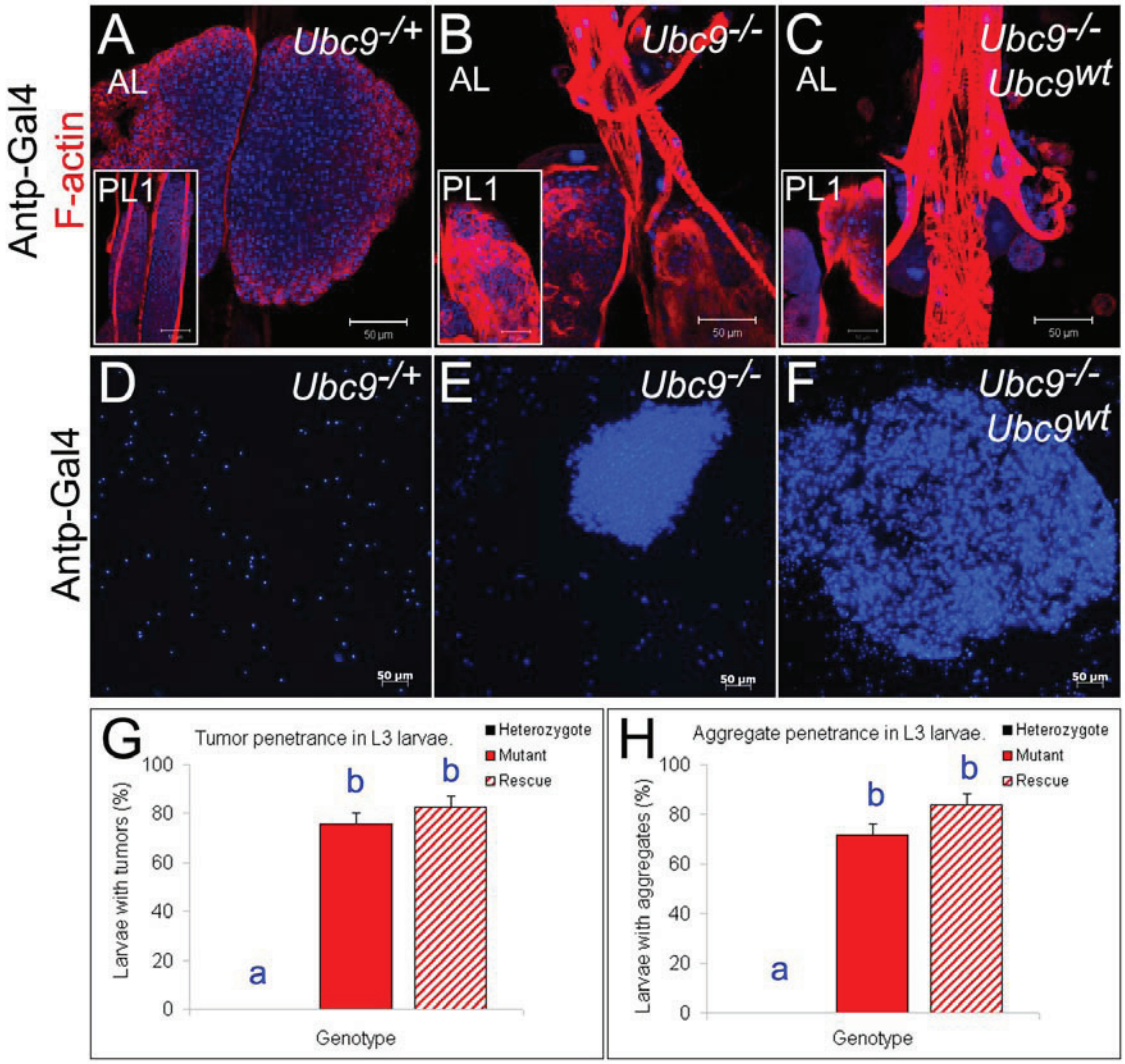
Antp-Gal4
F-actin
A
AL
Ubc9-/+
PL1
50 μm
B
AL
Ubc9-/-
PL1
50 μm
C
AL
Ubc9-/-
Ubc9wt
PL1
50 μm
Antp-Gal4
D
Ubc9-/+
50 μm
E
Ubc9-/-
50 μm
F
Ubc9-/-
Ubc9wt
50 μm
G
Tumor penetrance in L3 larvae.
Heterozygote
Mutant
Rescue
Larvae with tumors (%)
100
80
60
40
20
0
a
b
b
Genotype
H
Aggregate penetrance in L3 larvae.
Heterozygote
Mutant
Rescue
Larvae with aggregates (%)
100
80
60
40
20
0
a
b
b
Genotype

Fig. 11. *Antp>Ubc9^{wt}* or *Collier>Ubc9^{wt}* expression does not rescue *Ubc9$^{-/-}$* mutants to adulthood.

(A-C) Ratios of pupariating larvae (A) and eclosing adults (B, females and C, males) of control *Ubc9$^{-/+}$* (black line and bars), mutant *Ubc9$^{-/-}$* (red bars and lines) and "rescue" *Ubc9$^{-/-}$* with *Antp>Ubc9^{wt}* classes (dashed red bars and lines) are represented in the graphs.

(A) The delayed pupariation of *Ubc9$^{-/-}$* mutants is accelerated at days 8-10 after egglay in *Ubc9$^{-/-}$* animals expressing *Antp>Ubc9^{wt}* (n > 200 animals scored). While very mild rescuing effect of *Antp>Ubc9^{wt}* on *Ubc9$^{-/-}$* adult eclosure is seen in female progeny (B), there is no such effect on male F1 flies (C). Results for a total of n > 90 flies are represented in graphs in B and C. The same trend was recorded in additional repeats of this experiment with a total of n > 600 flies.

(D) Adult eclosure was not rescued by expression of *Collier>Ubc9^{wt}* in mutant *Ubc9$^{-/-}$* background (data shown for n > 190 adults, experiments were repeated with a total of n > 500 flies yielding similar results).

Figure 11.

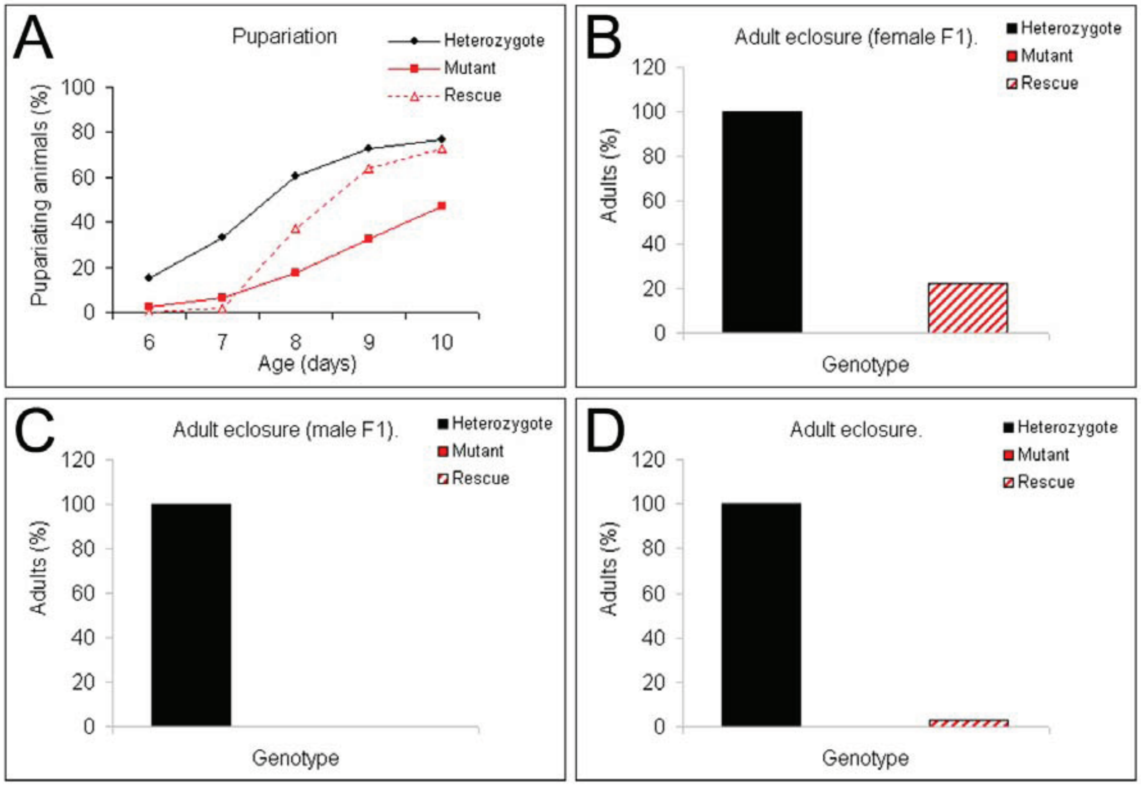
A
Pupariation
Heterozygote
Mutant
Rescue
Pupariating animals (%)
100
80
60
40
20
0
6
7
8
9
10
Age (days)
B
Adult eclosure (female F1).
Heterozygote
Mutant
Rescue
Adults (%)
120
100
80
60
40
20
0
Genotype
C
Adult eclosure (male F1).
Heterozygote
Mutant
Rescue
Adults (%)
120
100
80
60
40
20
0
Genotype
D
Adult eclosure.
Heterozygote
Mutant
Rescue
Adults (%)
120
100
80
60
40
20
0
Genotype

Fig. 12. Dacapo expression is reduced in misdifferentiated progenitor cells. Human p21 rescues *Ubc9* tumorogenesis.

(A, D) Dacapo (red) expression in third instar *Ubc9*$^{-/+}$ lymph glands expressing *Dome>GFP* (green, A); white dotted lines outline the medullary zone, yellow dotted lines outline the cortical zone; compare to (D) where the green and blue channels have been removed for clarity of the Dacapo staining.

(B, E) Dacapo (red) staining in *Ubc9*$^{-/-}$ mutant third instar lymph gland (B) where the *Dome>GFP* (green) is downregulated; orange dotted lines outline areas of putative post-medullary zone where Dacapo expression is reduced; only red channel showing Dacapo presented in (E).

(C, F) An example of *Ubc9*$^{-/-}$ anterior and a fragment of posterior mutant lobes (C) where the *Dome>GFP* (green) is downregulated but a fragment of posterior lobe still expresses Dacapo at a relatively high level; only red channel of this image is presented in (F).

(G-I) *76B>p21* (GFP) expression rescues *Ubc9*$^{-/-}$ mutant. *76B* expression in *Ubc9*$^{-/+}$ control (G) and *Ubc9*$^{-/-}$ (H) glands. Arrows in panels G and H point to the GFP-expressing cells in the posterior lobes. Mutant lobes *Ubc9*$^{-/-}$ with *76B>p21, GFP* (green) transgenes show reduction in level of *76B>GFP* expression and number of GFP-positive cells. Glands are counterstained with rhodamine-labelled phalloidin.

Samples were stained with Hoechst to visualize nuclei (blue), omitted in D, E and F for clarity. AL – anterior lobe(s), PL1 – set of first posterior lobes. Confocal sections (A-F) and images acquired in Zeiss fluorescent microscope (G-I). Scale bars correspond to 50 μm.

Figure 12.

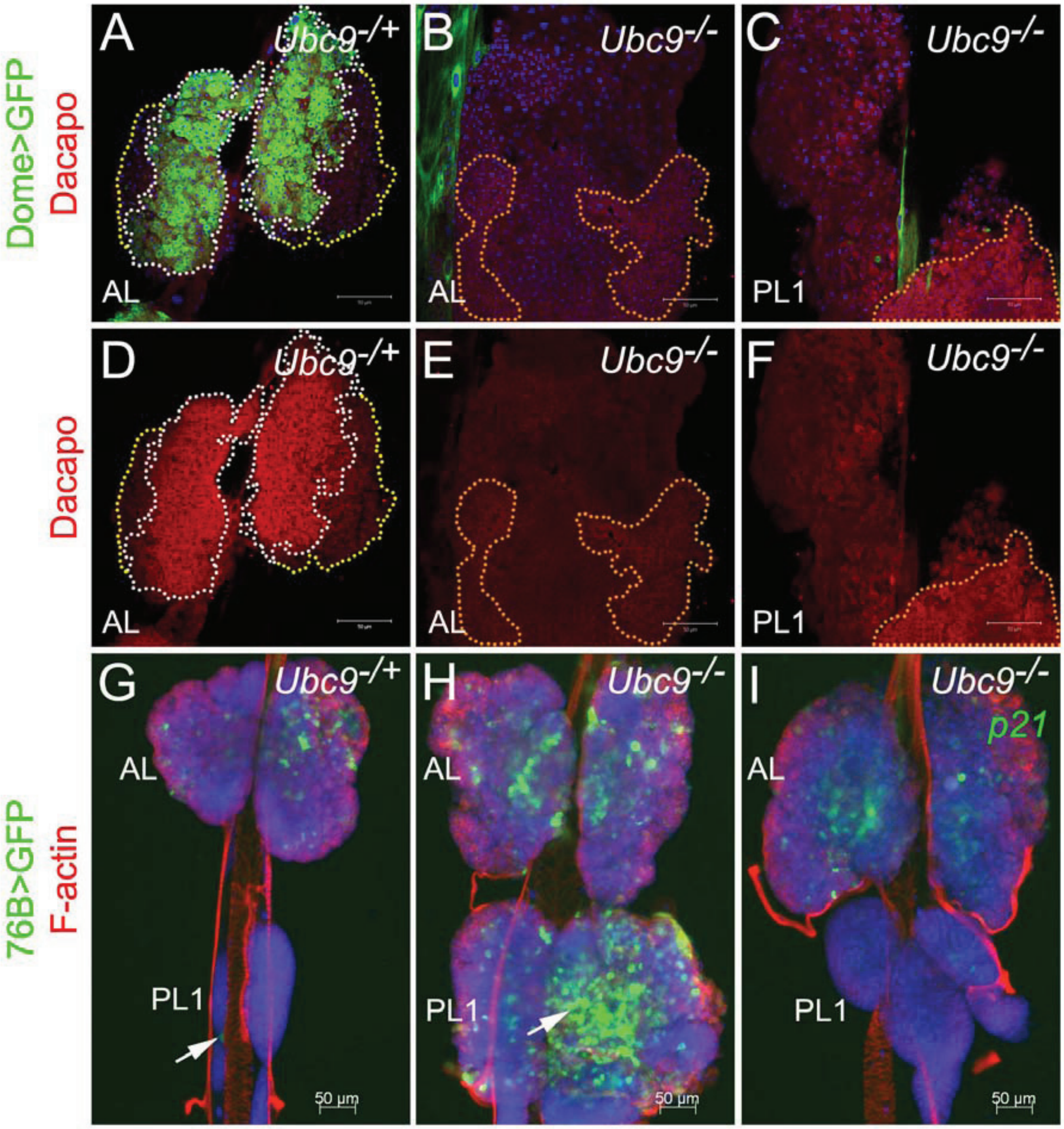
A
Ubc9-/+
B
Ubc9-/-
C
Ubc9-/-
Dome>GFP
Dacapo
AL
AL
PL1
D
Ubc9-/+
E
Ubc9-/-
F
Ubc9-/-
Dacapo
AL
AL
PL1
G
Ubc9-/+
H
Ubc9-/-
I
Ubc9-/-
p21
76B>GFP
F-actin
AL
AL
AL
PL1
PL1
PL1
50 µm
50 µm
50 µm

Fig. 13. *Dome>p21* rescue of *Ubc9* phenotype.

Lymph gland of a heterozygous control (A) with *Dome>GFP* expression (green). Overgrowth of the *Ubc9*$^{-/-}$ lymph gland (B) is suppressed by expression of *Dome>p21* in the *Ubc9*$^{-/-}$ background (C). Samples were stained with Hoechst and Phalloidin to visualize nuclei (blue) and F-actin (red) respectively. AL – anterior lobe(s), PL1 – set of first posterior lobes. Images acquired in Zeiss fluorescent microscope (A-C). Scale bars correspond to 50 µm.

Figure 13.

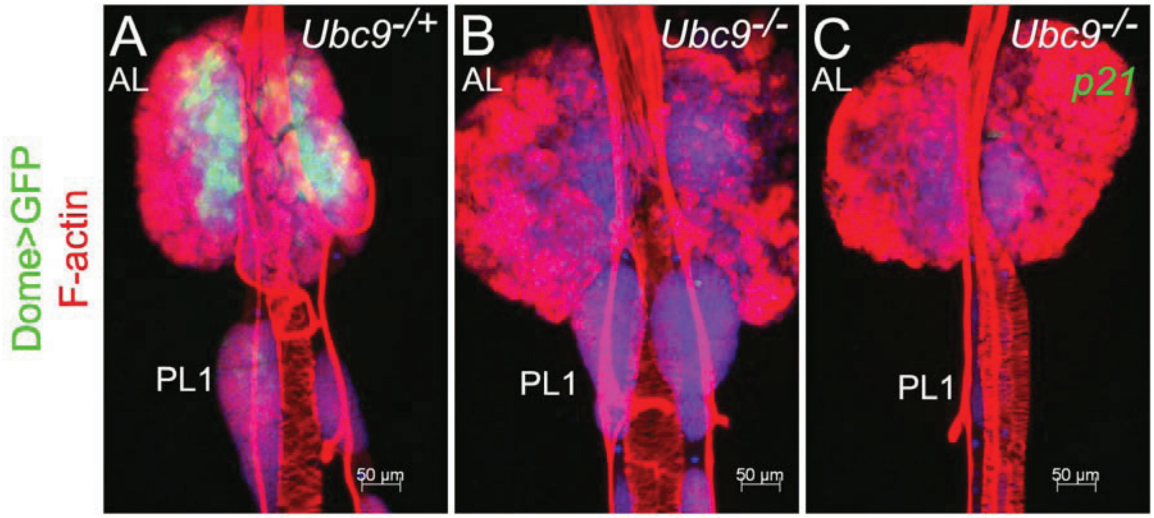
A
AL
Ubc9-/+
PL1
50 µm
B
AL
Ubc9-/-
PL1
50 µm
C
AL
Ubc9-/-
p21
PL1
50 µm
Dome>GFP
F-actin

Fig. 14. Loss of Ubc9 has no observable effect on SUMO expression in lymph gland tissue.

(A-F) Anterior lobes of the *Dome>GFP* (green) *Ubc9*$^{-/+}$ lymph gland show nuclear expression of SUMO protein (purple, A). The expression level varies among individual nuclei (magnified fragment of panel A is presented in panels B and C) but this difference appears to be random in terms of location of cells within the organ. *Dome>GFP* and SUMO staining shown in (B), while the green channel is omitted for clarity in panel (C). Control posterior lobes (D) show similar staining pattern as anterior lobes. (E, F) show zoomed regions of the posterior lobes corresponding to the white square in panel D. The green channel was omitted in panel F.

(G-L) Anterior lobes of *Ubc9*$^{-/-}$ mutant (G; magnified fragment of panel G with *Dome>GFP* shown in panel H, and without the green channel, in panel I). Posterior lobes (J) show similar pattern of staining as controls; magnification of the selected area from (J) with *Dome>GFP* expression in panel K, and without the green channel in L. Hoechst staining was omitted in this figure for clarity of SUMO staining. Confocal sections (A-L). Scale bars correspond to 50 μm.

Figure 14.

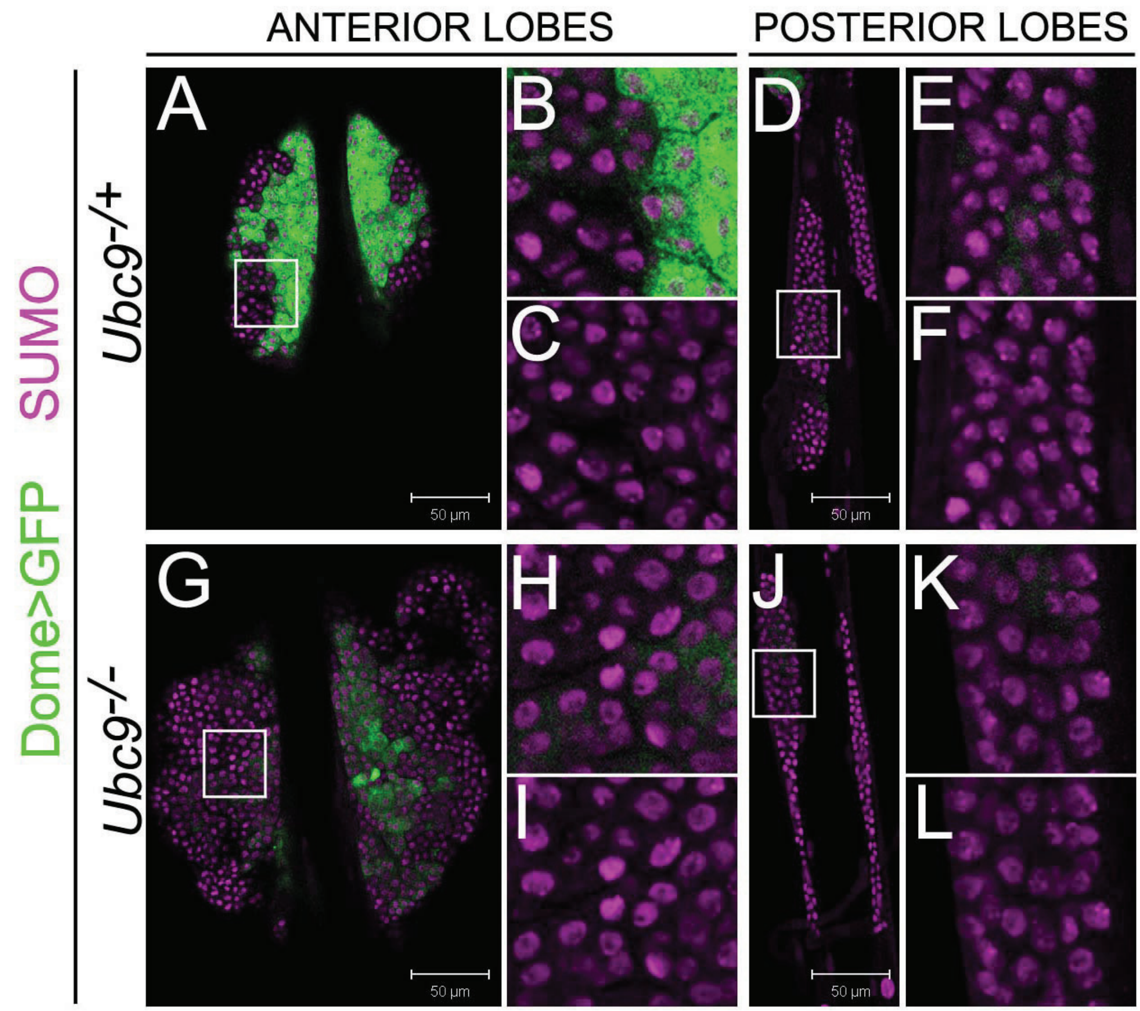
ANTERIOR LOBES
POSTERIOR LOBES
SUMO
Dome>GFP
Ubc9-/+
Ubc9-/-
A
B
C
D
E
F
G
H
I
J
K
L
50 µm
50 µm
50 µm
50 µm

Fig. 15. Sumoylation enzymes in larval hematopoiesis.

(A-C) Loss of function of *Aos1* and *PIAS* leads to upregulation of *ZCL2897* expression (green, A-C); main panels show anterior lobes and insets represent corresponding posterior lobes; control wild type lymph gland (A), *Aos1*$^{-/-}$ (B) and *PIAS*$^{-/-}$ (C).

(D-E) Tumors of *Aos1*$^{-/-}$ (D) and *PIAS*$^{-/-}$ (E) mutant larvae also express high levels of *ZCL2897* (green).

(F, J) Selective RNAi of *Aos1* or *Uba2* downregulates *Dome>GFP* (green) expression; control lymph gland (F) does not carry RNAi constructs and shows normal *Dome>GFP* expression, while *Dome>Aos1*^{RNAi}, *GFP* (green, G) and *Dome>Uba2*^{RNAi}, *GFP* (green, H) exhibit decrease in *Dome>GFP* expression.

(I, J) Tumors form in animals expressing *Dome>Aos1*^{RNAi}, *GFP* (I) and *Dome>Uba2*^{RNAi}, *GFP* (J). Parental classes of *UAS-Aos1*^{RNAi} and *UAS-Uba2*^{RNAi} show normal lymph glands and have no tumors in their hemolymph.

Samples were stained with Hoechst and Phalloidin to visualize nuclei (blue) and F-actin (red), respectively. AL – anterior lobe(s), PL1 – set of first posterior lobes. Confocal sections (A-C, F, H, J) and images acquired in Zeiss fluorescent microscope (D, E, G, I). Scale bars correspond to 50 μm.

Figure 15.

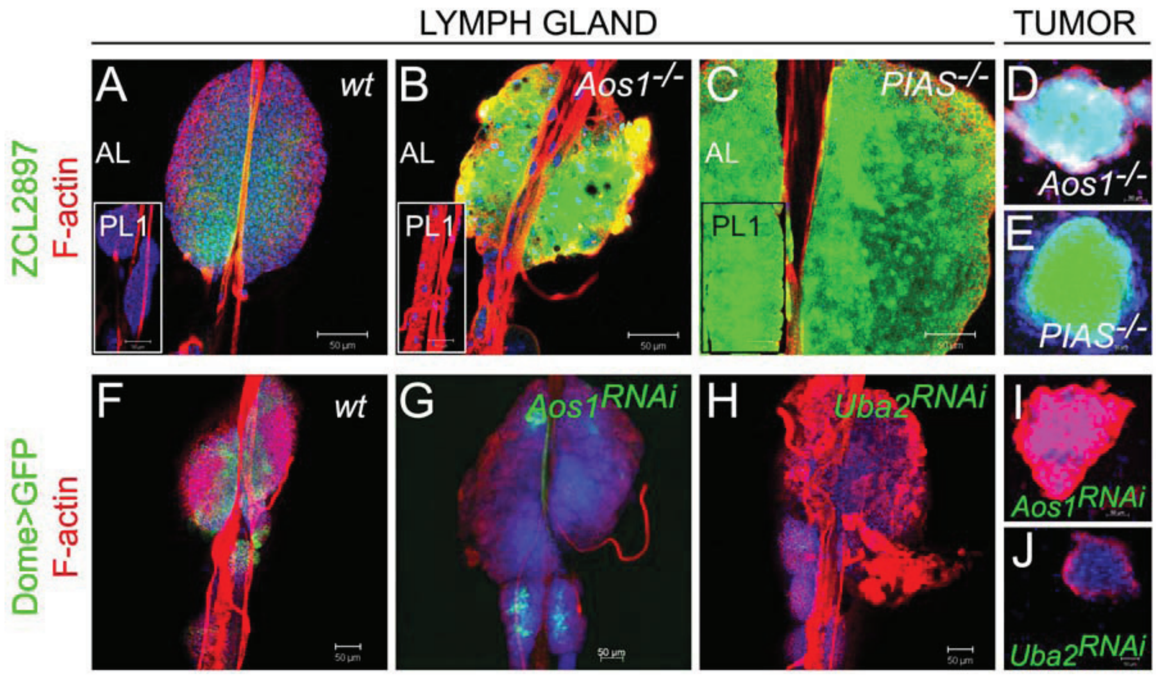
LYMPH GLAND
TUMOR
ZCL2897
F-actin
A
wt
AL
PL1
50 µm
B
Aos1-/-
AL
PL1
50 µm
C
PIAS-/-
AL
PL1
D
Aos1-/-
E
PIAS-/-
Dome>GFP
F-actin
F
wt
50 µm
G
Aos1RNAi
50 µm
H
Uba2RNAi
50 µm
I
Aos1RNAi
J
Uba2RNAi

Fig. 16. *Dome>GFP* expression is developmentally regulated in wild type lymph glands.

Dome>GFP (green) expression decreased over time in anterior (A-H) and posterior (I-P) lobes of wild type animals.

Anterior lobe of wandering larva (A, zoom in panel B), early prepupa (C, zoom in panel D), late prepupa (E, zoom in panel F), early pupa (G, zoom in panel H). Posterior lobes of wandering larva (I, zoom in panel J), early prepupa (K, zoom in panel L), late prepupa (M, zoom in panel N), early pupa (O, zoom in panel P).

Samples were stained with Hoechst to visualize nuclei (blue) and with rhodamine-phalloidin to visualize F-actin (red). AL – anterior lobe(s), PL1 – set of first posterior lobes. Confocal sections (A-P). Scale bars correspond to 50 µm.

Figure 16.

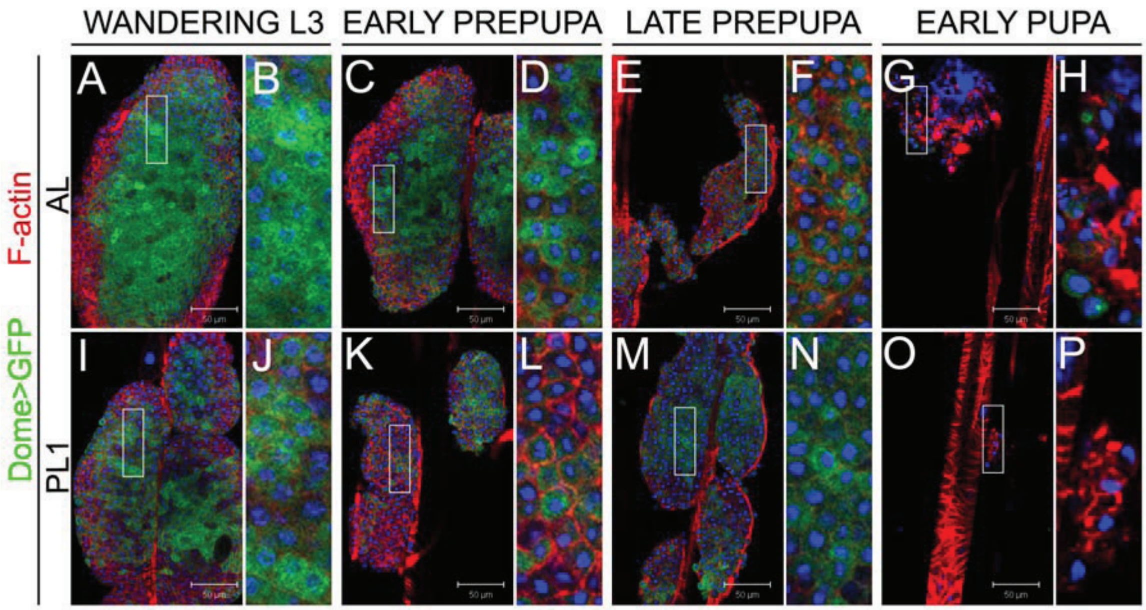

WANDERING L3
EARLY PREPUPA
LATE PREPUPA
EARLY PUPA
F-actin
Dome>GFP
AL
PL1
A
B
C
D
E
F
G
H
I
J
K
L
M
N
O
P

Fig. 17. Loss of heterochronic development and developmental delay in mutants supports the growth of microtumors.

Larval to pupal stages of *Drosophila* development encompassing days 4 to 8 of development. Days labeled on the central axis correspond to developmental stages of heterozygous or *Ubc9* mutant animals. Mutants lose heterochrony, persist in third instar stage past 8 day of development, while their heterozygous siblings transition into pupation by this time. As larval development progresses from second to third instar, the wild type lymph gland lobes expand until the onset of metamorphosis; at this time anterior and first posterior lobes downregulate their *Dome>GFP* expression and become smaller as they disperse or lose cells. The second set of posterior lobes remains relatively small and intact until late pupal stage. The anterior lobes of *Ubc9* mutants begin to disintegrate precociously at mid-to-late third instar and both posterior lobes grow significantly but remain intact. The process begins at day 6 and affects all animals by day 8. Microtumors are thus hyperplastic lobes detached from the dorsal vessel and found free in the hemolymph of 6 days and older animals.

Figure 17.

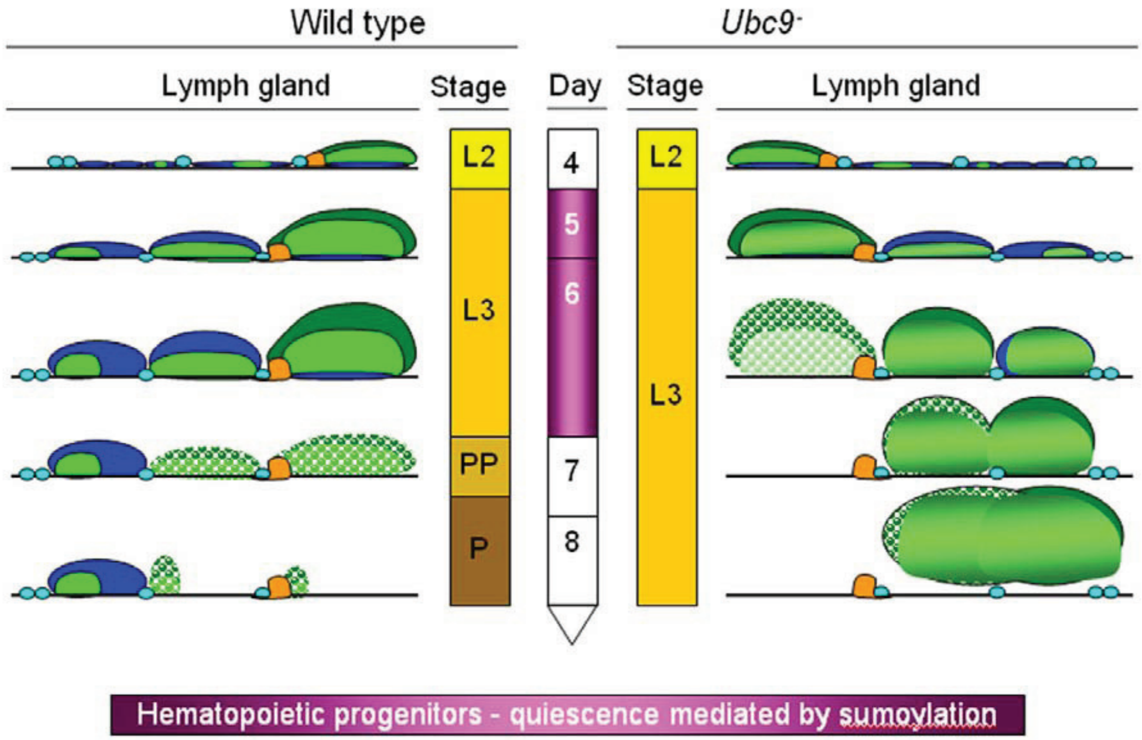
Wild type
Ubc9⁻
Lymph gland
Stage
Day
Stage
Lymph gland
L2
L3
PP
P
4
5
6
7
8
L2
L3
Hematopoietic progenitors - quiescence mediated by sumoylation

Fig. 18. Sumoylation controls proliferation of progenitor cells through Dacapo. Hematopoietic progenitors express either one or both, *ZCL2897* or *Dome>GFP*, and are maintained in their undifferentiated and proliferatively quiescent state by sumoylation through high levels of Dacapo. Loss of sumoylation correlates with low Dacapo/p21. Cells lose quiescence and initiate division, misdifferentiation and tumorgenesis.

Figure 18.

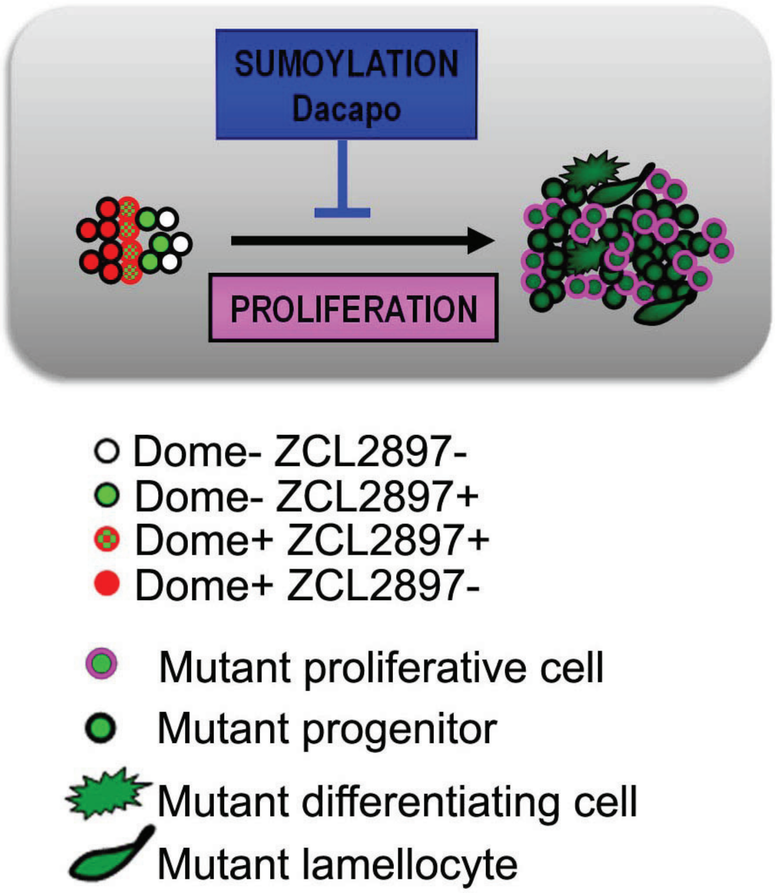
SUMOYLATION
Dacapo
PROLIFERATION
Dome- ZCL2897-
Dome- ZCL2897+
Dome+ ZCL2897+
Dome+ ZCL2897-
Mutant proliferative cell
Mutant progenitor
Mutant differentiating cell
Mutant lamellocyte

REFERENCES

Apionishev, S., Malhotra, D., Raghavachari, S., Tanda, S. and Rasooly, R. S. (2001). The Drosophila UBC9 homologue lesswright mediates the disjunction of homologues in meiosis I. *Genes Cells* 6, 215-224.

Asha, H., Nagy, I., Kovacs, G., Stetson, D., Ando, I. and Dearolf, C. R. (2003). Analysis of Ras-induced overproliferation in Drosophila hemocytes. *Genetics* 163, 203-215.

Bourbon, H. M., Gonzy-Treboul, G., Peronnet, F., Alin, M. F., Ardourel, C., Benassayag, C., Cribbs, D., Deutsch, J., Ferrer, P., Haenlin, M. et al. (2002). A P-insertion screen identifying novel X-linked essential genes in Drosophila. *Mech Dev* 110, 71-83.

Brand, A. H. and Perrimon, N. (1993). Targeted gene expression as a means of altering cell fates and generating dominant phenotypes. *Development* 118, 401-415.

Brown, S., Hu, N. and Hombria, J. C. (2001). Identification of the first invertebrate interleukin JAK/STAT receptor, the Drosophila gene domeless. *Curr Biol* 11, 1700-1705.

Bruckner, K., Kockel, L., Duchek, P., Luque, C. M., Rorth, P. and Perrimon, N. (2004). The PDGF/VEGF receptor controls blood cell survival in Drosophila. *Dev Cell* 7, 73-84.

Chiu, H., Sorrentino, R. P. and Govind, S. (2001). Suppression of the Drosophila cellular immune response by Ganaspis xanthopoda. *Adv Exp Med Biol* 484, 161-167.

Chiu, H., Ring, B. C., Sorrentino, R. P., Kalamarz, M., Garza, D. and Govind, S. (2005). dUbc9 negatively regulates the Toll-NF-kappa B pathways in larval hematopoiesis and drosomycin activation in Drosophila. *Dev Biol* 288, 60-72.

Crozatier, M., Ubeda, J. M., Vincent, A. and Meister, M. (2004). Cellular immune response to parasitization in Drosophila requires the EBF orthologue collier. *PLoS Biol* 2, E196.

de Nooij, J. C. and Hariharan, I. K. (1995). Uncoupling cell fate determination from patterned cell division in the Drosophila eye. *Science* 270, 983-985.

Emerald, B. S. and Cohen, S. M. (2004). Spatial and temporal regulation of the homeotic selector gene Antennapedia is required for the establishment of leg identity in Drosophila. *Dev Biol* 267, 462-472.

Ghiglione, C., Devergne, O., Georgenthum, E., Carballes, F., Medioni, C., Cerezo, D. and Noselli, S. (2002). The Drosophila cytokine receptor Domeless controls border cell migration and epithelial polarization during oogenesis. *Development* 129, 5437-5447.

Hari, K. L., Cook, K. R. and Karpen, G. H. (2001). The Drosophila Su(var)2-10 locus regulates chromosome structure and function and encodes a member of the PIAS protein family. *Genes Dev* 15, 1334-1348.

Harrison, D. A., Binari, R., Nahreini, T. S., Gilman, M. and Perrimon, N. (1995). Activation of a Drosophila Janus kinase (JAK) causes hematopoietic neoplasia and developmental defects. *EMBO J* 14, 2857-2865.

Holz, A., Bossinger, B., Strasser, T., Janning, W. and Klapper, R. (2003). The two origins of hemocytes in Drosophila. *Development* 130, 4955-4962.

Huang, L., Ohsako, S. and Tanda, S. (2005). The lesswright mutation activates Rel-related proteins, leading to overproduction of larval hemocytes in Drosophila melanogaster. *Dev Biol* 280, 407-420.

Jung, S. H., Evans, C. J., Uemura, C. and Banerjee, U. (2005). The Drosophila lymph gland as a developmental model of hematopoiesis. *Development* 132, 2521-2533.

Krzemien, J., Oyallon, J., Crozatier, M. and Vincent, A. (2010). Hematopoietic progenitors and hemocyte lineages in the Drosophila lymph gland. *Dev Biol*.

Krzemien, J., Dubois, L., Makki, R., Meister, M., Vincent, A. and Crozatier, M. (2007). Control of blood cell homeostasis in Drosophila larvae by the posterior signalling centre. *Nature* 446, 325-328.

Kurucz, E., Vaczi, B., Markus, R., Laurinyecz, B., Vilmos, P., Zsamboki, J., Csorba, K., Gateff, E., Hultmark, D. and Ando, I. (2007a). Definition of Drosophila hemocyte subsets by cell-type specific antigens. *Acta Biol Hung* 58 Suppl, 95-111.

Kurucz, E., Markus, R., Zsamboki, J., Folkl-Medzihradszky, K., Darula, Z., Vilmos, P., Udvardy, A., Krausz, I., Lukacsovich, T., Gateff, E. et al. (2007b). Nimrod, a putative phagocytosis receptor with EGF repeats in Drosophila plasmatocytes. *Curr Biol* 17, 649-654.

Lane, M. E., Sauer, K., Wallace, K., Jan, Y. N., Lehner, C. F. and Vaessin, H. (1996). Dacapo, a cyclin-dependent kinase inhibitor, stops cell proliferation during Drosophila development. *Cell* 87, 1225-1235.

Lanot, R., Zachary, D., Holder, F. and Meister, M. (2001). Postembryonic hematopoiesis in Drosophila. *Dev Biol* 230, 243-257.

Mandal, L., Banerjee, U. and Hartenstein, V. (2004). Evidence for a fruit fly hemangioblast and similarities between lymph-gland hematopoiesis in fruit fly and mammal aorta-gonadal-mesonephros mesoderm. *Nat Genet* 36, 1019-1023.

Mandal, L., Martinez-Agosto, J. A., Evans, C. J., Hartenstein, V. and Banerjee, U. (2007). A Hedgehog- and Antennapedia-dependent niche maintains Drosophila haematopoietic precursors. *Nature* 446, 320-324.

Minakhina, S. and Steward, R. (2006). Melanotic mutants in Drosophila: pathways and phenotypes. *Genetics* 174, 253-263.

Minakhina, S. and Steward, R. (2010). Hematopoietic stem cells in Drosophila. *Development* 137, 27-31.

Morin, X., Daneman, R., Zavortink, M. and Chia, W. (2001). A protein trap strategy to detect GFP-tagged proteins expressed from their endogenous loci in Drosophila. *Proc Natl Acad Sci U S A* 98, 15050-15055.

Morrison, S. J. and Spradling, A. C. (2008). Stem cells and niches: mechanisms that promote stem cell maintenance throughout life. *Cell* 132, 598-611.

Nam, H. J., Jang, I. H., Asano, T. and Lee, W. J. (2008). Involvement of pro-phenoloxidase 3 in lamellocyte-mediated spontaneous melanization in Drosophila. *Mol Cells* 26, 606-610.

Nie, M., Xie, Y., Loo, J. A. and Courey, A. J. (2009). Genetic and proteomic evidence for roles of Drosophila SUMO in cell cycle control, Ras signaling, and early pattern formation. *PLoS One* 4, e5905.

Ohsako, S. and Takamatsu, Y. (1999). Identification and characterization of a Drosophila homologue of the yeast UBC9 and hus5 genes. *J Biochem* 125, 230-235.

Paddibhatla, I., Lee, M. J., Ferrarese, R., Kalamarz, M. E. and Govind, S. (2010). Role for sumoylation in systemic inflammation and immune homeostasis in Drosophila larvae.

Passegue, E., Jamieson, C. H. M., Ailles, L. E. and Weissman, I. L. (2003). Normal and leukemic hematopoiesis: Are leukemias a stem cell disorder or a reacquisition of stem cell characteristics? *P Natl Acad Sci USA* 100, 11842-11849.

Qiu, P., Pan, P. C. and Govind, S. (1998). A role for the Drosophila Toll/Cactus pathway in larval hematopoiesis. *Development* 125, 1909-1920.

Rizki, T. M. and Rizki, R. M. (1980). Developmental Analysis of a Temperature-Sensitive Melanotic Tumor Mutant in Drosophila-Melanogaster. *Roux Arch Dev Biol* 189, 197-206.

Rizki, T. M. and Rizki, R. M. (1992). Lamellocyte differentiation in Drosophila larvae parasitized by Leptopilina. *Dev Comp Immunol* 16, 103-110.

Shrestha, R. and Gateff, E. (1982). Ultrastructure and Cyto-Chemistry of the Cell-Types in the Larval Hematopoietic Organs and Hemolymph of Drosophila-Melanogaster. *Dev Growth Differ* 24, 65-82.

Sinenko, S. A. and Mathey-Prevot, B. (2004). Increased expression of Drosophila tetraspanin, Tsp68C, suppresses the abnormal proliferation of ytr-deficient and Ras/Raf-activated hemocytes. *Oncogene* 23, 9120-9128.

Sinenko, S. A., Mandal, L., Martinez-Agosto, J. A. and Banerjee, U. (2009). Dual role of wingless signaling in stem-like hematopoietic precursor maintenance in Drosophila. *Dev Cell* 16, 756-763.

Smith, M., Bhaskar, V., Fernandez, J. and Courey, A. J. (2004). Drosophila Ulp1, a nuclear pore-associated SUMO protease, prevents accumulation of cytoplasmic SUMO conjugates. *J Biol Chem* 279, 43805-43814.

Sorrentino, R. P., Carton, Y. and Govind, S. (2002). Cellular immune response to parasite infection in the Drosophila lymph gland is developmentally regulated. *Dev Biol* 243, 65-80.

Stanyon, C. A., Liu, G., Mangiola, B. A., Patel, N., Giot, L., Kuang, B., Zhang, H., Zhong, J. and Finley, R. L., Jr. (2004). A Drosophila protein-interaction map centered on cell-cycle regulators. *Genome Biol* 5, R96.

Talamillo, A., Sanchez, J. and Barrio, R. (2008). Functional analysis of the SUMOylation pathway in Drosophila. *Biochem Soc Trans* 36, 868-873.

Trumpp, A., Essers, M. and Wilson, A. (2010). Awakening dormant haematopoietic stem cells. *Nat Rev Immunol* 10, 201-209.

Vidal, M. and Cagan, R. L. (2006). Drosophila models for cancer research. *Curr Opin Genet Dev* 16, 10-16.

Vilmos, P., Nagy, I., Kurucz, E., Hultmark, D., Gateff, E. and Ando, I. (2004). A rapid rosetting method for separation of hemocyte sub-populations of Drosophila melanogaster. *Dev Comp Immunol* 28, 555-563.

Wang, J. C. (2010). Good cells gone bad: the cellular origins of cancer. *Trends Mol Med* 16, 145-151.

Watson, K. L., Justice, R. W. and Bryant, P. J. (1994). Drosophila in cancer research: the first fifty tumor suppressor genes. *J Cell Sci Suppl* 18, 19-33.

Zettervall, C. J., Anderl, I., Williams, M. J., Palmer, R., Kurucz, E., Ando, I. and Hultmark, D. (2004). A directed screen for genes involved in Drosophila blood cell activation. *Proc Natl Acad Sci U S A* 101, 14192-14197.